LAMELLAR SPIRALLING
IN
DIRECTIONALLY FROZEN EUTECTICS

by

Teresa S. Attallah
B.Sc. in Materials Engineering
American University in Cairo
(1973)

A thesis submitted to the Faculty of Graduate Studies
and Research in partial fulfilment of the
requirements for the degree of
Master of Engineering

Department of Metallurgical Engineering,
McGill University,
Montreal, Canada. August, 1975

TO MY PARENTS
WITH ALL MY GRATITUDE

"Felix Qui Potuit Rerum Cognoscere Causas"

Virgil

ABSTRACT

A study of lamellar spiralling was carried out on the Sn-Cd, Sn-Zn, Pb-Sn, Cd-Zn and Al-$CuAl_2$ eutectic systems. A technique was developed to measure lamellar orientations from which the spiralling rate could be determined.

Results indicated that the Sn-Cd system whether in the faulted or fault-free state does not exhibit lamellar spiralling. Cd-Zn and Sn-Zn also were found to not spiral. Pb-Sn spiralled at 160°/cm when frozen at a growth rate of 2.3 cm/hr. under a temperature gradient of 7.1°C/cm while degenerate Pb-Sn grains failed to exhibit lamellar spiralling. Al-$CuAl_2$ lamellae were observed to twist during growth about the growth axis. Mold shape and temperature gradient were found to affect lamellar spiralling in the sense that an increase in the imposed G enhanced lamellar spiralling by inducing an increase in subgrain density and grain misorientation; while increasing the aspect ratio of the sample was found to reduce the spiralling rate. Metallographic studies indicated that the lamellae of all systems investigated (except Sn-Zn) were bent when observed across sections cut at right angles to the growth axis.

A spiral growth analysis is presented based on the anisotropic growth tendency of both eutectic phases combined with eutectic coupled growth. The analysis is applied to the equilibrium interface of all the systems investigated as well as others which have been reported to exhibit lamellar spiralling. The results are in agreement with the experimental observations.

RESUME

Une étude de la croissance en spirale des eutectiques lamellaires Sn-Zn, Pb-Sn, Cd-Zn et Al-$CuAl_2$ a été réalisée. Une technique de mesure des orientations de lamelles a été mise au point, permettant la détermination du taux de croissance en spirale.

Les résultats montrent que les lamelles des systèmes Sn-Cd, Cd-Zn et Sn-Zn ne croissent pas en spirale, que les lamelles présentent des fautes ou non. L'eutectique Pb-Sn, solidifié sous un gradient de température de 7.1^{0}C/cm et à une vitesse de 2.3 cm/hr croît en spirale à un taux de 160^{0}/cm; alors que les grains Pb-Sn dégénérés ne le font pas. Les lamelles de l'eutectique Al-$CuAl_2$, comme celles de Pb-Sn, croissent selon une hélice dont l'axe est perpendiculaire à l'interface de solidification. Une augmentation du gradient de température favorise la croissance en spirale en élevant la densité de fautes et la désorientation des grains. La forme du moule affecte également la croissance en spirale, plus le rapport longueur sur largeur du moule est grand, moins les lamelles spiralent.

Les observations métallographiques montrent que les lamelles des systèmes étudiés (sauf Sn-Zn) apparaissent courbées lorsqu'on observe des sections perpendiculaires à la direction de solidification.

Une analyse de la croissance en spirale est présentée, basée sur la croissance anisotrope mais couplée des deux phases de l'eutectique. L'analyse est appliquée aux interfaces lamellaires de tous les systèmes étudiés, ainsi qu'à d'autres pour lesquels la croissance en spirale a déjà été observée. Les résultats sont en accord avec les observations expérimentales.

ACKNOWLEDGEMENTS

The author would like to express her deepest gratitude and appreciation to her Research Director, Dr. J.E. Gruzleski, for his guidance and encouragement which have made this work both fruitful and enjoyable.

Thanks are due to Dr. W.M. Williams, Chairman of the Department of Mining and Metallurgical Engineering for providing the laboratory facilities required for the investigation.

Particular gratitude is also expressed to Dr. W.A. Miller for his stimulating discussions and suggestions.

The assistance of Mr. Knoepfel in the laboratory work and sample preparation is also gratefully acknowledged.

The author extends her thanks to Mr. A. Rizkalla for the help promptly provided during the experimental work.

A final tribute is due to the National Research Council of Canada and Quebec Iron and Titanium Corporation who provided financial assistance.

TABLE OF CONTENTS

APPENDIX

LIST OF FIGURES

Page

LIST OF TABLES

CHAPTER I

INTRODUCTION

In a binary eutectic phase diagram (Figure 1.1) the liquidus lines of each eutectic phase slope downward as the solute content increases until they meet at the eutectic equilibrium temperature below which the eutectic reaction takes place by the simultaneous crystallization of two phases. Many different types of eutectic microstructure have been reported, these being strongly dependent on the nature of the nucleation process (Mondolfo 1965) and the growth characteristics of each of the solid phases (Hunt and Jackson 1966; Davies 1964).

Eutectics were known as early as Roman times when Pb-Sn alloys were used for joining lead pipes and plating drinking vessels. More recently eutectic or near-eutectic cast irons have been used extensively for a variety of purposes, and Al-Si eutectic alloys have become important because of their high strength-to-weight ratio. Many eutectics form lamellar or rod-like (fibrous) structures (Figures 1.2(a) and 1.2(b)). Recently, by using a controlled directional solidification technique, extremely high strengths have been obtained in composite materials which consist of strong fibres or lamellae embedded in a ductile matrix (Bibring 1973). Eutectics are also useful as superconducting materials where fibre textures play an important role (Yue et al. 1972; Hurles and Hunt 1967).

Even though eutectics have been used for a long time, it is only within the past thirty years that the mechanism of eutectic solidi-

FIGURE 1.1 Typical binary eutectic phase diagram

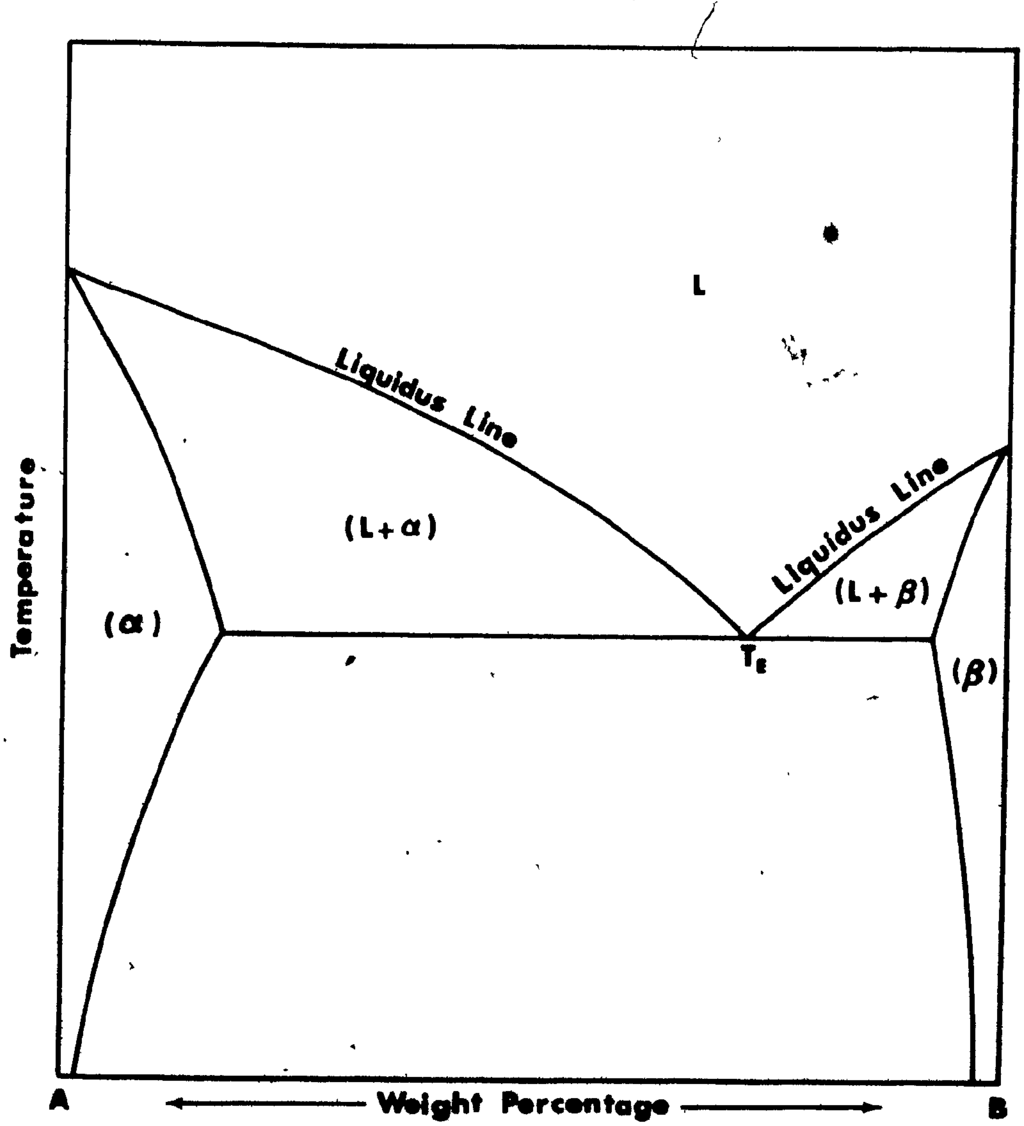
L
Liquidus Line
Liquidus Line
(L+α)
(L+β)
(α)
(β)
T_E
Temperature
A
Weight Percentage
B

FIGURE 1.2 Regular eutectic structures:
(a) lamellar, $Al-CuAl_2$ transverse section;
(b) rod-like, $Al-Al_3Ni$
(i) transverse section,
(ii) longitudinal section (Hertzberg et al. 1965)

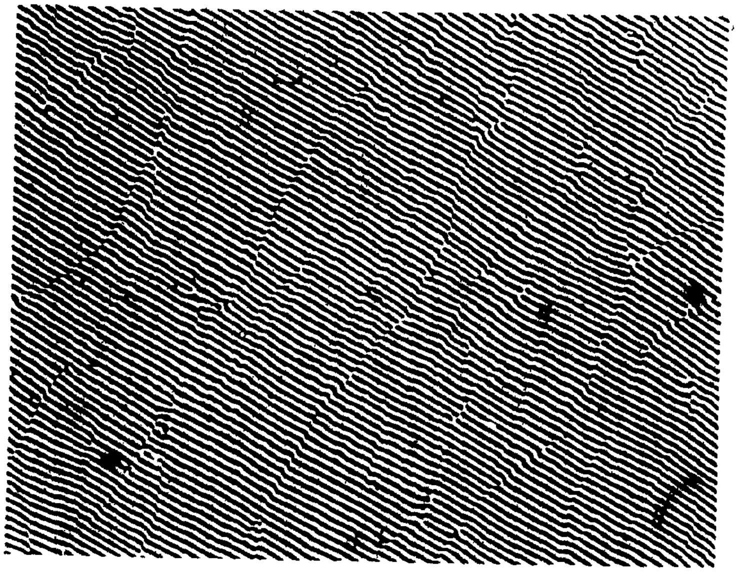

(a)

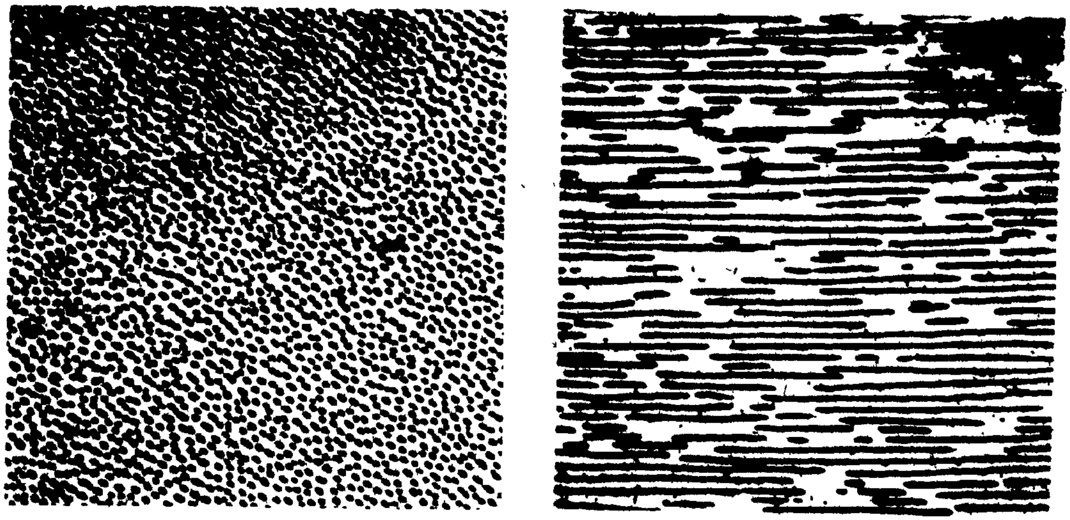

(i)

(ii)

(b)

fication has been given much attention. Many attempts have been made (Hunt and Jackson 1966; Scheil 1946, 1959; Hogan 1961; Jackson 1958a, 1958b) to classify the various types of observed eutectic morphologies, but a completely satisfactory classification covering the whole range of structures has never been put forward. A great deal of effort has also been devoted to explaining how eutectic nucleation takes place, and although theories have been postulated, no firm conclusions have yet been reached and the problem still remains open.

The work to be described in this thesis will be concerned with lamellar eutectics, concentrating on a particular aspect of lamellar growth known as spiralling.

1.1 LITERATURE REVIEW

1.1.1 Classification of Eutectics

One of the most widely accepted classifications of eutectics is that by Scheil (1946,1959) based on the mode of crystallization of the two eutectic phases individually rather than on the morphological characteristics of the composite on which previous investigators had relied. All binary eutectic microstructures were divided into two classes, viz. "normal" and "abnormal". Scheil placed the lamellar and rod-like structures (Figures 1.2(a) and 1.2(b)) in the first category, wherein the two phases were assumed to grow at equal velocities with a fixed orientation relationship between themselves, the growth direction being at right angle to a locally planar solid/liquid interface.

Abnormal eutectics (Figure 1.3(a)) were said to form when one of the phases tends to grow ahead of the other, producing no fixed crystallographic orientation relationship at the solid/solid interface.

Scheil's conclusions were reconsidered by Hogan (1961) who suggested that "normal" structures (rod-like and lamellar) result from the epitaxial nucleation of one phase on the other, while "anomalous" morphologies (Figure 1.3(a)) are obtained when the growth is coupled without a fixed orientation relation between the two eutectic phases. "Degenerate" microstructures (Figure 1.3(b)) were thought to occur when the two phases tend to grow independently.

Based on a study of transparent organic eutectics which freeze like metals, Hunt and Jackson (1966) proposed a new classification of eutectics involving the entropies of melting of the individual eutectic phases. Single phase materials were found to grow with faceted or non-faceted solid/liquid interfaces (Figures 1.4(a) and 1.4(b)) depending upon the magnitude of a computed parameter, α. Jackson (1958a, 1958b) showed that $\alpha = \xi \frac{\Delta S_F}{R}$, where ΔS_F is the entropy of fusion, R, the universal gas constant and ξ, a crystallographic factor which is less than, but almost, unity. He succeeded in showing from a thermodynamic argument that the growth morphology is largely dependent on the α factor. In general for non metals, α exceeds two owing to a high entropy of fusion, and as a consequence these crystals grow with faceted solid/liquid interfaces. On the other hand, metals have low entropies of melting ($\alpha < 2$) and hence they grow with non-faceted interfaces. On

FIGURE 1.3 Irregular eutectic structures:
(a) abnormal (anomalous), Al-Si longitudinal section (Day and Hellawell 1968);
(b) degenerate, Al-$CuAl_2$ transverse section

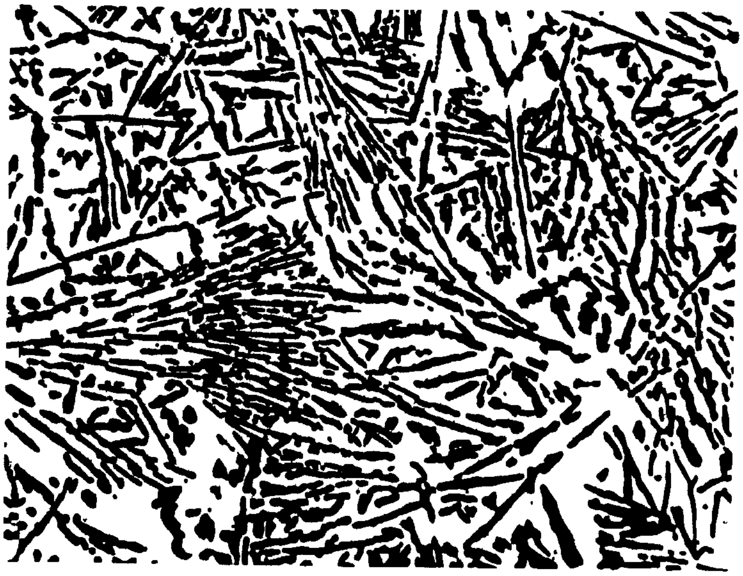

(a)

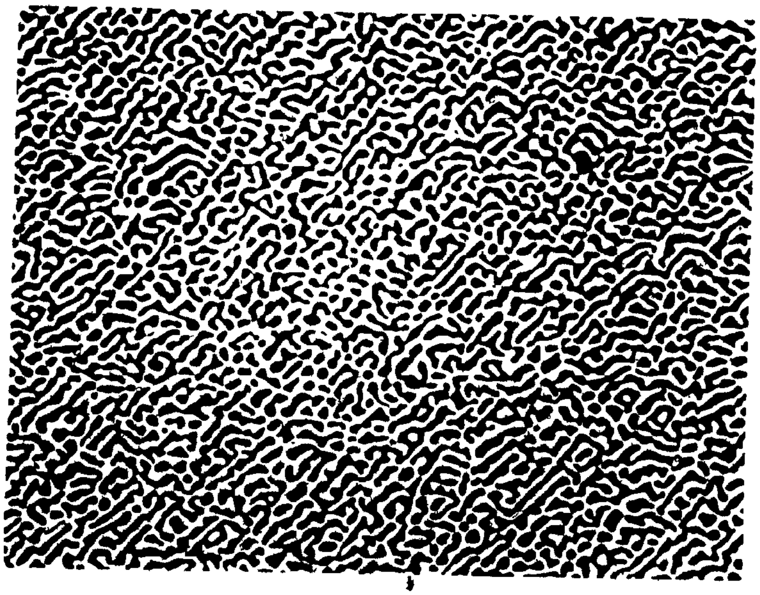

(b)

FIGURE 1.4 Types of solid/liquid interface:
(a) non-faceted, carbon tetrabromide-hexachloroethane eutectic (Hunt and Jackson 1966);
(b) faceted, salol ($\alpha \simeq 7$) (Jackson 1967)

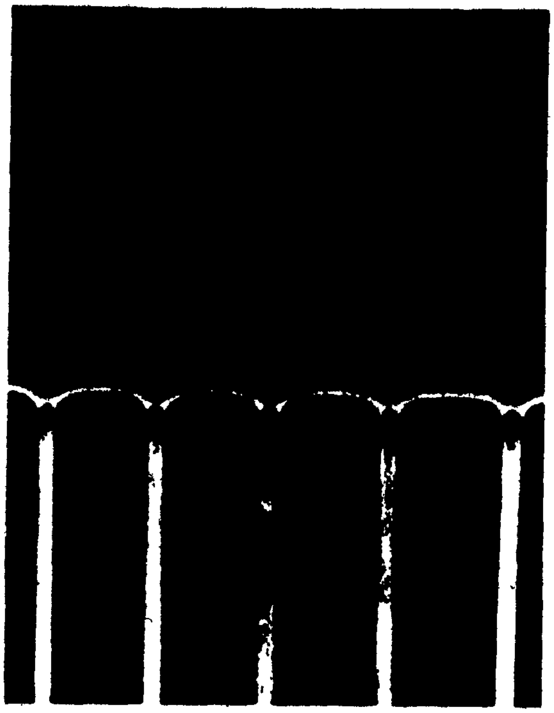

(a)

(b)

the same basis Hunt and Jackson (1966) divided eutectics into three groups, viz. those in which both phases have low entropies of melting, those in which only one phase has a low entropy of melting, and those in which both phases have high entropies of melting (this case never occurs in strictly metallic systems but may occur when two intermetallic compounds or metalloids such as Si, Ge or Bi are involved). Lamellar and rod-like structures belong to the first group, while irregular morphologies were said to belong to the second and third groups.

1.1.2 Nucleation of Eutectics

The nucleation stage is definitely of significance during controlled eutectic solidification since it is the stage at which coupled growth is established. Certain authors (Cooksey et al. 1964; Kraft 1962) have proposed that the preferred eutectic orientation relationship develops through repeated nucleation events until energetically stable grains suitably oriented for growth are produced.

After intensive studies on the nucleation of eutectic alloys, Mondolfo(1965) came to the conclusion that all the various structures can be explained in terms of the nucleation process. In fact, normal eutectics (rod-like and lamellar) were said to be expected when one of the phases acts as nucleating agent for the other, with a definite crystallographic relationship being established at the solid/solid interface. Anomalous eutectics are observed when both phases are nucleated by foreign impurities with the result that no mutual preferred orientation relationship is obtained. Degenerate (divorced) structures were said to be obtained when the second phase nucleates only after the first has completely solidified. These are generally formed in alloys far from the eutectic composition in which it is impossible for the primary phase to act as a nucleating agent for the second eutectic phase. Sundquist and Mondolfo (1961a,1961b) showed that: (1) nucleation is non-reciprocal, (2) epitaxy does in general exist between nucleant and nucleus although there exists a variety of crystallographic orientations leading to good matching between the two planes in contact at the solid/solid interface, (3) lattice disregistry between the phases seems not to be important, and (4) good nucleating agents tend to have high entropies of fusion and are themselves hard to nucleate.

Hogan (1965) carried out some experiments on quenched samples of Al-$CuAl_2$ eutectic in order to study eutectic nucleation. He observed very small eutectic nodules (previously detected by Chadwick (1965) in the Pb-Sn system) surrounding minute $CuAl_2$ nuclei. From a study of sections of quenched ingots he was able to show that the nodules did indeed nucleate the eutectic. In agreement with Mondolfo's concept of one-way nucleation, he found that Al primary dendrites had no effect on eutectic nucleation, while the $CuAl_2$ primaries were always associated with it. The results of more recent studies on the nucleation of eutectic alloys (Davies 1964; Cooksey et al. 1964; Hogan 1964-1965) have generally been found to agree with the conclusions of Mondolfo and his co-workers.

1.1.3 Growth and Crystallography of Lamellar Eutectics

Because the major concern of this work is with lamellar eutectics, it is appropriate to concentrate the remainder of this chapter on nucleation and growth of lamellar eutectics.

Lamellar eutectic growth is a diffusion-controlled process which can occur only if an undercooling below the equilibrium eutectic temperature is attained. Following Zener's work (1946) on the eutectoid austenite-to-pearlite transformation, Tiller (1958) determined the minimum undercooling, ΔT, required for lamellar growth, expressing it in the following form:

$$\Delta T = \Delta T_C + \Delta T_D + \Delta T_K$$

where ΔT_C and ΔT_D refer to the undercoolings due to interfacial curvature and diffusion controlled solute rejection respectively, and ΔT_K is a kinetic undercooling term which is usually neglected for non-faceted-non-faceted growth. Summing the ΔT_C and ΔT_D undercoolings, Tiller was able to correlate the interlamellar spacing with growth rate and total undercooling. In order to specify a unique relationship between any two of the variables, an optimizing condition had to be specified. While Zener in his treatment maximized the growth rate, Tiller obtained the same result by minimizing the total undercooling. The lamellar spacing, λ, was predicted to be related to the growth rate, R, by an equation of the form $\lambda = A(R)^{-1/2}$, where A is a constant, and the total undercooling was found to be related to the growth rate by the relationship $\Delta T = BR^{1/2}$ where B is another constant. This analysis proved to be extremely successful in predicting the nature of the experimental relationship between the three variables, λ, R and ΔT (Cooksey et al. 1964; Moore and Elliot 1968; Hunt and Chilton 1962).

In the period 1952-1962, Elbaum and Chalmers (1955) developed a model for the growth of crystals from the melt in which growth was assumed to take place by the side-propagation of low-index steps across the solid/liquid interface. This model was based on the results of decanting experiments which revealed crystallographic facets on the exposed solid surfaces, the decanted surface structure being assumed to be identical to the actual interface structure during growth. This platelet theory was discredited by Chadwick (1962) who showed that surface tension causes a thin layer of liquid to remain on any decanted surface and that solidification of this layer obscures the nature of the real solid/liquid interface.

The growth of a lamellar eutectic from its melt is thought to take place according to the "normal growth" mechanism depicted in Figure 1.5. Regardless of its crystallographic orientation, the solid/liquid interface moves parallel to itself and perpendicular to the lamellar interphase boundary without need for linear growth steps across the interface. As a lamella of the α phase solidifies, it rejects atoms of component B and correspondingly the β phase rejects atoms of component A, with the result that the liquid ahead of the β lamella is depleted

FIGURE 1.5 Schematic representation of the steady-state growth of a lamellar eutectic (Tiller 1958)

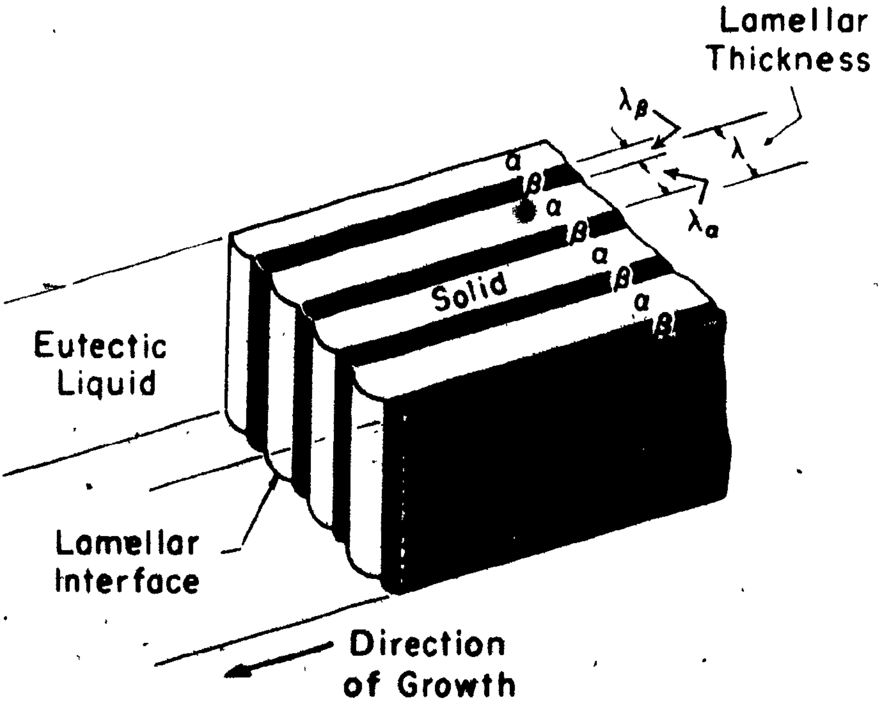
Lamellar Thickness
λ_β
λ
λ_α
α
β
α
β
α
β
α
β
Solid
Eutectic Liquid
Lamellar Interface
Direction of Growth

in the B component and that ahead of the α lamella is depleted in A component. Thus, lateral diffusion ahead of the interface is an important step in the growth of lamellar eutectics. The large area of the lamellar interface makes this morphology energetically unfavourable, but the occurence of a consistent orientation relationship between the phases leads to the conclusion that the growth can be stabilized by selection of a low-energy interface. The preferred crystallographic orientation relationship established at the lamellar interface may be a function of the freezing conditions. In fact, Takahashi and Ashinuma (1958-1959) and Takakashi (1960) examined thin films of Al-$CuAl_2$ by selected-area electron diffraction analysis and observed orientation relationships which were different from those previously reported (Kraft and Albright 1961; Kraft 1961). Kraft (1962) later investigated the same eutectic alloy and found a third set of orientation relationships, while other workers (Davies and Hellawell 1970; Cantor and Chadwick 1974) showed that different relationships can be obtained even when two identical specimens are frozen in an identical manner. Changes in growth kinetics with orientation, anisotropy of solid/liquid interfacial energy as well as anisotropy of heat flow are thought to be responsible for the various crystallographic relationships observed under various freezing conditions (Kraft 1961; Chadwick 1967).

A convenient way of describing lamellar growth is to specify the planes in contact at the solid/solid interface, as well as the direction in each which is parallel to the growth axis of the system. Two statements are therefore used to describe the five degrees of freedom of the eutectic interface:

LAMELLAR INTERFACE // $(hkl)_\alpha$ // $(hkl)_\beta$ STATEMENT A
GROWTH DIRECTION // $[uvw]_\alpha$ // $[uvw]_\beta$ STATEMENT B

From studies on the Al-$CuAl_2$ and Mg-Mg_2Sn eutectics, Kraft (1962,1963) came to the conclusion that a low-energy interface is usually parallel to crystallographic planes of wide spacing and nearly equal atomic densities in each of the two phases. A comprehensive list defining the crystallography of unidirectionally solidified eutectics is given in a review article by Hogan et al. (1970).

With one exception (Gruzleski and Winegard 1968; Berthou and Gruzleski 1971), lamellar structures in bulk specimens have been found to contain structural imperfections (named faults) such as those shown in Figure 1.2(a). The reason for the occurence of such imperfections is not yet very well understood, although they are believed to play a role during growth in causing changes of orientation related to the development of preferred orientation and the spiral growth phenomenon (Double 1973).

1.1.4 Spiralling in Lamellar Eutectics

Many grains are usually nucleated during directional eutectic solidification, some being more suitably oriented for growth than others. The energetically stable grains will grow at the expense of less stable ones thus considerably reducing the number of persisting grains.

While studying the crystallographic relationships in those grains which survived some several centimeters of growth, Kraft and Albright (1962) found that the preferred lamellar orientation in the Al-$CuAl_2$ eutectic is subject to microscopic deviations of a few degrees. More recently, progressive changes of the lamellar orientation within single eutectic grains have been observed (Double et al. 1968; Hopkins and Kraft 1968). Most crystallographic studies have been made near the end of directionally solidified ingots where lamellar growth was almost a steady state process. Very little is known about crystallographic orientations in a given grain at the moment of nucleation. It is possible that the preferred crystallographic orientation relationship between the lamellar phases does not exist at the point of nucleation, but develops gradually during growth, probably requiring relative rotation of the two lattices until a low energy interface containing the growth direction is attained.

Hogan et al. (1970) have summarized the reported observations on orientation changes during eutectic grain growth as follows:

(1) Rotation of lamellar normals about the growth axis, probably necessitating changes in the crystallographic planes in contact at the solid/solid interface.

(2) After a low energy interface has been selected, the two phases may rotate during growth about an axis normal to the growth direction of the system until a preferred texture is attained.

(3) Lamellae can spiral progressively about an axis parallel to the growth direction with both phases maintaining a fixed orientation relationship.

(4) Small changes in crystallographic orientation can occur across mismatch surfaces.

Rotations of type 2 were observed by Hopkins and Kraft (1968) in lamellar grains of Pb-Sn seeded by Sn crystals of known orientation. After a few centimeters of directional growth the orientation of both seeded and unseeded grains could be described as:

LAMELLAR INTERFACE // $(0\bar{1}1)$ Sn // $(1\bar{1}\bar{1})$ Pb   STATEMENT A
GROWTH DIRECTION // [211] Sn // [211] Pb   STATEMENT B

When the [211] in the Sn seed was parallel to the overall growth direction, statements A and B were observed after 3 mm. of directional growth, but when the [100] was coincident with the growth direction, the crystals rotated almost 30° about an axis perpendicular to the growth direction during the first 4.5 cm. of growth, until the directions described in statement B were observed. In this case, the preferred interfacial habit plane seems to have been established immediately upon nucleation.

Rotations of type 3, being of major interest in the present work, will be treated in more detail. They have been observed in Pb-Sn (Hopkins and Stewart 1970) and in Al-$CuAl_2$, Al-Zn and Al-Ag_2Al directionally solidified eutectics (Double et al. 1968). The spiral growth of the lamellae of an Al-Zn grain is represented in a schematic way in

Figure 1.6, the spiralling rate calculated from the experimental data being 11°/inch or 4.3°/cm. Double and co-workers (1968) found that the spiralling rate, regardless of growth rate, was constant for all grains and directly related to the subgrain density which in turn decreases by increasing the imposed temperature gradient. Clockwise and counterclockwise rotations were observed in the same sample (Al-Zn), the sense of rotation being constant for a given grain. Spiralling in lamellar eutectics was linked to the subgrain density: for a given temperature gradient, the Al-$CuAl_2$ system was found to spiral less rapidly than the Al-Ag_2Al which contained a wider range of misorientations between subgrains. X-ray studies on the Zn-rich phase of the Al-Zn system (Double et al. 1968) showed that the lamellar planes instead of coinciding with the growth axis were often inclined by up to 25°. From the examination of a tapered longitudinal section of a directionally solidified Al-$CuAl_2$ eutectic specimen (Figure 1.7) (Double 1973; Double et al. 1968), lamellar orientation changes could be followed and the average rate of rotation was found to be about 6°/cm. It is evident from the micrograph that the mean lamellar trace is rotating, but moreover it may be seen that rotations can be followed within a given subgrain as well as discontinuously across the sub-boundaries.

Hopkins and Stewart (1970) measured lamellar rotations in Pb-Sn eutectic samples grown both from [100] Sn seeds by the Czochralski technique and by unseeded Bridgeman growth. The spiralling rate, $\frac{d\phi}{dx}$, was found to be constant for any grain during growth and dependent upon the growth method. In fact, $\frac{d\phi}{dx}$ was nearly twice as large in Bridgeman-

FIGURE 1.6 Heavily etched specimen of directionally frozen Al-Zn alloy in which the orientation has changed progressively. The diagrammatic sections show the relative positions, 1-6, of mean lamellar traces (Double 1971)

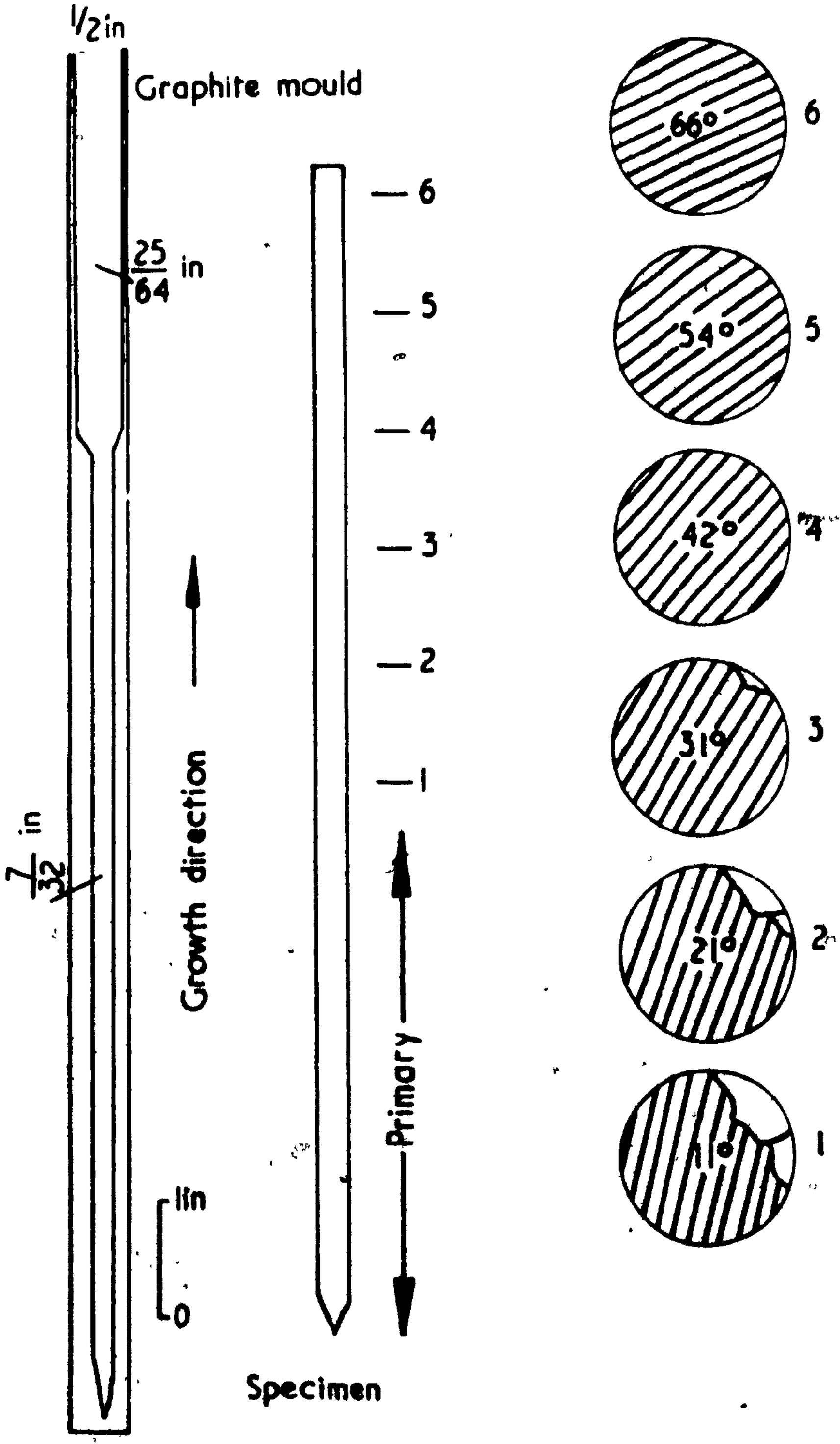
1/2 in
Graphite mould
25/64 in
7/32 in
Growth direction
1in
0
Specimen
6
5
4
3
2
1
Primary
66°
54°
42°
31°
21°
11°
6
5
4
3
2
1

FIGURE 1.7. Al-$CuAl_2$ lamellar rotations:

(a) a near longitudinal (<5^o) taper section through a eutectic specimen showing lamellar rotations within subgrains and across sub-boundaries. The observed general rotation of 30^o corresponds to a true rotation of less than 2^o;

(b) the orientation of the lamellar traces within individual subgrains in the above taper section is plotted as a function of distance along the specimen. The angles measured on the taper section are converted to true values. The straight line represents the observed average rate of rotation of some 6^o/cm. The graph shows that the angular rotations of the lamellar traces are irregular but with an overall tendency in one sense. (Double 1971,1973)

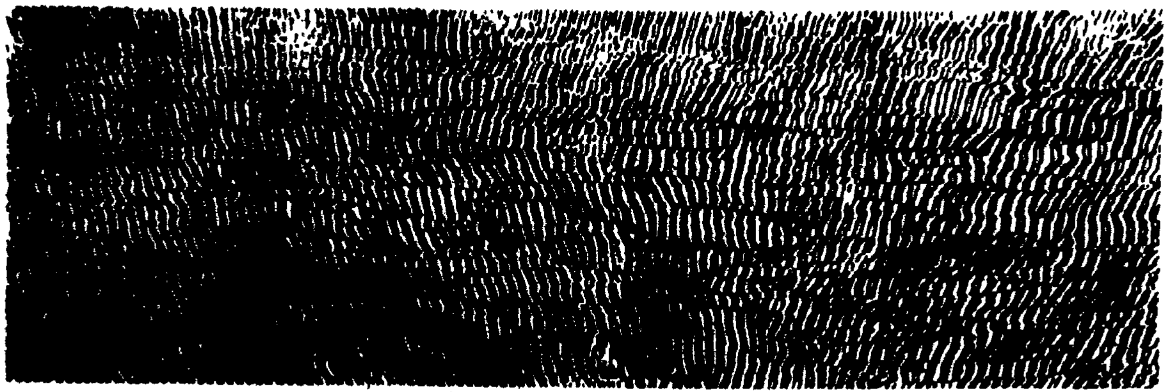
Growth direction ▶
Al–CuAl₂

(a)

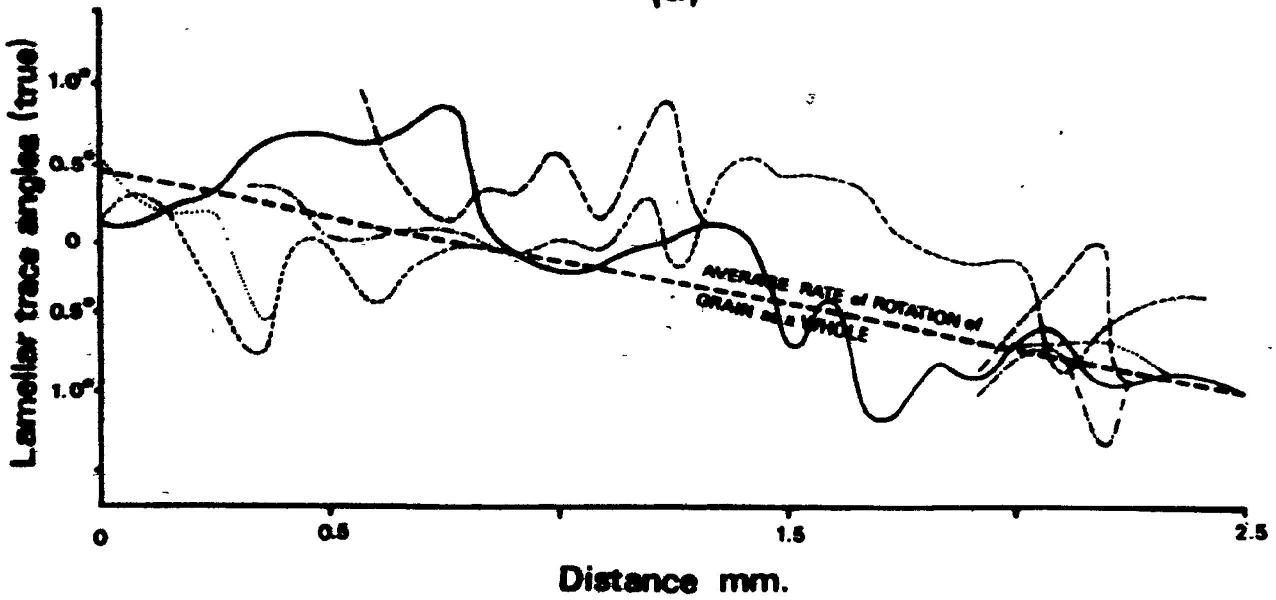
Lamellar trace angles (true)
1.0°
0.5°
0
0.5°
1.0°
0
0.5
1.5
2.5
Distance mm.
AVERAGE RATE of ROTATION of GRAIN as a WHOLE

(b)

grown ingots as in the Czochralski samples even though the growth rates were almost the same in each case and the fault densities were comparable, indicating that the spiralling rate is probably not determined only by substructural perfection.

Hogan and co-workers (1970) suggested that the effect of steep temperature gradients would be to make the solid/liquid interface flatter, thus decreasing the variations in local growth direction along the interface and therefore decreasing the spiralling rate. Such a suggestion was discredited by Hopkins' and Stewart's results (1970) since interfacial curvature is more convex during Czochralski growth than during Bridgeman growth.

No complete explanation of spiral growth in lamellar eutectics has been given to date, although it is believed by certain authors (Double et al. 1968; Hopkins and Stewart 1970; Double and Hellawell 1969a) that the eutectic substructure might be related in some way to this phenomenon. Double (1973) stated that "the mechanism by which the rotation effect operates is that it involves some asymmetric bias either in the solid/solid interfacial energy associated with the epitaxial arrangement of the phases and/or in the mechanism which the subgrain boundaries themselves are formed (and thus ultimately on the evolutionary process), or in the combination of a preferred habit plane with a tendency to anisotropic growth of one or both phases." Double and Hellawell (1969a) using a simple interference technique showed that in Al-CuAl$_2$ sub-grains, the lamellae have a tendency to form a fan-like pattern. The effect is obtained by superimposing upon a micrograph running transverse to the growth direction a grid of parallel lines as shown in Figure 1.8. If a micrographic section makes an angle with the lamellar plane, successive sections through the fan-like arrangement will simulate a progressive twisting of the grain as shown in Figure 1.9.

1.2. AIMS OF THE PRESENT WORK

The present investigation was undertaken with the following objectives:

(1) To study the effect of microstructural perfection on the spiralling rate by comparing the lamellar rotation of Sn-Cd fault-free grains with the spiralling of faulted grains. The Sn-Cd system was chosen because it is the only known system in which perfect eutectic grains may be obtained in bulk specimens.

(2) To determine whether eutectics formed from phases having the same crystal structure will exhibit the spiralling effect previously observed only in systems in which the unit cells of the two phases were of different types.

(3) To investigate the effect of growth rate, temperature gradient and asymmetrical heat flow on the spiralling phenomenon.

(4) To attempt to find an explanation for the origin and mechanism of lamellar spiralling.

FIGURE 1.8 Super-imposition of a perfect grid of parallel lines upon a typical micrograph of the lamellar eutectic, Al-$CuAl_2$, producing divergent interference fringes (Double and Hellawell 1969a)

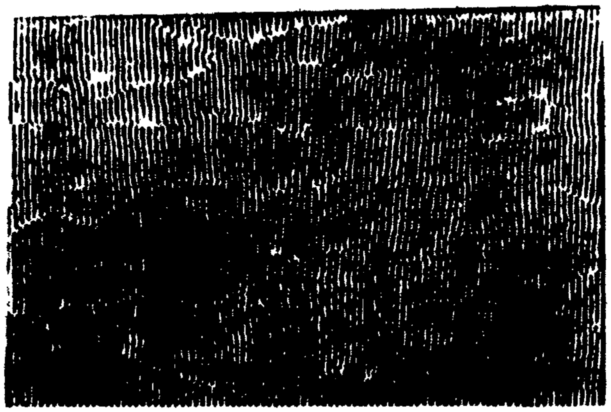

+

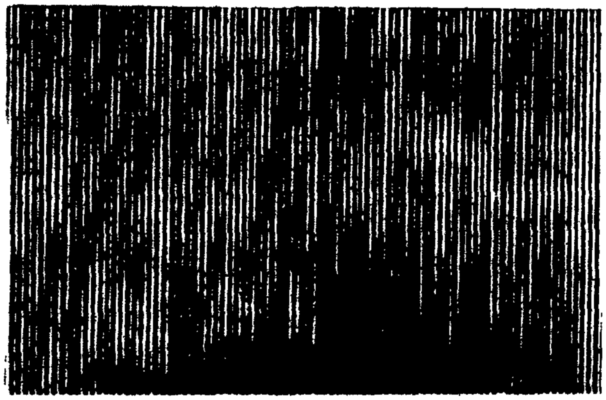

=

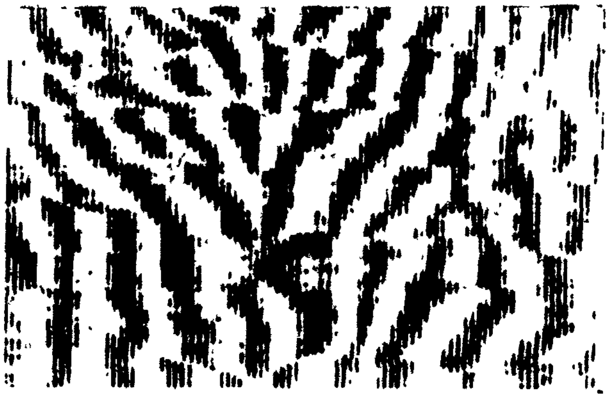

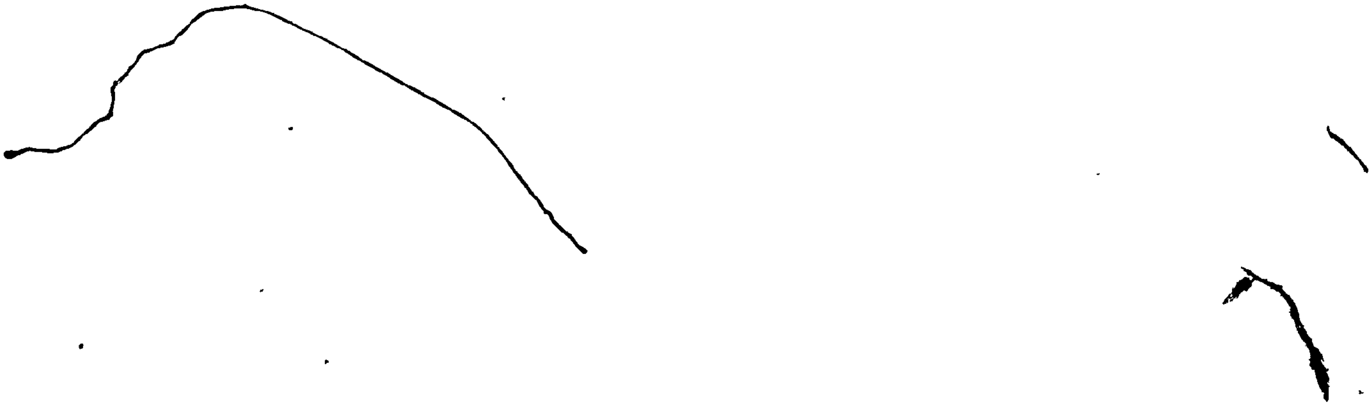

FIGURE 1.9 Schematic representation of how successive sections through a fan-like lamellar arrangement include different lamellae and therefore give an impression of helical growth if the sections are not normal to the rotational axis. Thus, Section a includes lamellae Nos. 1 and 2, Section b - Nos. 2 and 3, Section c - Nos. 4, 5 and 6, etc. (Double and Hellawell 1969a)

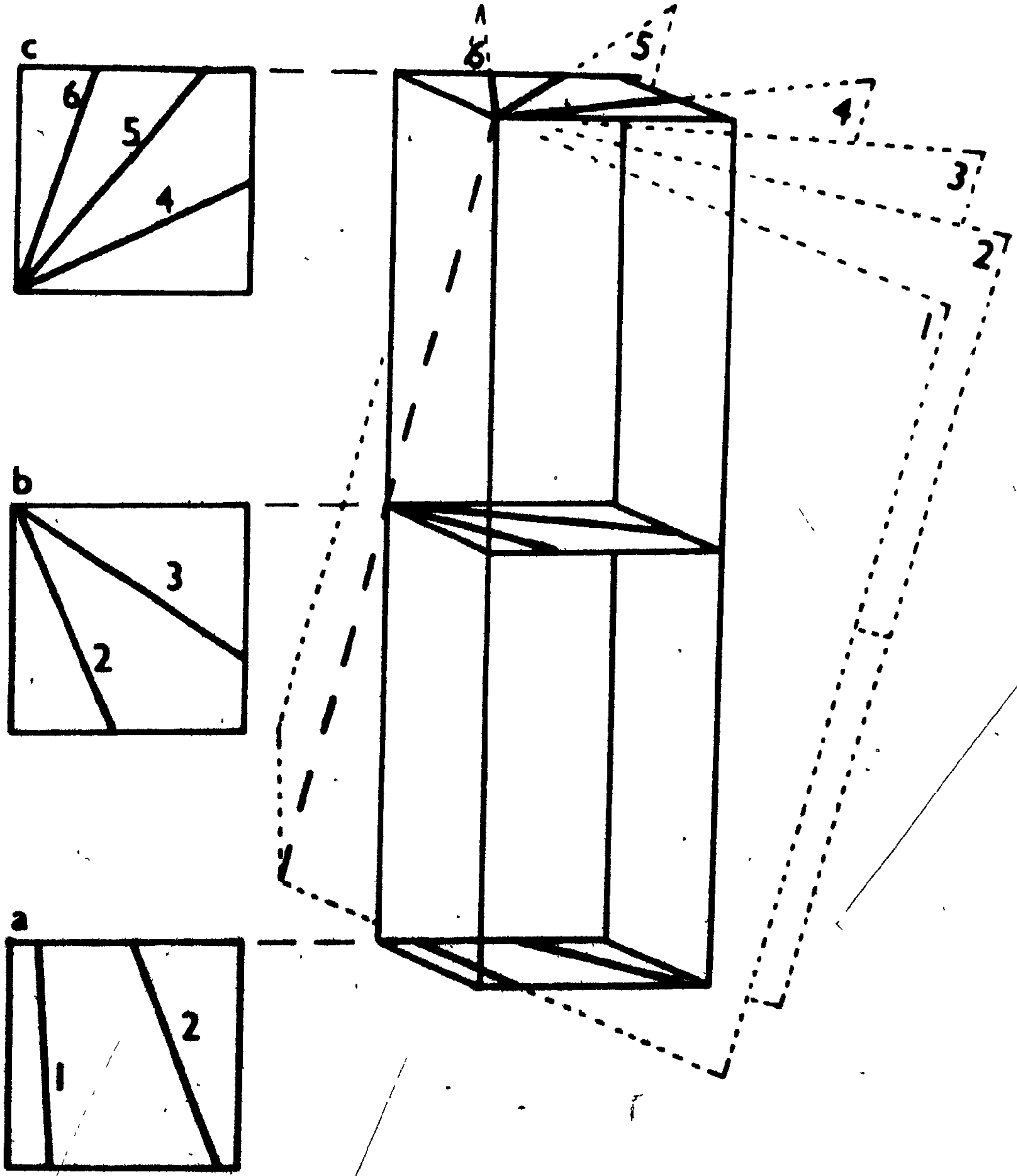
c
6
5
4
b
3
2
a
1
2
6
5
4
3
2
1

CHAPTER II

EXPERIMENTAL PROCEDURE

When directionally solidified, certain lamellar eutectics have been found to grow by spiralling about an axis parallel to the overall growth direction of the system. Such behaviour was previously thought to be common to all lamellar systems. The spiralling of lamellae is undesirable because of the serious effects it may have on the anisotropic properties of directionally solidified composites. The following experimental procedure was undertaken in order to prepare directionally solidified alloys of eutectic composition for the purpose of studying lamellar spiralling.

2.1 ALLOY PREPARATION

The eutectic systems selected for this study were Sn-Cd, Cd-Zn, Pb-Sn, Sn-Zn and Pb-Cd because their low eutectic temperatures make them favourable for experimental work. In addition, these systems show some variations in their lamellar microstructure: e.g., Sn-Cd has been shown to exist in the fault-free condition (Gruzleski and Winegard 1968; Berthou and Gruzleski 1971), Gd-Zn, Pb-Sn and Pb-Cd are normal lamellar eutectics, while Sn-Zn forms a broken lamellar structure (Jaffrey and Chadwick 1969).

The metals used were of 99.999% purity supplied in the form of shot by Cominco Ltd.. Master heats of eutectic composition were prepared by weighing the appropriate amounts of the constituents according to the phase diagrams shown in Figure 2.1. The metallic shot was mixed and then placed in a pyrex tube measuring 12 mm. in diameter and about 60 cm. in length. In order to prevent oxidation, the metals were melted by means of an oxygen-butane torch under a vacuum of $10^{-2}\mu$ or better. After the entire charge of about 125 gm. was melted, the tube was sealed at a position approximately 10 cm. above the liquid metal surface, tilted a few times to insure proper mixing and finally allowed to cool slowly under a glass wool bed. Since it is difficult to obtain the exact eutectic composition by simply weighing the components, the alloys were zone refined in sealed pyrex tubes for about 20 passes (Chalmers 1964). Samples measuring about one centimeter in length were then cut from each end of the zone refined ingots for metallographic analysis.

2.2 SPECIMEN PREPARATION

Samples of each zone refined eutectic master alloy (weighing about 50 gm.) were cast under vacuum in a 6 mm. I.D. by 30 cm. long pyrex tube inside a three zone vertical furnace as shown in Figure 2.2(a). The cast eutectic sample was placed in a high purity graphite crucible measuring 10 mm. O.D., 6 mm. I.D. and 30 cm. in length. Three small holes were drilled to a depth of 1.5 mm. on the external surface of the mold, one at the top, one at the center and the third at the bottom. A chromel-alumel thermocouple tip was inserted into each hole, fixed with refractory cement and connected to a temperature recorder. The central thermocouple was used in the calculation of the average temperature gradient during solidification while the top and bottom thermocouples indicated when to stop or start the run, respectively.

FIGURE 2.1 Phase diagrams for the studied systems:
(a) Sn-Cd;
(b) Cd-Zn;
(c) Pb-Sn;
(d) Sn-Zn. (ASM Metals Handbook 1973)

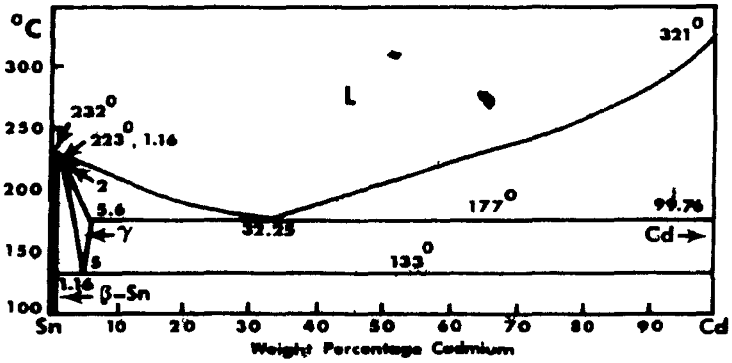
°C
300
250
200
150
100
L
321°
232°
223°, 1.16
2
5.6
32.23
177°
99.76
γ
Cd
5
133°
1.16
β-Sn
Sn
10
20
30
40
50
60
70
80
90
Cd
Weight Percentage Cadmium

(a)

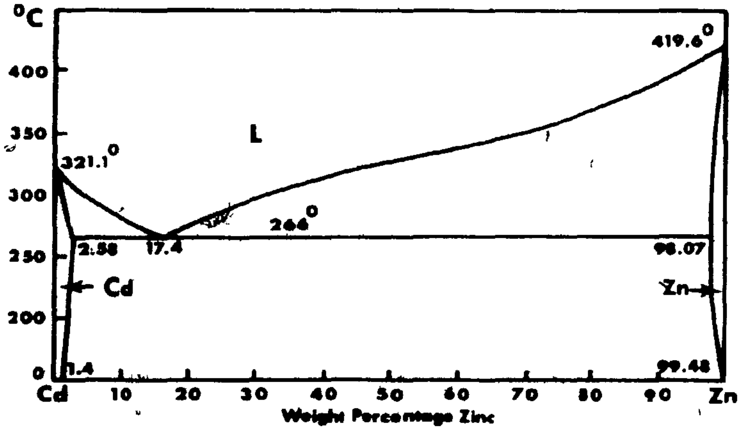
°C
400
350
300
250
200
0
L
419.6°
321.1°
266°
2.58
17.4
98.07
Cd
Zn
1.4
99.48
Cd
10
20
30
40
50
60
70
80
90
Zn
Weight Percentage Zinc

(b)

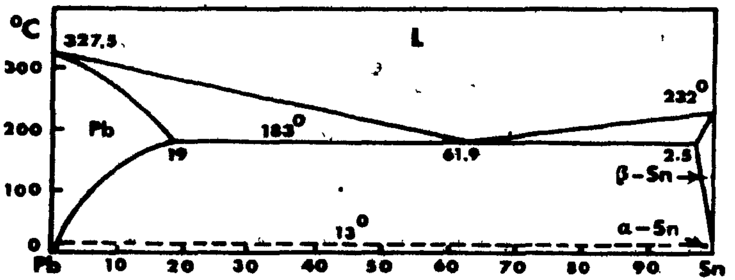
°C
300
200
100
0
327.5
L
Pb
183°
232°
19
61.9
2.5
β-Sn
13°
α-Sn
Pb
10
20
30
40
50
60
70
80
90
Sn
Weight Percentage Tin

(c)

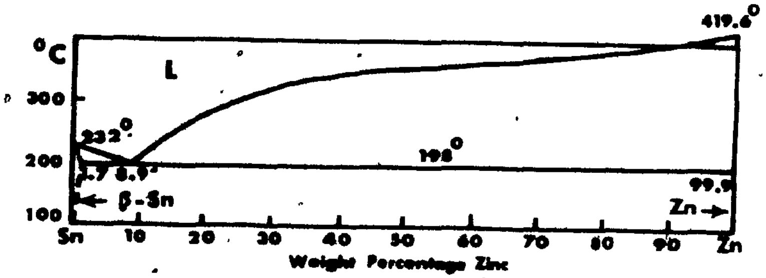
°C
300
200
100
L
419.6°
232°
198°
2.7
8.9
99.9
β-Sn
Zn
Sn
10
20
30
40
50
60
70
80
90
Zn
Weight Percentage Zinc

(d)

FIGURE 2.2 Casting techniques:
(a) circular glass mold;
(b) rectangular graphite mold

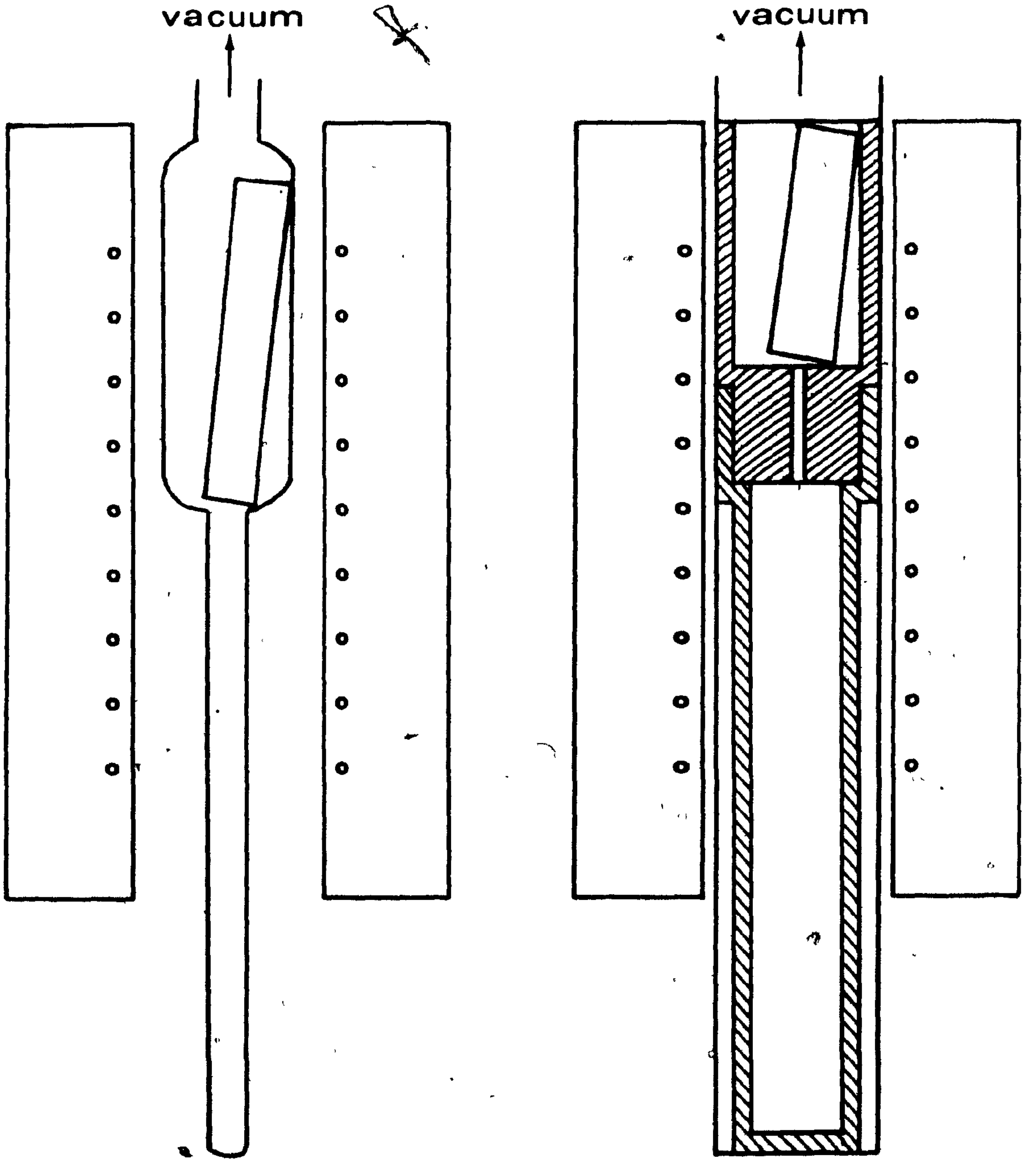

(a) (b)

Experiments on asymmetrical heat flow were carried out using rectangular high purity molds measuring 2 x 0.5 x 20 cm. with a 3 mm. wall thickness. The molds were machined in two parts and were held together with refractory cement. A graphite funnel containing the eutectic alloy to be cast was placed in the upper part of the mold and the unit placed in a vycor tube as shown in Figure 2.2(b). Melting was carried out under vacuum with the samples (in either round or rectangular molds) placed between two steel discs bolted together as shown in Figure 2.3. The discs were used to hold the specimen in the vertical position.

2.3 GROWTH PROCEDURE

All specimens were directionally grown by the Bridgeman technique employing a constant vertical movement of the furnace. A schematic diagram of the directional solidification apparatus used is shown in Figure 2.3. The furnace, powered by a controlled variable drive motor attached to a gear reducer by a chain linkage, was connected to a counterweight by a braided steel wire. As the motor started, the wire moved around the pulley of the gear reducer and the furnace was smoothly lifted at a speed ranging from between 1 and 30 cm./hr., constant to within ±0.5%. The whole set up was designed to be almost vibration free in order to prevent erratic growth fluctuations.

High temperature gradients were established in some runs by using a cooling system consisting of a water-cooled copper disc in contact with the bottom of the graphite crucible. By varying the water

FIGURE 2.3 Schematic diagram of the unidirectional solidification apparatus

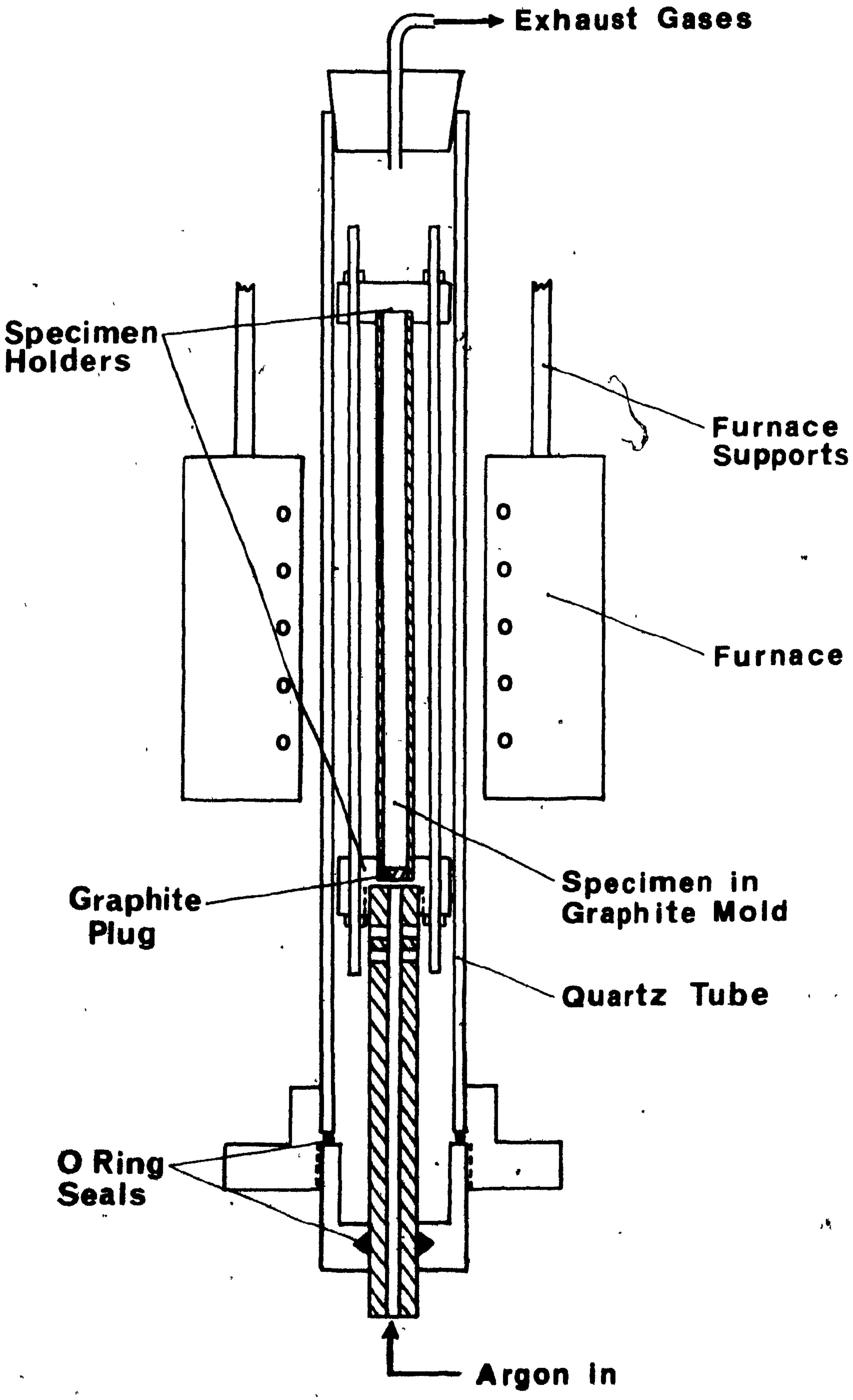
Exhaust Gases
Specimen Holders
Furnace Supports
Furnace
Specimen in Graphite Mold
Graphite Plug
Quartz Tube
O Ring Seals
Argon in

pressure recorded by a manometer gauge, a range of temperature gradients could be obtained.

Prior to the directional solidification of a specimen, the furnace elements were turned on for one day to allow the temperature to stabilize. Once the furnace was at its lowest position, the sample could be inserted, fixed in the quartz tube, and allowed to heat up for about one hour while argon was allowed to flow through the tube. The motor was then set for the desired furnace speed and the temperature at the lower, central and uppermost parts of the sample recorded by means of a Leeds and Northrup temperature recorder.

A special growth technique (Berthou and Gruzleski 1971) was used in order to produce perfect Sn-Cd eutectic grains. This technique consisted of using a very high growth rate for the first centimeter in order to promote the nucleation of many grains, followed by a slower growth rate to favour the growth of the most stable grains.

2.3.1 Growth Rate Measurement

The rate of freezing of a directionally solidified eutectic alloy can be measured by one of three methods as follows:

(1) From the rate of cooling, (dT/dt), and the temperature gradient, G, in the liquid ahead of the solid/liquid interface, using the relationship

$$R = (dT/dt)_L/G$$

(2) From the equation relating the interlamellar spacing to the growth rate, viz.

$$\lambda^2 R = \text{constant}$$

(3) From the expression $R = x/t$, where x is the distance travelled by the furnace in time t.

The first method is the most accurate but is also the most difficult experimentally because it requires accurate thermocouple measurements in the melt. The second method requires knowledge of the precise value of a constant which was often unavailable for the systems investigated during the present work. The third method was generally used for measuring the growth rate in this work, although method (2) was used where variable freezing conditions were employed during a single experiment.

2.4 METALLOGRAPHY AND SPIRALLING RATE MEASUREMENTS

When removed from the graphite molds, the directionally solidified samples measured about 23 cm. in length. It is important to have long specimens in controlled directional solidification since growth conditions are steady only in the central region which constitutes about 80% of the specimen length. At the beginning of freezing the metal at the bottom of the mold undercools, nucleates and grows rapidly, while towards the end of solidification there is little sensible heat left, so that the growth rate increases.

A flat surface was machined along the length of each sample, and for reasons to be explained later, a V-notch was made along the sample length as shown in Figure 2.4(a). Sections transverse to the growth direction were cut with a hack saw at various intervals along the specimen axis and these were then cold mounted. The number of sections prepared per specimen ranged up to a maximum of 26. Lubricated surfaces were ground through 600 grit paper on a Buehler Handimet grinder and were polished and etched as indicated in Table 2.1. Smoother and cleaner surfaces were obtained by dipping the sections in alcohol after each polishing step and cleaning in an ultrasonic cleaner for about 10-15 minutes. This procedure was found to be necessary to remove all particles which had become attached to the soft alloy surfaces.

From examination of serial sections along the length of each eutectic ingot, three regions were found to exit. At the initial region of the crucible where solidification began, there was a zone between 0.5-1 cm. long containing randomly nucleated fine eutectic grains. From this region several grains, evidently of preferred orientation, grew in a columnar fashion and as growth proceeded certain grains grew at the expense of their neighbours thus reducing to a few the number of persisting grains. A colony structure was sometimes observed in the last centimeter of growth. All spiralling measurements were made on ingot zones in which steady state heat flow prevailed and an aligned morphology was obtained. In some cases it was not possible to take measurements from the initial region of the ingot because the large number of nucleated grains presented difficulties in attempting to distinguish between grains from one section to the next.

FIGURE 2.4 Technique used for measuring lamellar orientations:
(a) directionally solidified sample (cylindrical);
(b) reference mark (v-notch) carved along the sample on a flat surface;
(c) section alignment;
(d) lamellar orientation measurement (ϕ)

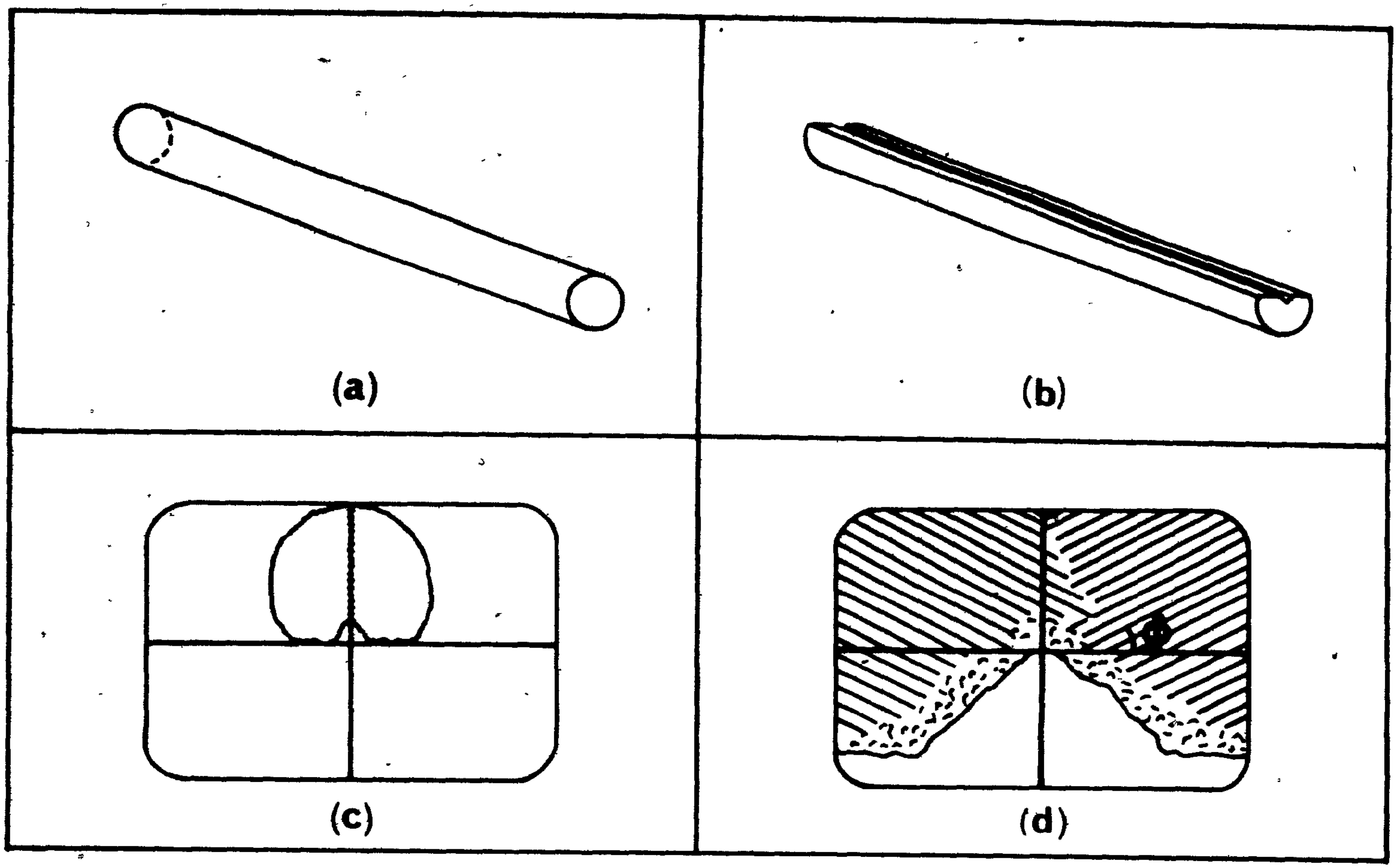
(a)
(b)
(c)
(d)

TABLE 2.1 Polishing Materials and Etching Solutions Used for the Systems Investigated in this Work.

System	Coarse Polishing	Intermediate Polishing	Fine Polishing	Etching Solution
Sn-Cd	14μ diamond paste	6μ diamond paste	1μ diamond paste	Aqueous $FeCl_3$ solution
Cd-Zn	Brasso	6μ diamond paste	-	5% nital
Pb-Sn	Brasso	6μ diamond paste	1μ diamond paste	HNO_3 1 part Acetic acid 1 part Glycerol 8 parts at 40°C
Sn-Zn	14μ diamond paste	6μ diamond paste	1μ diamond paste	1% HCl in alcohol
Pb-Cd	Brasso	6μ diamond paste	-	HNO_3 4 parts Acetic acid 4 parts H_2O 16 parts freshly prepared

The spiralling rate was determined by following the average lamellar orientation of the grains from section to section along the directionally solidified sample. The technique used (see Figure 2.4 (a-d)) consisted of measuring the angle between lamellar traces and a reference line within each eutectic grain. All measurements were made on the screen of a Quantimet television microscope. At first the flat portion of the section containing the reference mark (V-notch) was aligned parallel to a horizontal line made on the screen at a magnification of 50X (Figure 2.4(c)). This was done through a rotational movement of the sample stage. At a higher magnification, usually 400X, the center of the groove was then translated vertically and horizontally by means of a mechanical stage until it coincided with the intersection made by the two lines on the screen. In this way the sections were all identically aligned when measurements were taken at the same reference point.

Lamellar orientations, defined as the angle between the lamellae and the horizontal line (Figure 2.4(d)), were measured every 1/10 of a millimeter running from the center of the notch to the opposite side of the section as shown in Figure 2.4(c), this path being referred to as the reference line. Angular measurements were plotted versus distance across the section and depending on the position of experimental points, grains could be identified and the average lamellar orientations estimated as represented in Figure 2.5.

FIGURE 2.5 Grain identification and average grain orientation determination from lamellar orientation measurements taken across section along the reference line

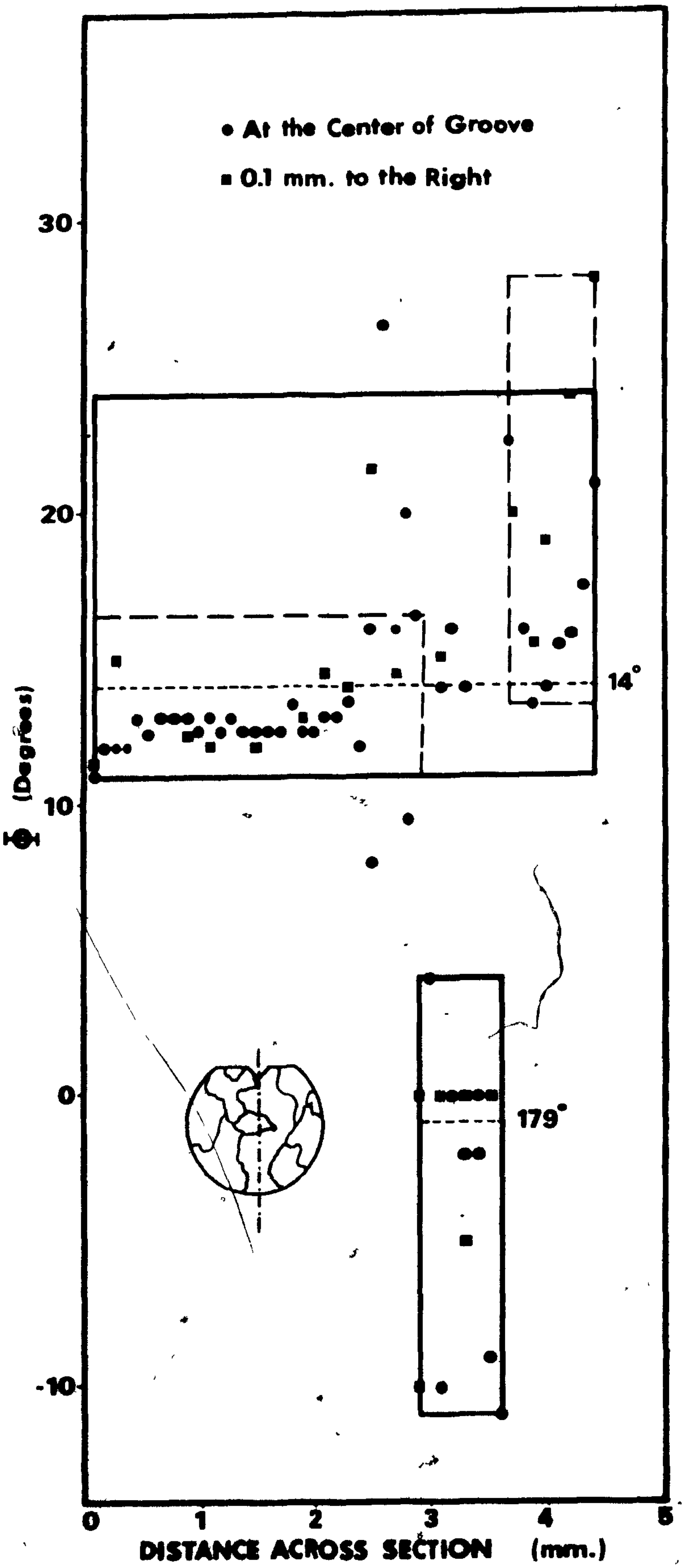
● At the Center of Groove
■ 0.1 mm. to the Right
30
20
10
0
-10
Θ (Degrees)
14°
179°
0
1
2
3
4
5
DISTANCE ACROSS SECTION (mm.)

Care had to be taken at this stage to make a net distinction between different grains. Sometimes owing to the irregular shape of the grain boundaries (see drawing on the left-hand side of Figure 2.5) one could identify the same grain twice as indicated in Figure 2.5. This occurred because a very small portion of a grain might intersect the reference line for a short distance only. In the successive sections, because of grain boundary migration, this small portion might no longer intersect the reference line or might even become larger in size. Another difficulty encountered in grain identification was in attempting to distinguish betwen grains and subgrains because of the difficulty of distinguishing grain boundaries from subgrain boundaries in eutectic structures. The presence of faults results in the production of many subgrains within each grain, and the subgrain misorientation can vary from a few degrees to several degrees. During the present work the allowable misorientations within a eutectic grain was chosen to be between 10^o and 20^o for relatively low temperature gradients, and between 30^o and 40^o for considerably higher temperature gradients. As will be shown later, the degree of misorientation increases with the imposed G. Very often, grains existing at the beginning of the sample disappeared after a certain growth distance probably because of grain boundary migration allowing for the expansion of more suitably oriented grains at the expense of less stable ones.

To show that the technique was reliable even if measurements were taken at an offset of 0.1 mm. from the center of the groove, lamellar orientations were measured under such conditions, and led to comparable values of the average grain orientation (Figure 2.5). Once the grains were identified, their mean lamellar orientation could be estimated and followed from section to section thus permitting the determination of the spiralling rate and sense of rotation in each grain. The results were presented on circular graphs by plotting the angular values of lamellar orientations around the circumference, and the distance in the growth direction along the diameter, as shown in Figure 3.7.

2.5 MOIRE PATTERNS AND LAMELLAR BENDING

Moiré patterns have been widely used for many years in various applications such as electron microscopy for the detection of lattice strains introduced by dislocations and local lattice misorientations. They are also employed for detecting machining defects in very accurately prepared work-pieces as well as in fingerprint characterization and classification. In this work Moiré patterns have been used to accentuate structural features such as lamellar bending observed across transverse sections of most of the investigated systems. Such patterns were obtained by superimposing either a perfect grid on the micrograph of a transverse section or vice versa, resulting in the production of Moiré fringes which showed the magnified curvature of the lamellae. More details about the patterns themselves will be given later in the Results section, while the technique used for the production of grids and patterns is discussed below.

2.5.1 Grids and Pattern Production

Perfect grids were obtained by photographing at different magnifications sets of parallel lines of equal or different spacings. Lettraset sheets of continuous straight lines were used for this purpose and when the spacings did not correspond to the required ones, sets of parallel lines were obtained by means of a hatching rule and rapido-pens of appropriate sizes.

Once the perfect grid with the appropriate spacing (see below) was produced either as a negative or as a positive, superposition of the perfect grid and transverse section transparency was done on top of the photographic paper followed by normal light exposure using the enlarger. The micrograph employed was always a 4 x 5 in. plate and the perfect grid was also a negative if the lettraset sheets were used. When the set of parallel bars was obtained by drawing lines with rapido-pens, the micrograph had to be placed on the top to make the pattern visible since the lines were drawn on a thin opaque paper. In both cases a print of the Moiré pattern could be obtained with no difficulty, the two superimposed grids being thin enough for light to pass through.

2.5.2 Quantitative Determination of Grid Spacing (Oster 1969)

a) Superposition of Identical Gratings

Figures 2.6(a) and 2.6(b) show the superposition of two identical grids of parallel equispaced lines. This very simple case,

FIGURE 2.6 Superposition of grids of parallel equispaced lines:

(a) coarse gratings at 45°;

(b) coarse gratings at a small angle (Oster 1969)

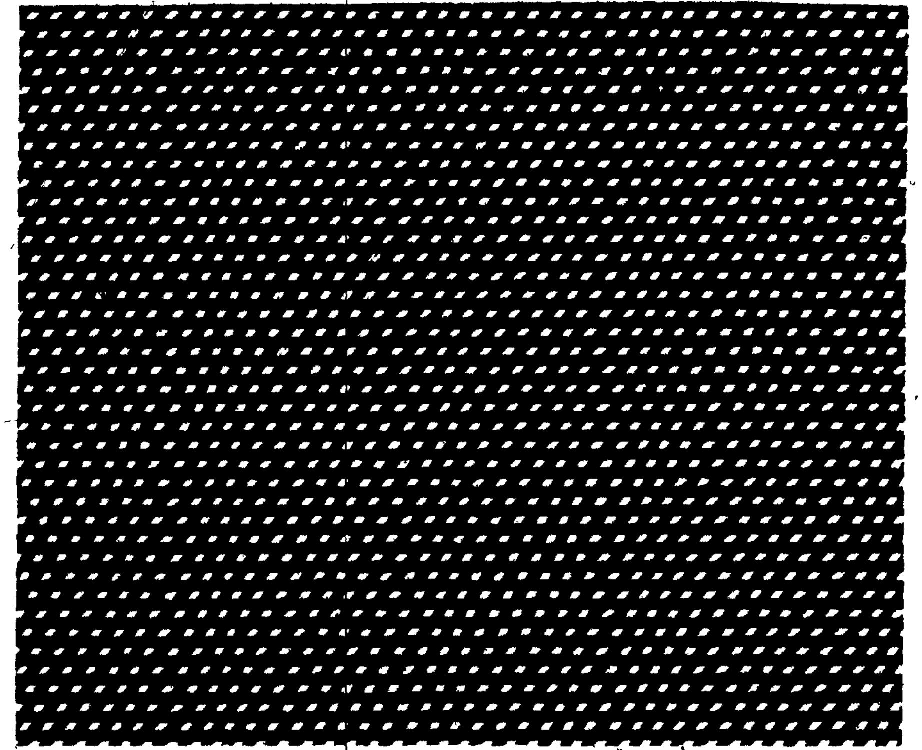

(a)

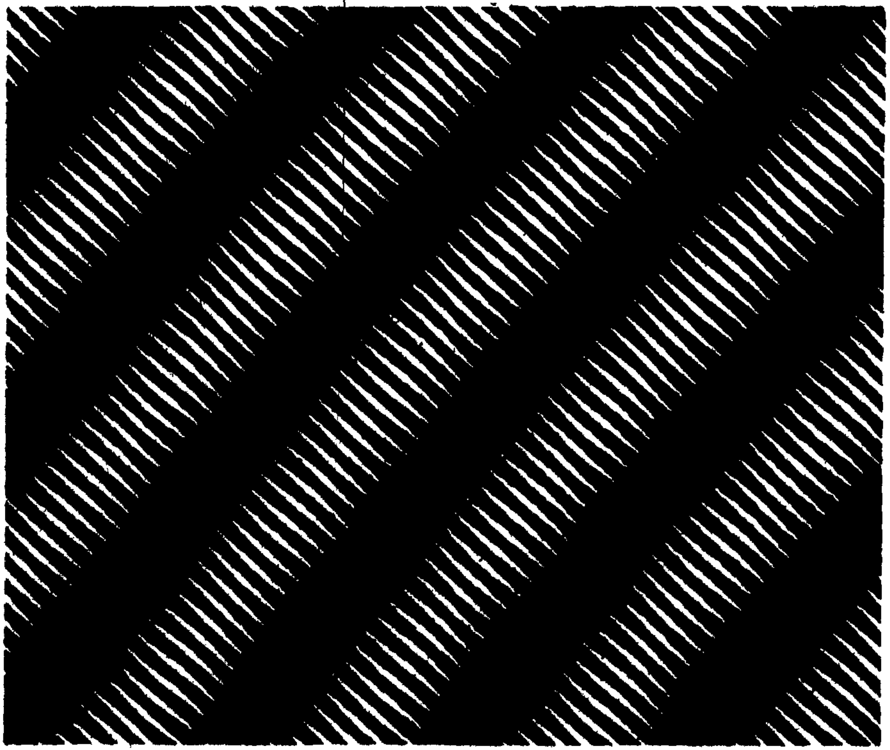

(b)

although not directly related to the observations made during the course of this work, helps in understanding the more complex case of mismatched pairs with which the investigation was concerned. When the lines of the two grids shown in Figures 2.6(a) and 2.6(b) coincide, two patterns result depending upon the way the bars overlap:

(1) If the white bars coincide with the white and hence the black with the black, the pattern will remain unchanged.

(2) If the black bars overlap on the white, a complete dark field will be obtained.

If the top transparency is rotated by a certain angle, a field of white diamonds surrounded by a black background is produced as shown in Figures 2.6(a) and 2.6(b) and the net result is a new set of lines, the Moiré fringes, which become more prominent as the angle of intersection is decreased. The distance between the fringes increases as the angle of intersection decreases, approaching infinity as this tends to zero. A quantitative relationship between the angle of intersection θ, fringe spacing d, and grating repeat unit (the width of a black bar or of a white bar) a, can be determined from Figure 2.7(a) which shows an enlarged portion of the network (a rhombus ABCD):

$$\overline{AC}^2 = \overline{AB}^2 + \overline{AD}^2 - 2\overline{AB}\,\overline{AD}\,\overline{CD}(180-\theta) \qquad (1)$$

or

$$\overline{AC}^2 = \overline{AB}^2 + \overline{AD}^2 - 2\overline{AB}\,\overline{AD}\cos\theta \qquad (1')$$

Since $|AB| = |AD|$ and $1 - \cos\theta = 2\sin^2\theta/2$, then

FIGURE 2.7 Elements of fields produced by the overlaying of:
(a) two identical gratings;
(b) two dissimilar size gratings (Oster 1969)

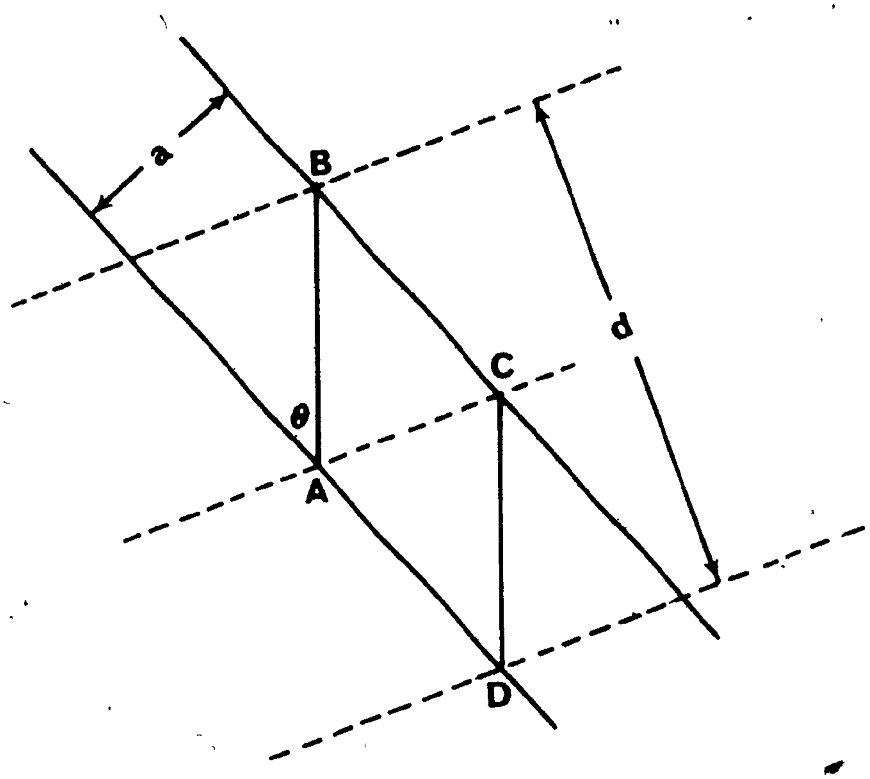

(a)

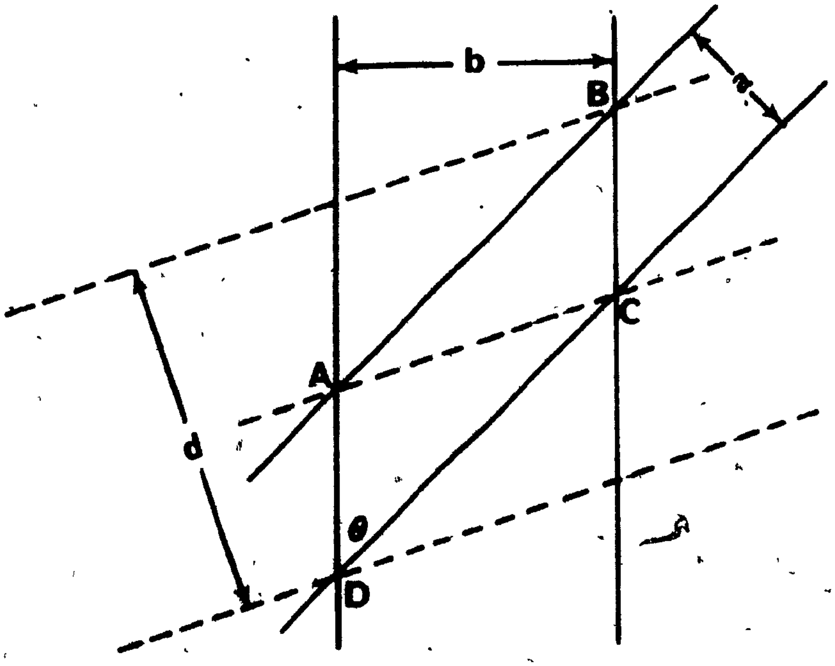

(b)

$$\overline{AC} = 2\overline{AB} \sin\frac{\Theta}{2} \tag{2}$$

From the area of a rhombus

$$a|AB| = d|AC| \tag{3}$$

From Equations (3) and (2), the Moiré fringe spacing d is given by

$$d = \frac{a}{2\sin\theta/2} \tag{4}$$

For small values of $\theta/2$, Equation (4) becomes

$$d \simeq \frac{a}{\Theta} \tag{5}$$

Therefore, by simply measuring the fringe spacing, one can determine very small angles of intersection from Equation (5).

b) Superposition of Two Dissimilar Gratings

When the two gratings do not have the same spacing, a mismatch is said to exist. As in the previous case the fringe distance increases as the angle of intersection is decreased, but it assumes a finite value at $\theta = 0^{\circ}$. Beats are observed when the lines of both grids overlap and the resulting beat pattern becomes a magnification of the original grating (Figure 2.8). If a and b are the spacings of the two gratings respectively, then the difference in frequency of the two gratings is given by

FIGURE 2.8 Illustration of how the superposition of two non-identical gratings lead to a beat pattern which is a magnification of the original grating

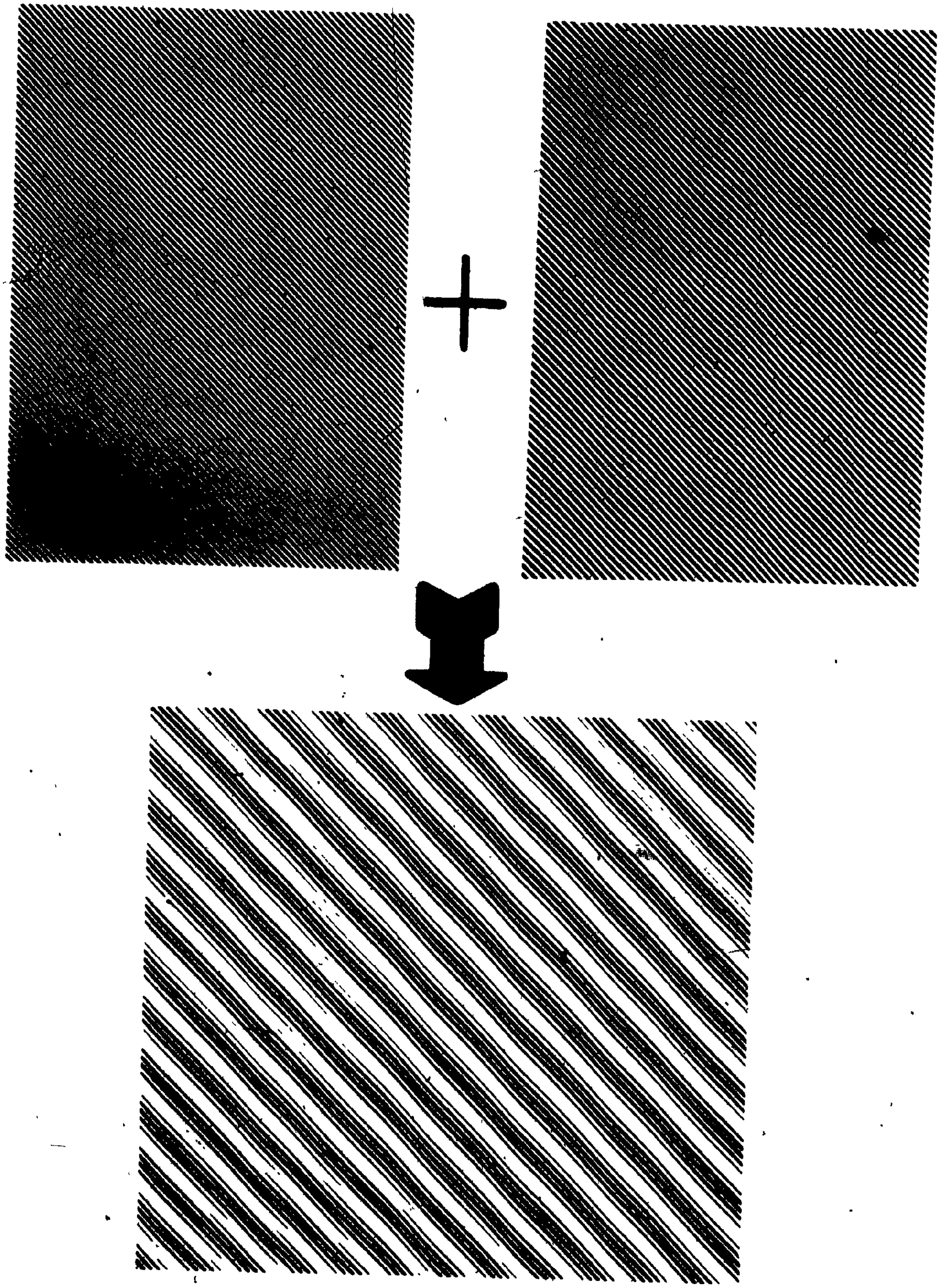

$$\frac{1}{d} = \left|\frac{1}{a} - \frac{1}{b}\right| \tag{6}$$

or

$$d = \frac{ab}{|a-b|} \tag{7}$$

From Equation (7) the fringe spacing d is the spacing a or b magnified by the factor $(\frac{a}{b} - 1)^{-1}$ or $(1 - \frac{b}{a})^{-1}$ respectively. The magnification increases as a becomes closer to b until it becomes infinity when a = b which is the case of superimposing two identical gratings. Having defined the fringe distance d and we wish to have a pattern consisting of 10 fringes in the 5 by 4 in. area of the plate, then knowing the spacing on the transverse micrograph transparency, one can determine the spacing of the perfect grid required to obtain the desired value of d.

If a grating of spacing b with its lines in the vertical position is superimposed on a grid of spacing a at an intersection angle Θ, the field will consist of parallelograms as shown in Figure 2.7(b), the fringe distance being given by (Oster 1969)

$$d = \frac{ab}{\sqrt{a^2+b^2-2ab\cos\Theta}} \tag{8}$$

When Θ = 0, Equation (8) becomes Equation (7) and when a = b, Equation (8) becomes Equation (4).

In the present study we were concerned with the superposition of two non-identical gratings which further differed in that the white and black bars were of different widths so that the white and black fringes were also differently spaced. Because mismatch exists between even the components of one grid, the best way to estimate roughly the spacing of the white and black bars, a_w and a_b, respectively, is to consider each case separately. The beat equation for this case includes the larger and smaller fringe distances:

$$\frac{1}{d_b+d_w} = \left|\frac{1}{a_b+a_w} - \frac{1}{b_b+b_w}\right| \tag{9}$$

or

$$\frac{1}{D} = \left|\frac{1}{A} - \frac{1}{B}\right| \tag{9'}$$

where $D = d_b+d_w$, $A = a_b+a_w$ and $B = b_b+b_w$

also

$$D = \frac{AB}{|A-B|} \tag{10}$$

from which the total fringe distance, D, is the spacing A or B magnified by the factor $(\frac{A}{B} - 1)^{-1}$ or $(1 - \frac{B}{A})^{-1}$, respectively.

For the present study a difference of 10-30% between grid spacings (either for white or black bars) was found to be adequate. It is to be noted that it did not really matter whether the spacings of the superimposed grid were both larger or if one was larger and the other smaller than those of the bottom grid provided that the difference was within the established range. An example of structural defect detection is presented in Figure 3.2 where the case of lamellar bending is displayed in a Sn-Cd transverse section. It is to be noted that if the structural defect is in the grating of larger spacing, the defect will appear reversed in the Moiré pattern (Hirsch et al. 1965) (see Figure 2.9). This can also be noticed from a comparison of Figure 3.2(c) which is exactly Figure 3.2(a) but magnified, with Figures 3.3(b), 3.5(b), 3.18(b) and 3.19(b) in which the sense of bending appears reversed since the grating of larger spacing was that of the transverse section micrographs while in the case of Figure 3.2(b) it was that of the perfect grid.

FIGURE 2.9 Optical analogue showing that:

(a) if the dislocation is in the grating of larger spacing, a dislocation of opposite sign will result;

(b) if the dislocation is in the grating of smaller spacing, a dislocation of the same sign will be produced. (Hirsch et al. 1965)

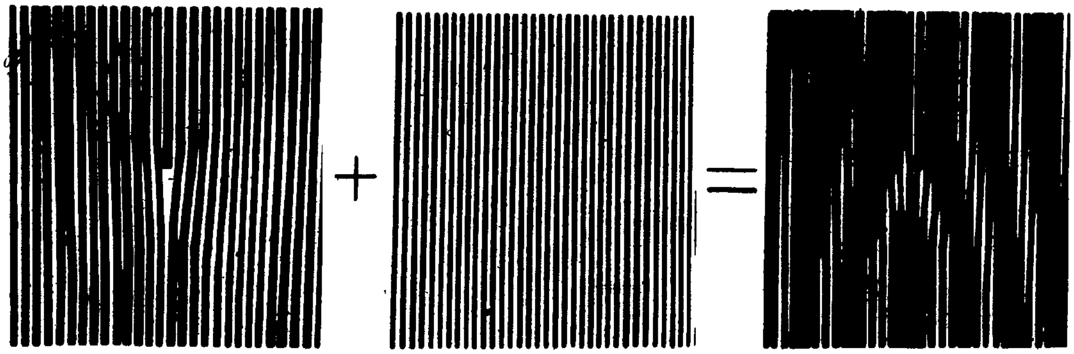

(a)

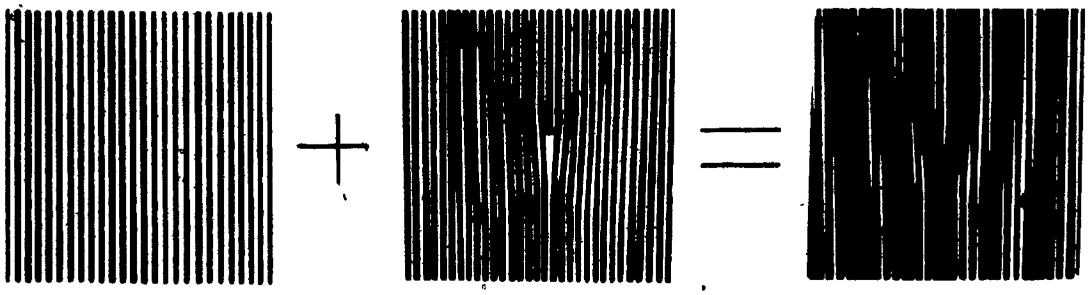

(b)

CHAPTER III

RESULTS

General data on the five systems investigated during the present work are first given in this chapter with special emphasis on the crystal structure of the eutectic phases which is thought to play an important role in lamellar spiral growth. Moiré patterns showing lamellar bending across transverse sections will be shown followed by presentation of the results on spiralling.

3.1 SOLIDIFICATION AND METALLOGRAPHY (LAMELLAR BENDING)

3.1.1 Tin-Cadmium

The Sn-Cd eutectic solidifies with a typical lamellar morphology composed of alternating plates of the Cd-rich phase containing 0.24 wt.% Sn on solidification and a Sn-rich or β phase containing 5.6 wt.% Cd (see Figure 2.1(a)). The faulted lamellar Sn-Cd structure is shown in Figures 3.1(a) and 3.1(c) representing the microstructure of sections taken at right angles to the growth axis of a directionally solidified sample. According to Hunt and Chilton (1962) the Cd-rich phase constitutes 25% of the eutectic by volume and appears dark after etching with the β phase appearing light. The two eutectic phases are both close packed hexagonal (ASM Metals Handbook 1973), the lattice parameters of the β phase being unknown while those of pure Cd at 20°C are: $a = 2.9787$ A° and $c = 5.617$ A° (Barrett 1952). At 133°C a solid state transformation takes place during which 3.5 to 4 vol.% of Cd (Racek et al. 1974) either precipitates within the Sn lamellae or diffuses

FIGURE 3.1 Faulted Sn-Cd lamellar structure:
(a) transverse section (x400). The tendency of the lamellae to bend is emphasized by the drawn lines: the dotted line represents the actual position of the lamellae while the full line stands for the position the lamellae would have had if straight;
(b) Moiré pattern showing lamellar bending;
(c) transverse section of another faulted grain also showing curvature of the lamellae (x300)

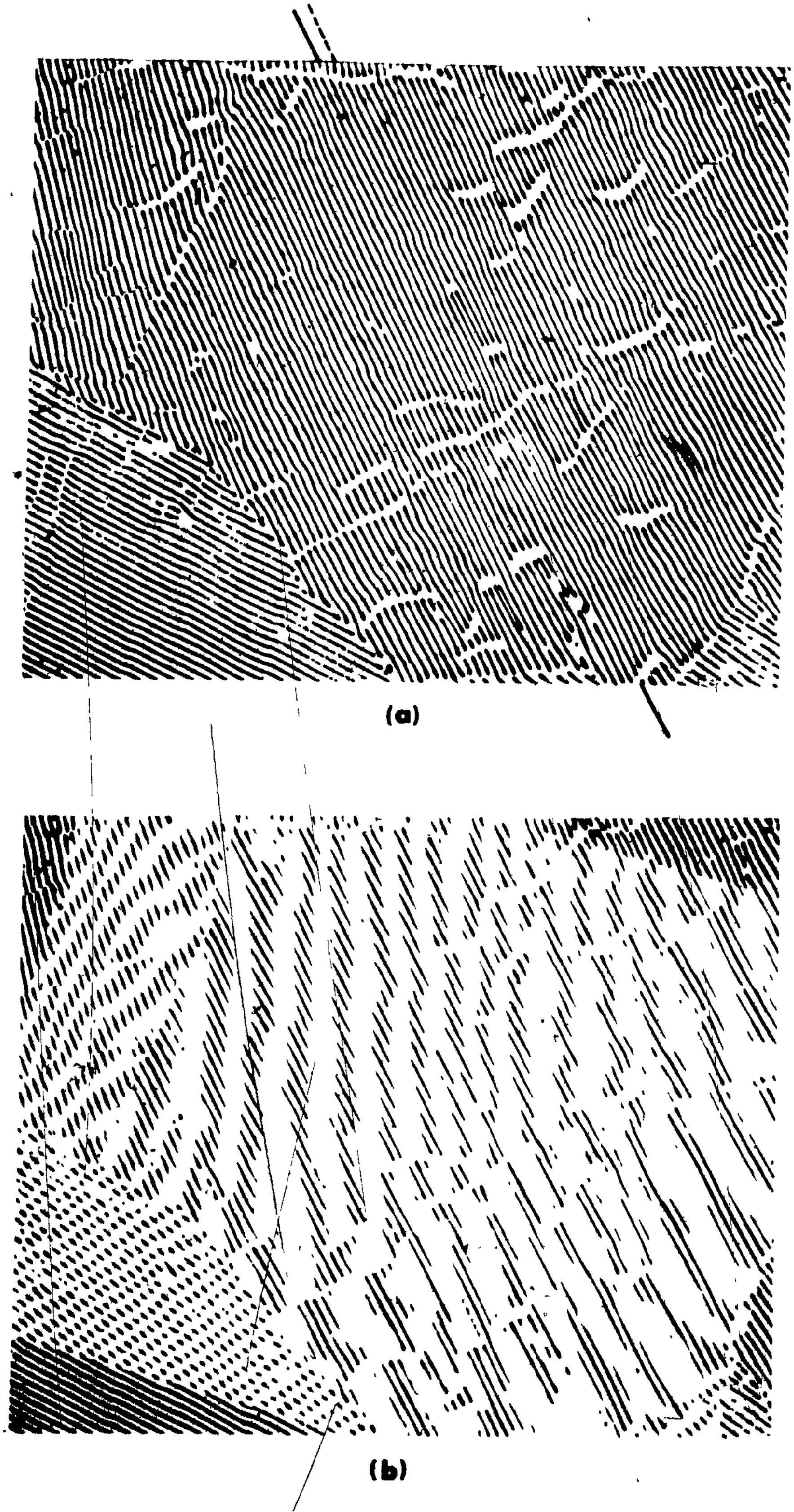
(a)
(b)

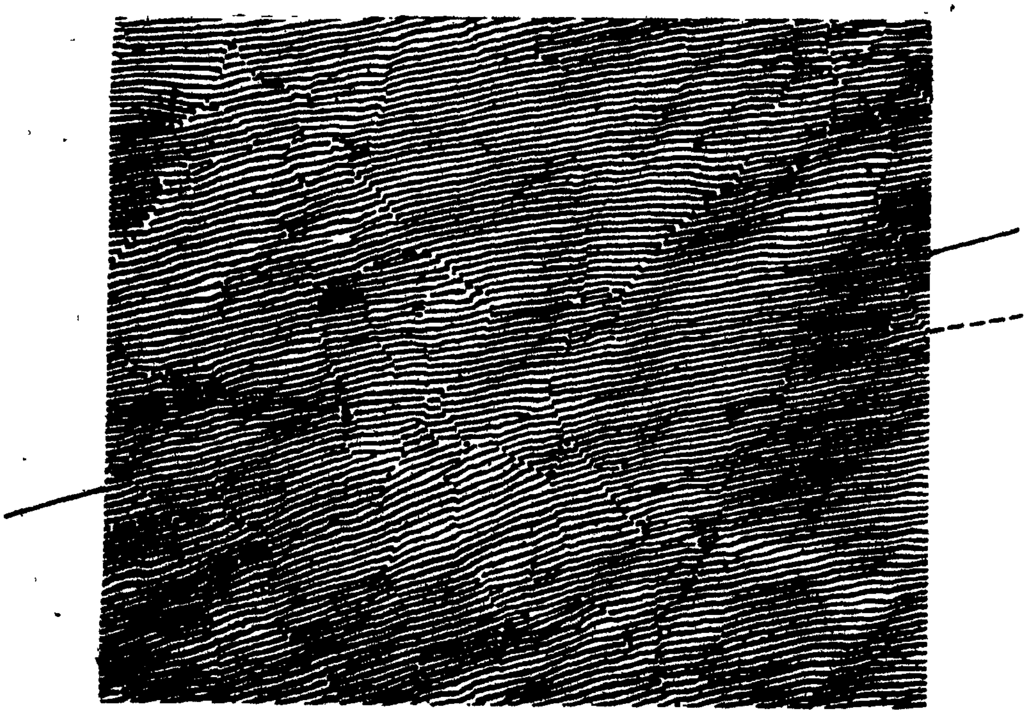

(c)

towards the adjacent Cd lamellae depending upon the freezing rate. As a consequence of this eutectoid reaction, the two eutectic phases assume different crystal structures, the Cd-rich phase remaining close packed hexagonal while the β phase becomes body centered tetragonal.

During the present work grains containing essentially no faults were found to grow adjacent to faulted grains as has been previously reported (Gruzleski and Winegard 1968). Specimens free of faults or with very low fault densities were produced by adopting the technique devised by Berthou and Gruzleski (1971). The method consisted of growing the first centimeter of the ingot very rapidly to induce the nucleation of as many grains as possible, thus increasing the probability of obtaining solid-solid interfaces of low energy. The remainder of the sample was then directionally frozen at a much lower rate to favour preferential growth of the most stable grains. Figure 3.2(a) shows the microstructure of a perfect grain as it appears on a section cut transverse to the growth direction.

The lamellae of perfect as well as faulted grains have been found to have a tendency to curve across transverse sections of any directionally solidified specimen. From this observation it might be deduced that the lamellar interphase boundary is curved rather than straight. Departures from parallelism in grains and subgrains can be detected on optical micrographs at relatively high magnifications (about 300x) by following any lamella for some distance as shown in Figures 3.1(a), 3.1(c) and 3.2(a). Here a lamella is selected and a continuous

FIGURE 3.2 Perfect Sn-Cd lamellar structure:
(a) transverse section (x400);
(b) perfect grid of appropriate spacing;
(c) Moiré pattern showing lamellar bending. Fringes are smoothly curved because of the absence of faults

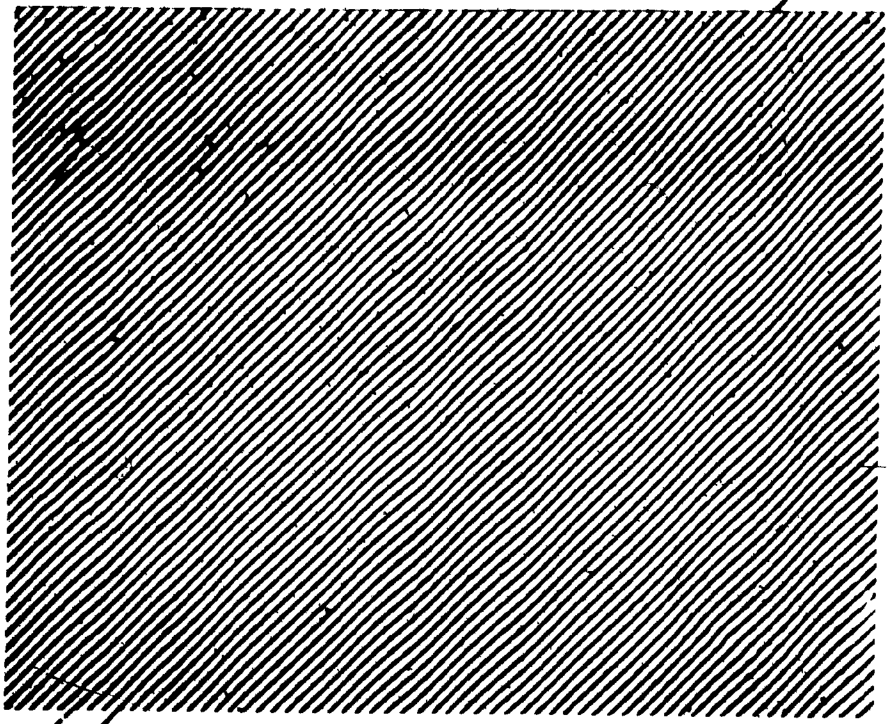

(a)

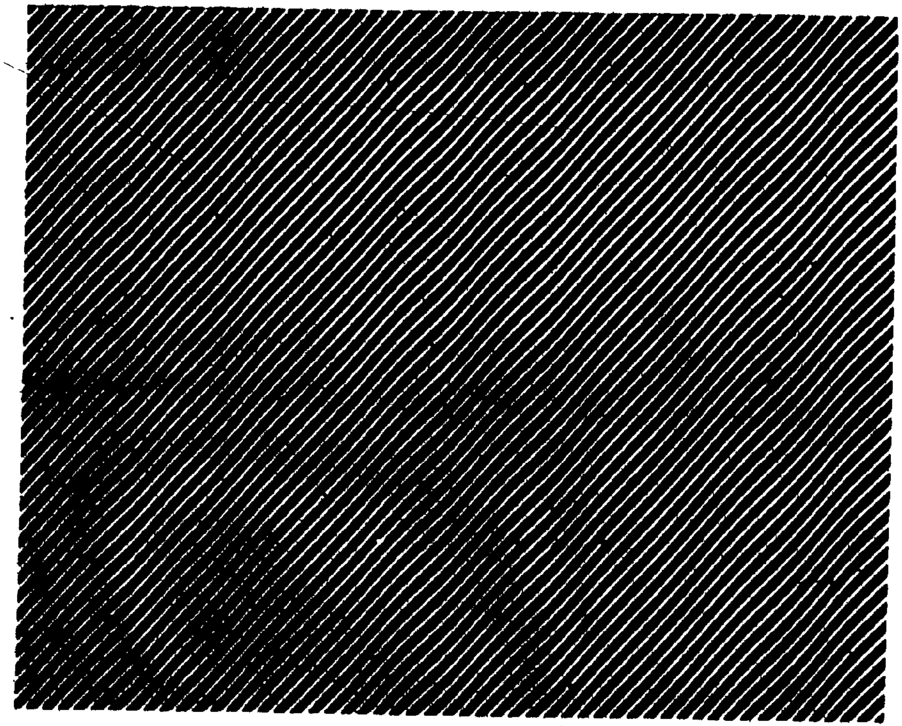

(b)

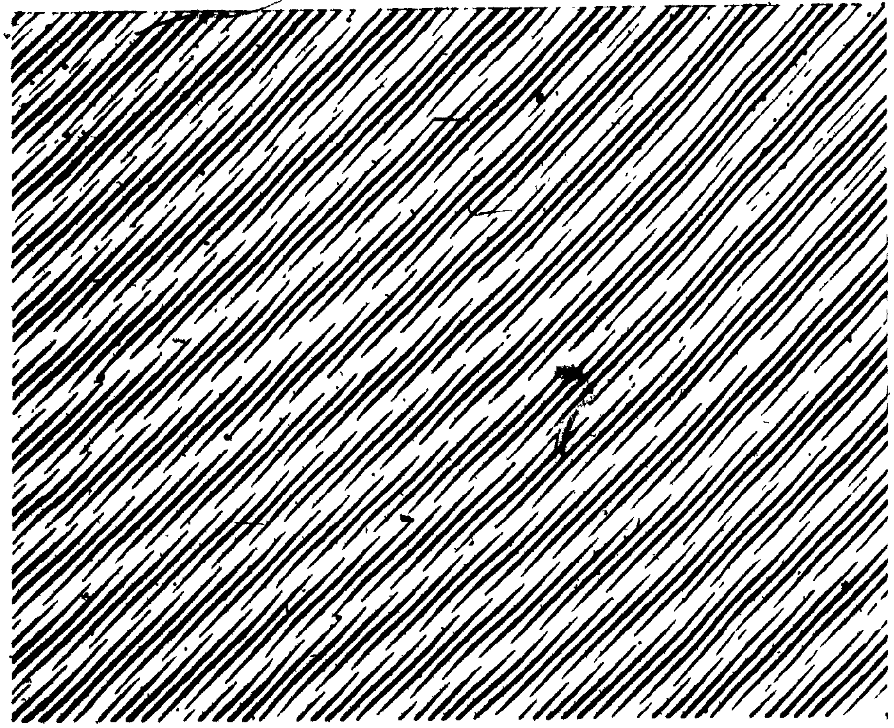

(c)

straight line is drawn coinciding with this lamella, and extending to the opposite side of the micrograph. It is seen that after some distance the lamella has bent away from the line. The deviation and new position of the lamella is indicated by the dotted line. It may be seen that the lamellae in Figures 3.1(a), 3.1(c) and 3.2(a) have rotated in a clockwise direction with respect to the lines drawn.

The bending effect can be directly detected without following the path of the lamellae by means of an interference technique described in the previous chapter. A perfect grid of spacing $B(b_w + b_b)$ is superimposed on the transverse micrograph whose spacing is $A(a_w + a_b)$ and a new grating is obtained of spacing $D(d_w + d_b)$, equal either to that of the micrograph, A, magnified by the factor $(A/B-1)^{-1}$ or to that of the perfect grating, B, magnified by the factor $(1-B/A)^{-1}$.

This effect is shown in Figure 3.2(c) which was obtained from the superposition of Figure 3.2(b) on Figure 3.2(a). The results are wide bundles called Moiré fringes and the bending of the lamellae is made very clear, the fringes being straight near the top of the figure and tending to curve as one moves to the bottom region. In Figures 3.1(b) and 3.2(c) the sense of the deviation is exactly the same as that shown in Figures 3.1(a) and 3.2(a), respectively, the bars of the perfect grid being overlapped on the bottom lamellae of Figure 3.1(a) and on the top right corner lamellae of Figure 3.2(a). In the case of the faulted lamellar Sn-Cd structure the bending effect in the Moiré patterns is less evident than in the case of the perfect morphology because of the discontinuity of the lamellae. The perfect grid superimposed on Figure 3.1(a) was not large enough to cover the entire field so that one can see the real structure at the corners of Figure 3.1(b). Regions containing subgrains and grains are shown in Figure 3.1(a) and because of the different orientation of the lamellae, the angle of intersection (see Section 2.5.2) increases and hence the Moiré fringes appear different (left side of Figure 3.1(b)).

3.1.2 Lead-Tin

From the phase diagram shown in Figure 2.1(c) it may be seen that the phases coexisting at the eutectic temperature (183°C) are solid solutions of Pb (19 wt.% Sn) and Sn (2.5 wt.% Pb). The eutectic point is at 61.90 wt.% Sn, the volume fractions of the two eutectic phases formed being approximately 63% Sn and 37% Pb (Hunt and Chilton 1962). The crystal structure of the Pb-rich phase is face-centred cubic although its lattice parameter is not accurately known. The lattice parameter of pure Pb is 4.9743 A^{o} at 183^{o}C according to Tyzack and Raynor (1954). They could not obtain data concerning the variation in the lattice parameter of Pb with Sn content above about 5% Sn due to the spontaneous decomposition of the high temperature solution at room temperature; however, they did observe a remarkable contraction of the Pb lattice with increasing Sn concentration. The crystal structure of the Sn-rich phase is body-centred tetragonal with lattice constants for the 2.5 wt.% Pb alloy at 183^{o}C being a = 5.8534 A^{o} and c = 3.2029 A^{o} (Lee and Raynor 1954).

The stable lamellar structure is shown on a transverse section in Figure 3.3(a), the Pb-rich phase appearing dark and the Sn-rich phase light. Under certain conditions the Pb-Sn lamellae tend to break down into wavy or degenerate lamellae instead of undergoing the lamellar-to-rod transition as observed in most lamellar structures (Hunt and Chilton 1962; Hunt 1963). During the present work this degenerate structure (Figure 3.4(a)) was observed at the beginning of the directionally solidified ingots, usually during the first two centimeters of growth, although stable lamellar grains were often found to have grown adjacent to degenerate ones as shown in Figure 3.4(b). Generally, the wavy lamellar grains tended to disappear after a few centimeter of growth even if a few persisted for longer distances. Only degenerate grains were produced in a sample grown at 11 cm/hr. under a temperature gradient of 5.5°C/cm., these grains persisting throughout the ingot. The reason for this behaviour is thought to be related to the fact that the volume fractions of the two phases are nearly equal.

Moiré fringes obtained for a stable Pb-Sn lamellar structure are shown in Figure 3.3(b) indicating that the lamellae were bent across the transverse section. The continuous and dotted lines indicate the magnitude and sense of the lamellar deviation (Figure 3.3(a)), the sense not being the same as that obtained by the interference technique (Figure 3.3(b)). It should be noted that the bending effect is best detected when a moderate magnification is used; in the present work a magnification of x300 was adequate. No Moiré patterns could be obtained for the wavy lamellae (Figure 3.4(b)) because of the structural degeneracy.

FIGURE 3.3 Stable Pb-Sn lamellar structure:
(a) transverse section (x300);
(b) Moiré pattern showing lamellar bending

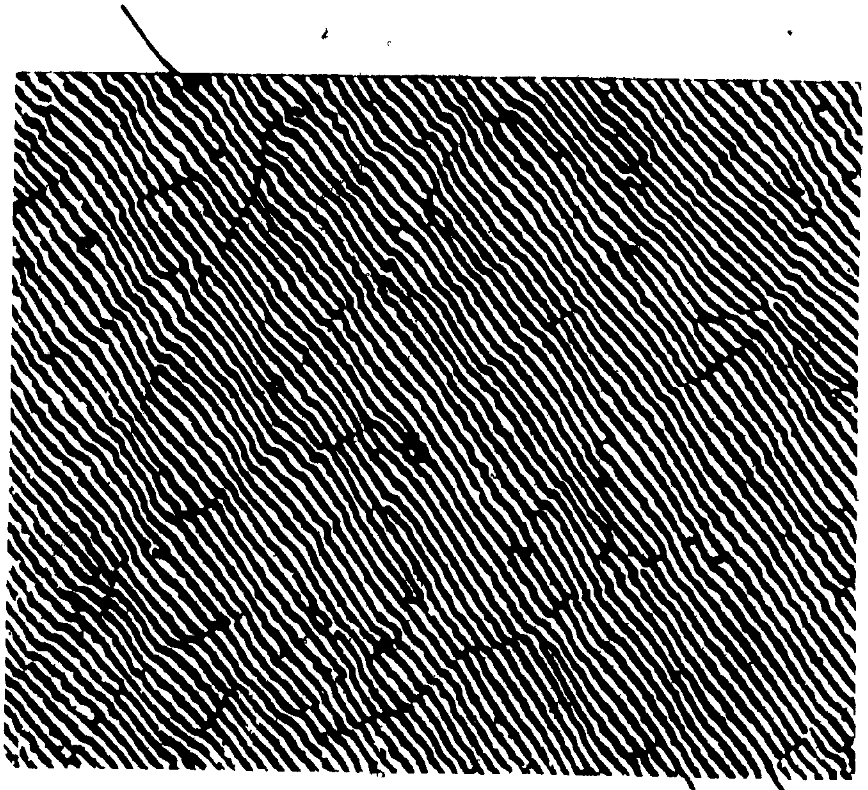

(a)

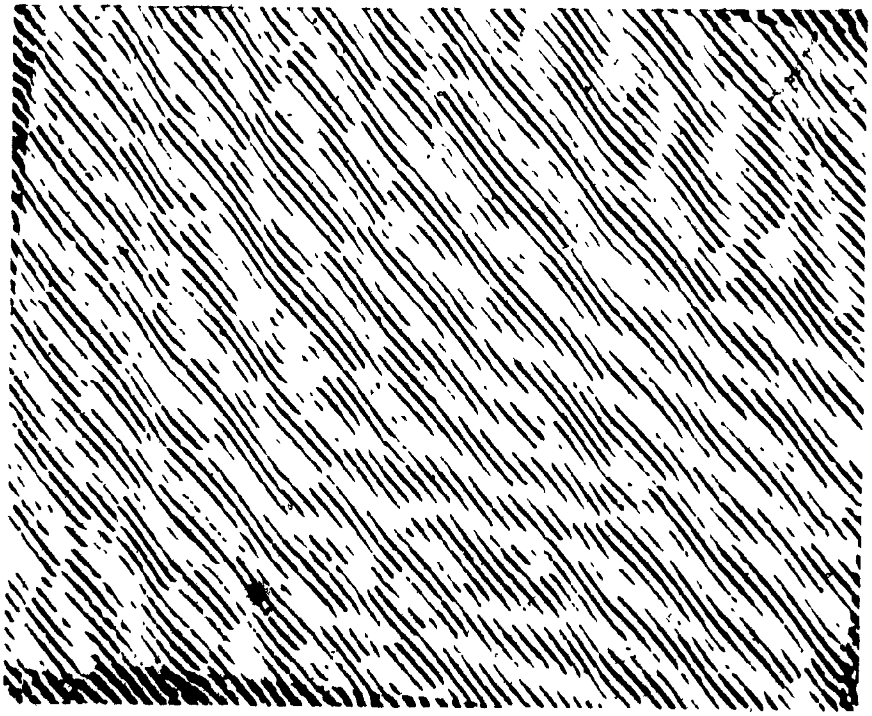

(b)

FIGURE 3.4 Degenerate Pb-Sn structure:
(a) transverse section (x300);
(b) stable lamellar grain growing adjacent to degenerate grains (x300)

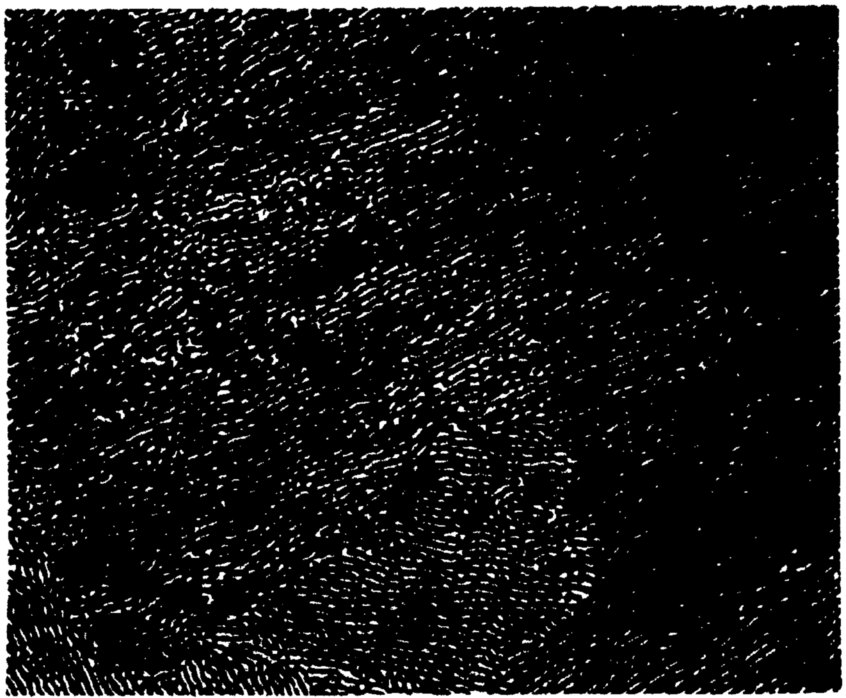

(a)

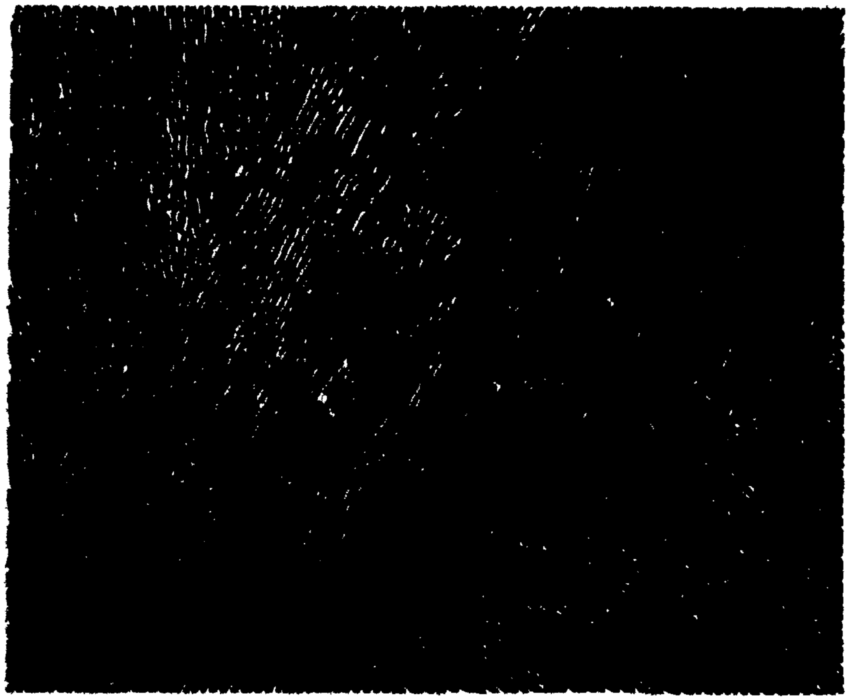

(b)

3.1.3 Cadmium-Zinc

The eutectic reaction occurs at 266°C yielding a Cd-rich phase containing 2.58 wt.% Zn and a Zn-rich phase consisting of 1.93 wt.% Cd. The eutectic composition is 82.6 wt.% Cd (Figure 2.1(b)), the Zn-rich phase having a volume fraction of 17% (Hunt and Chilton 1962). The microstructure on a transverse section of a directionally frozen sample is shown in Figure 3.5(a), the Cd lamellae appearing dark and the Zn lamellae light. The crystal structure of both the Cd-rich and Zn-rich phases is close packed hexagonal ($a_{Zn} = 2.664$ A^{o}, $c_{Zn} = 4.945$ A^{o} and $a_{Cd} = 2.9787$ A^{o}, $c_{Cd} = 5.617$ A^{o} for the pure metals at 20^{o}C) (Barrett 1952).

Instability in the Cd-Zn system during growth leads to a breakdown of the Zn-rich lamellae into rods (Hunt and Chilton 1962; Hunt 1963). This is evident at subgrain boundaries in Figure 3.5(c). Despite the fact that the two solid phases are crystallographically similar as was the case for the Sn-Cd eutectic, fault-free grains could not be obtained even with the technique devised by Berthou and Gruzleski (1971).

Lamellar bending was also observed in this system and is magnified by the Moiré fringes of Figure 3.5(b).

FIGURE 3.5 Cd-Zn lamellar structure:
(a) transverse section (x300);
(b) Moiré pattern showing lamellar bending;
(c) beginning of structural breakdown along grain boundaries (x250)

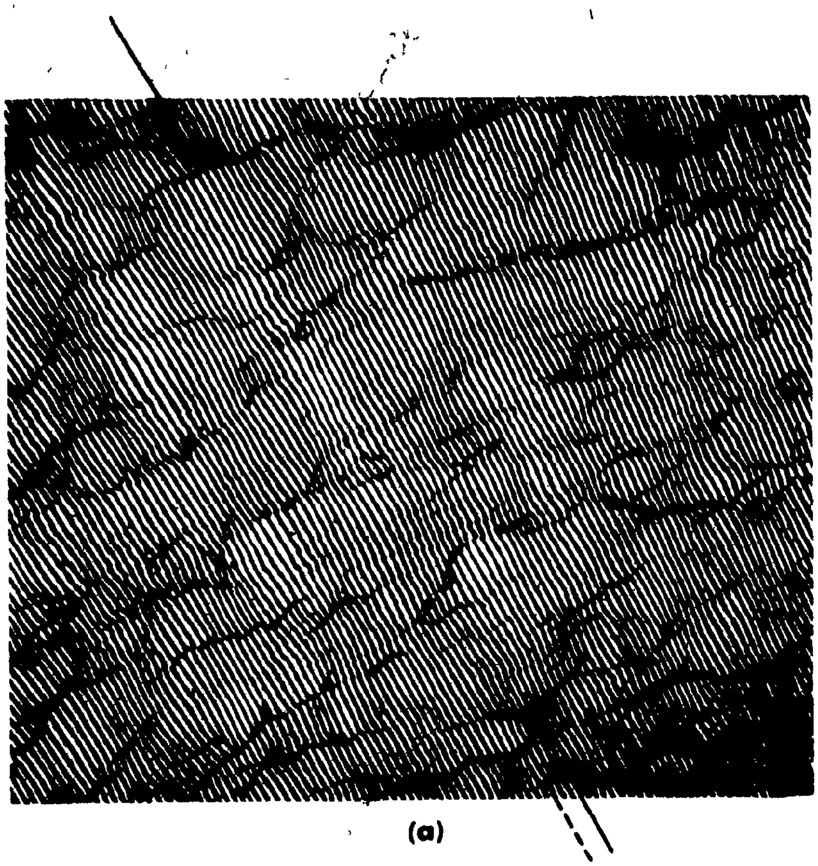

(a)

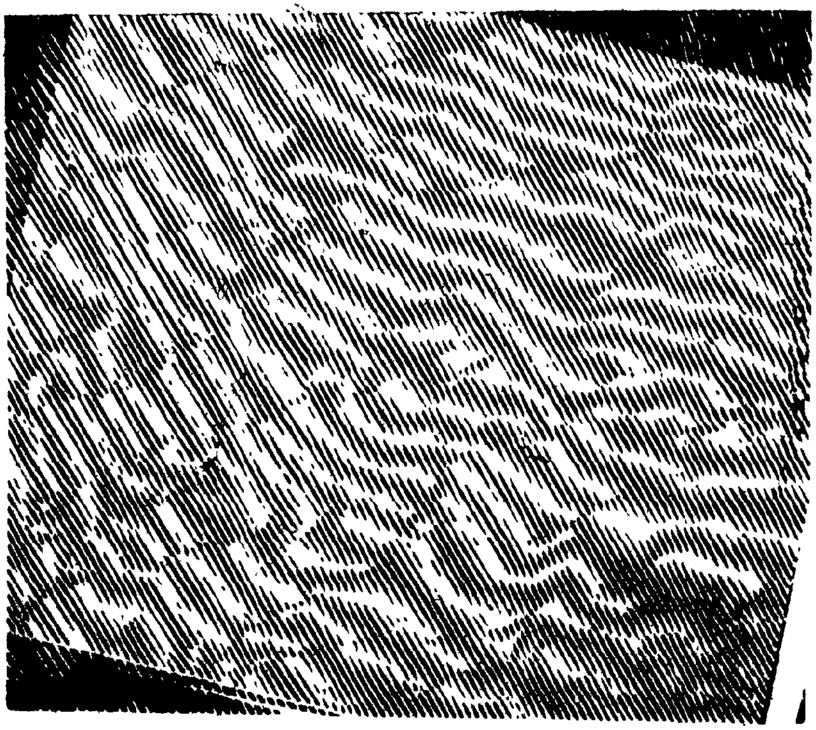

(b)

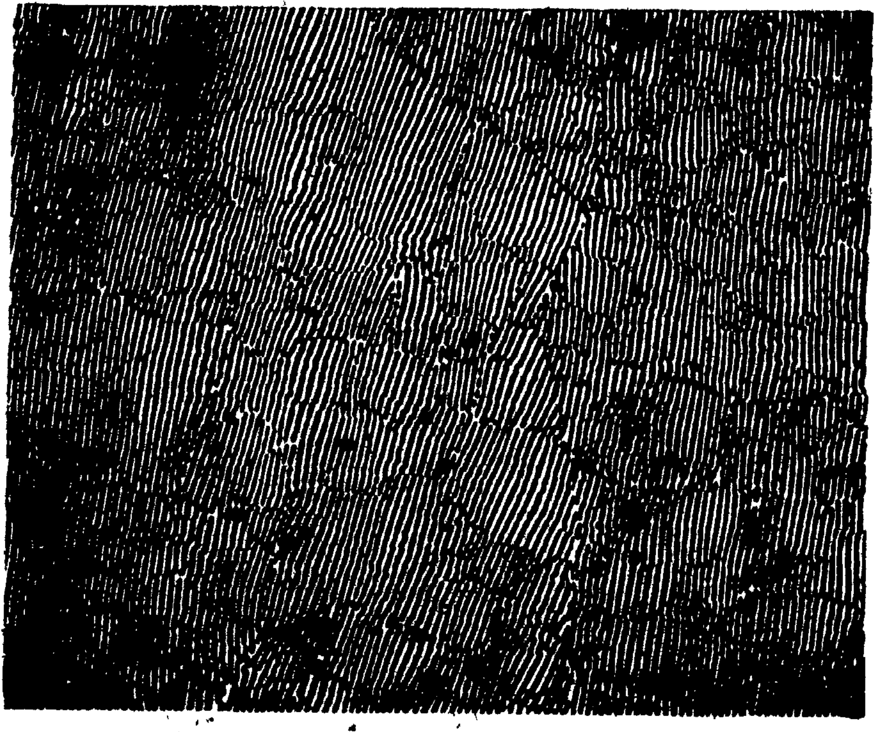

(c)

3.1.4 Tin-Zinc

The Sn-Zn eutectic reaction occurs at a temperature of 198°C and a composition of 8.9 wt.% Zn yielding solid solutions of Zn (.1% Sn) and of Sn (1.7 wt.% Zn) (see Figure 2.1(d)). The volume fraction of the Zn-rich phase is very low and amounts to only 9% (Hunt and Chilton 1962). For this reason the Zn-rich lamellae (dark-etching) have a tendency to be discontinuous or broken as shown in Figure 3.6(a). The two solid phases are crystallographically dissimilar, Sn being body-centred tetragonal and Zn close packed hexagonal. It is believed by certain authors (Taylor et al. 1964) that the Zn-rich phase assumes the form of sheets containing regularly spaced holes although more recently it has been reported to be ribbon-like (Southin and Jones reported by Jaffrey and Chadwick 1969, p.118). When the system is rapidly solidified the Zn-rich phase grows with a fibrous morphology (Taylor et al. 1964; Moore 1967) making the Sn-Zn one of the few systems that exhibit a natural lamellar-to-fibrous transition.

Faults were found to be present in all grains from the beginning to the end of each sample but unlike the other systems studied, the lamellae were observed to be straight across transverse sections as shown in Figures 3.6(a) and 3.6(b).

FIGURE 3.6 Sn-Zn lamellar structure:
(a) transverse section (x400);
(b) Moiré pattern showing the straightness of the lamellae

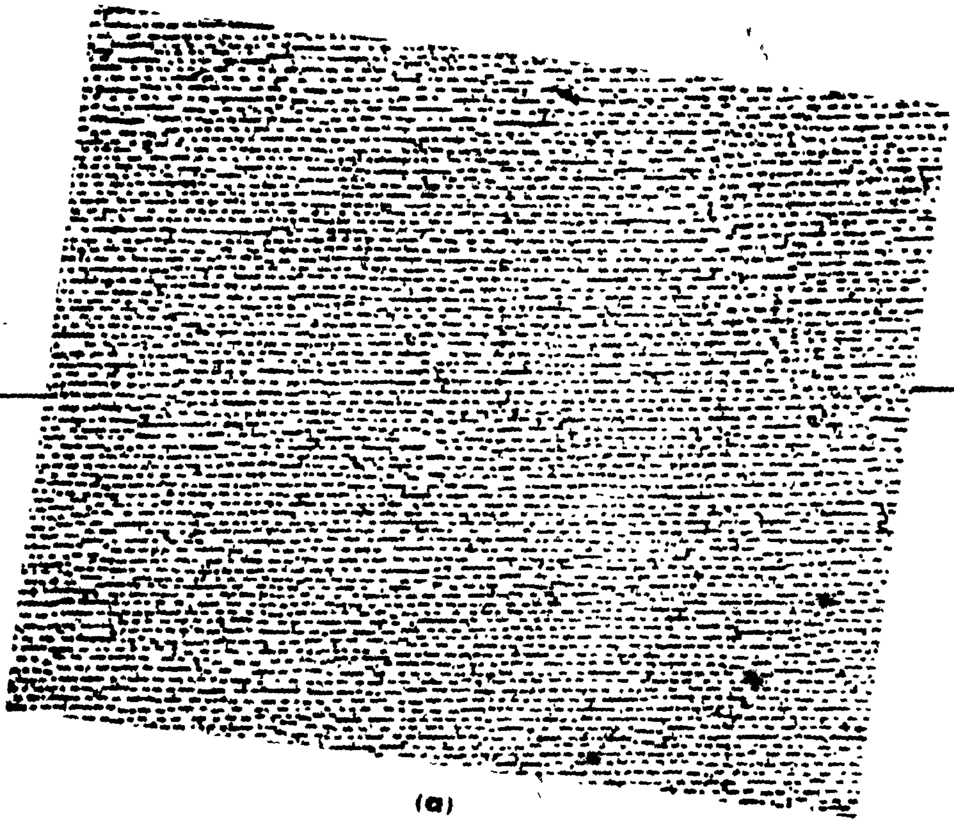

(a)

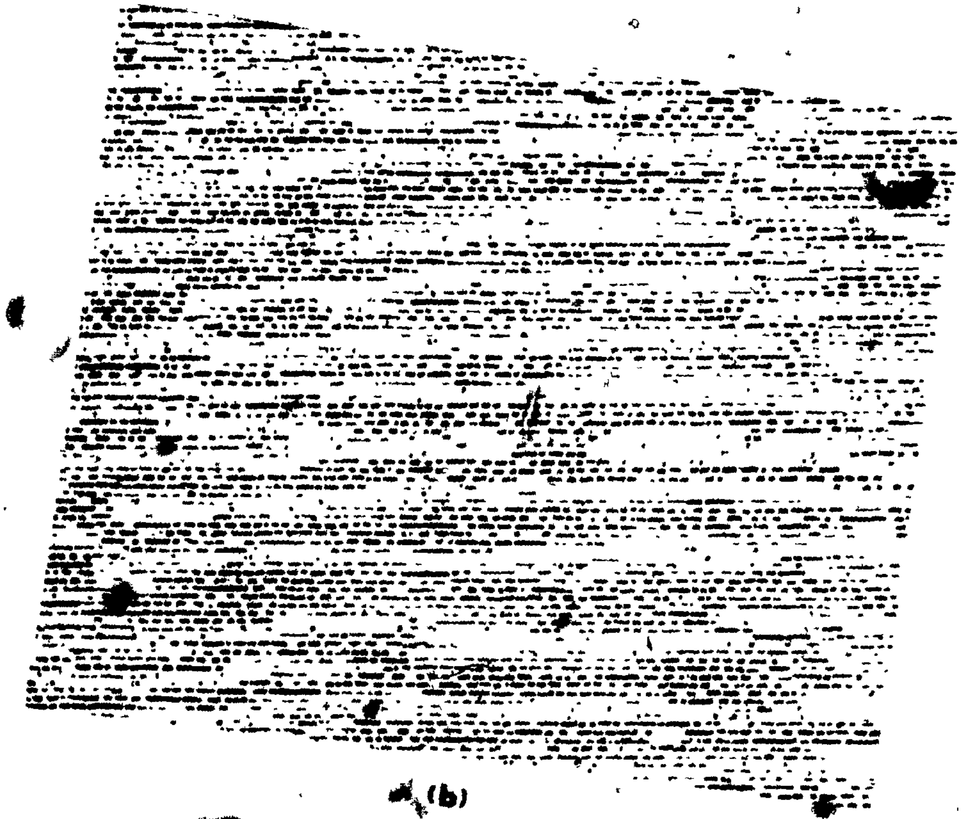

(b)

3.2 LAMELLAR SPIRALLING

3.2.1 Tin-Cadmium

Lamellar spiralling in the Sn-Cd system was investigated in four specimens grown under different freezing conditions as shown in Table 3.1.

TABLE 3.1 Growth Conditions used for Sn-Cd Specimens

Sample #	R(cm/hr)	G(^{o}C/cm)	Remarks
A1	15.0 - 3.1	12.5	varying R - perfect structure
A2	2.7	7.4	constant R - faulted structure
A3	15.0	3.7	constant R - faulted structure
A4	1.3	8.0	constant R - faulted structure

The technique devised for measuring lamellar spiralling has been explained previously. Briefly the method consisted of a comparison of the mean orientation of each grain from section to section along the length of the sample. Circular graphs were constructed by plotting the average lamellar orientation of each grain along the circumference of the circle versus distance along the growth direction plotted on the diameter of the circle.

The first centimeter of sample A1 was grown at 15.0 cm/hr., the furnace speed then being lowered to 3.1 cm/hr. for the remainder of the ingot. With this method essentially fault-free grains were obtained (Figure 3.2(a)). Two grooves instead of one were then carved along the length of the sample as shown on the right hand side of Figure 3.7 and lamellar orientation measurements were taken twice on each section following paths at right angles to one another, one starting from groove A and the other from groove B. This was done only on one sample to ensure that the lamellar behaviour was the same throughout the specimen.

Figure 3.7 is a plot of average grain orientation versus growth distance. In the upper and lower semicircles are plotted the lamellar orientation of grains detected during motion along the reference line extending from the apex of each groove to the opposite side of the section. At the beginning of the sample the total number of grains encountered was eight and after about 4 cm. of growth this was reduced to five. It is evident from Figure 3.7 that the mean lamellar orientation of each grain along the sample was reasonably constant implying that the lamellae did not spiral.

Similar measurements were carried out on sample A2 containing faulted grains (Figure 3.1(a)). The average lamellar orientations versus solidified distance are plotted in Figure 3.8 for three eutectic grains which intersected the reference line. The mean orientation of the three faulted grains remained roughly constant from one end of the

FIGURE 3.7 Plot of lamellar orientations from the beginning (S) to the end (E) of a directionally frozen Sn-Cd sample containing perfect grains (R = 15.0 - 3.1 cm/hr, G = 12.5°C/cm)

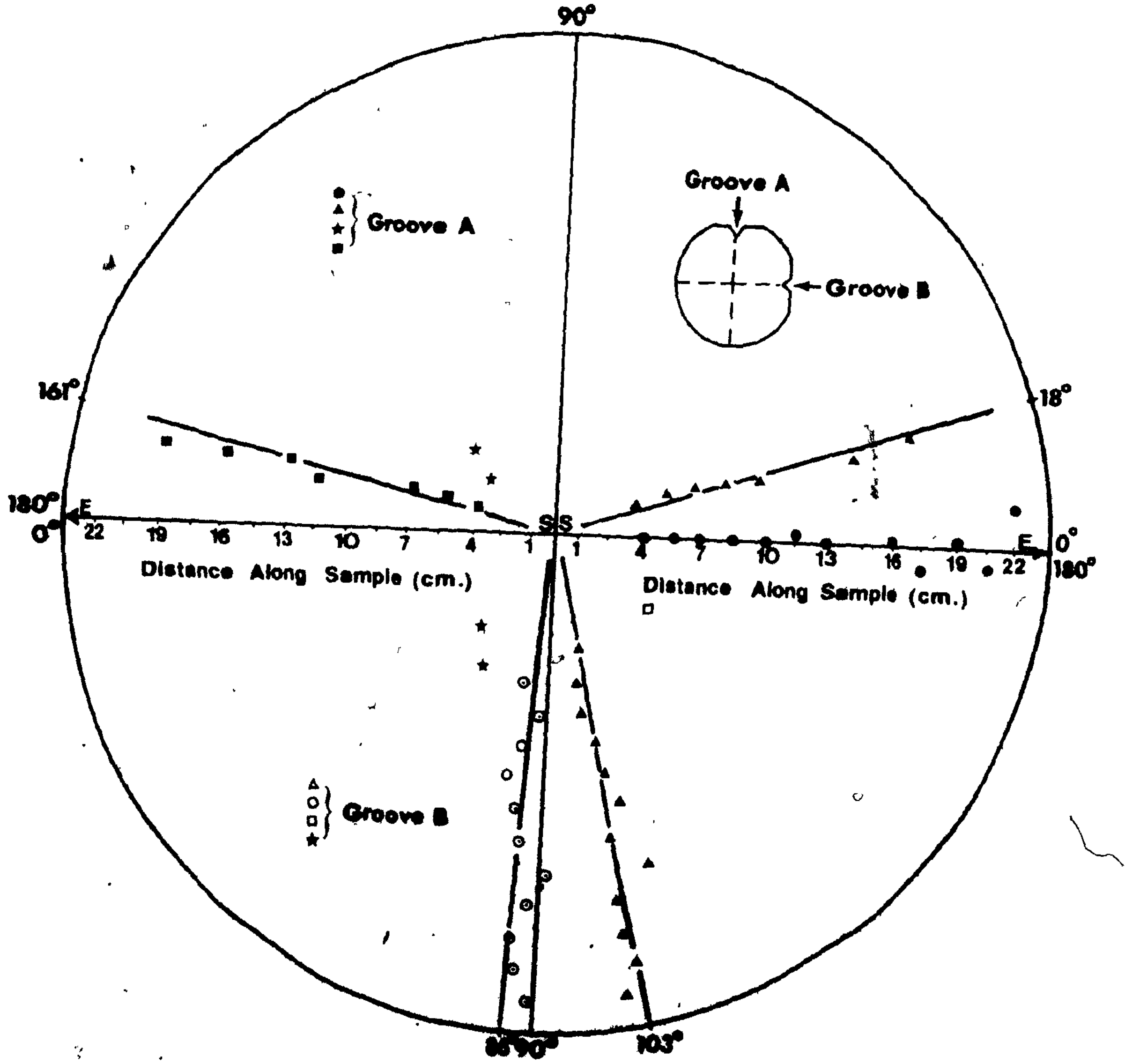
90°
Groove A
Groove B
Groove A
Groove B
161°
18°
180°
0°
E
22
19
16
13
10
7
4
1
S
S
1
4
7
10
13
16
19
22
E
0°
180°
Distance Along Sample (cm.)
Distance Along Sample (cm.)
86°
90°
103°

FIGURE 3.8 Plot of lamellar orientations as a function of solidification distance for a directionally frozen Sn-Cd sample containing faulted grains (R = 2.7 cm/hr, G = 7.4°C/cm)

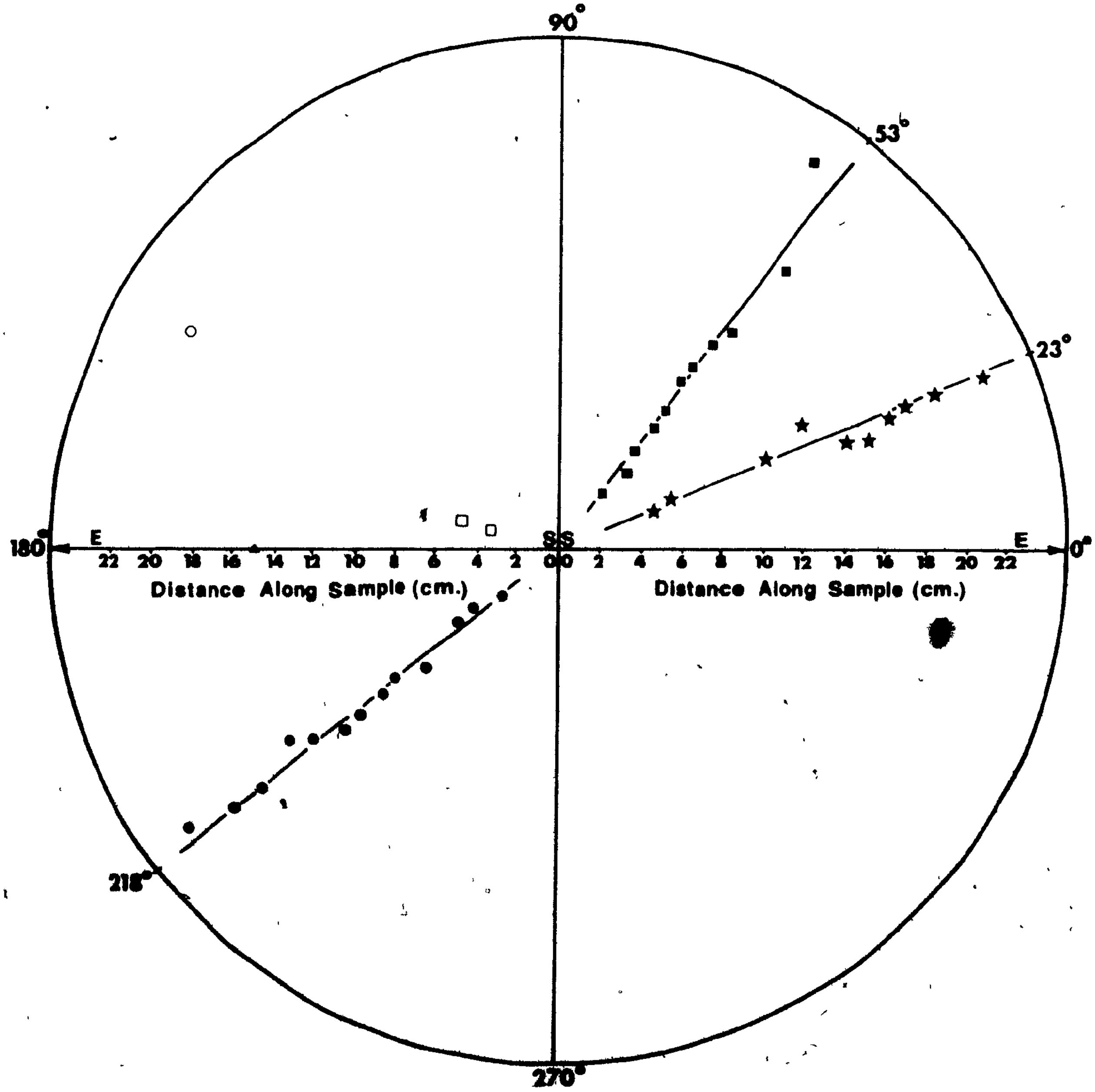
90°
53°
23°
180°
0°
218°
270°
E
S S
E
22 20 18 16 14 12 10 8 6 4 2 0
0 2 4 6 8 10 12 14 16 18 20 22
Distance Along Sample (cm.)
Distance Along Sample (cm.)

directionally solidified sample to the other. Two additional samples were directionally solidified under different freezing conditions (samples A3 and A4 in Table 3.1) and again no twisting was detected as may be seen from the results plotted in Figures 3.9 and 3.10.

To conclude this section on the Sn-Cd eutectic, no spiralling was observed in either perfect or faulted grains. To the author's knowledge this is the first system in which spiralling has been searched for and not found (Section 3.2.4 reports on a second system, Sn-Zn, which also failed to exhibit lamellar spiralling).

3.2.2 Lead-Tin

Spiralling in the Pb-Sn eutectic was studied previously by Hopkins and Stewart (1970) who measured the rate of lamellar rotation in specimens grown both by the Czochralski and Bridgeman techniques. During the present investigation the spiralling rate was determined in sample B1 (Table 3.2) grown under conditions similar to those used by Hopkins and Stewart. This was done for the purpose of comparing the results of this work with published results as a check on the experimental technique. Lamellar spiralling measurements in Pb-Sn were made on two samples frozen under the conditions shown in Table 3.2. The regular lamellar structure was obtained in sample B1 (Figure 3.3(a)) while sample B2 contained only degenerate grains (Figure 3.4(a)) which persisted throughout the directionally solidified ingot. It should be noted that Pb-Sn samples tend to solidify with large grain sizes, so

FIGURE 3.9 Plot of lamellar orientations as a function of solidification distance for a directionally frozen Sn-Cd sample (23 cm. long) containing faulted grains (R = 15.0 cm/hr., G = 3.7°C/cm)

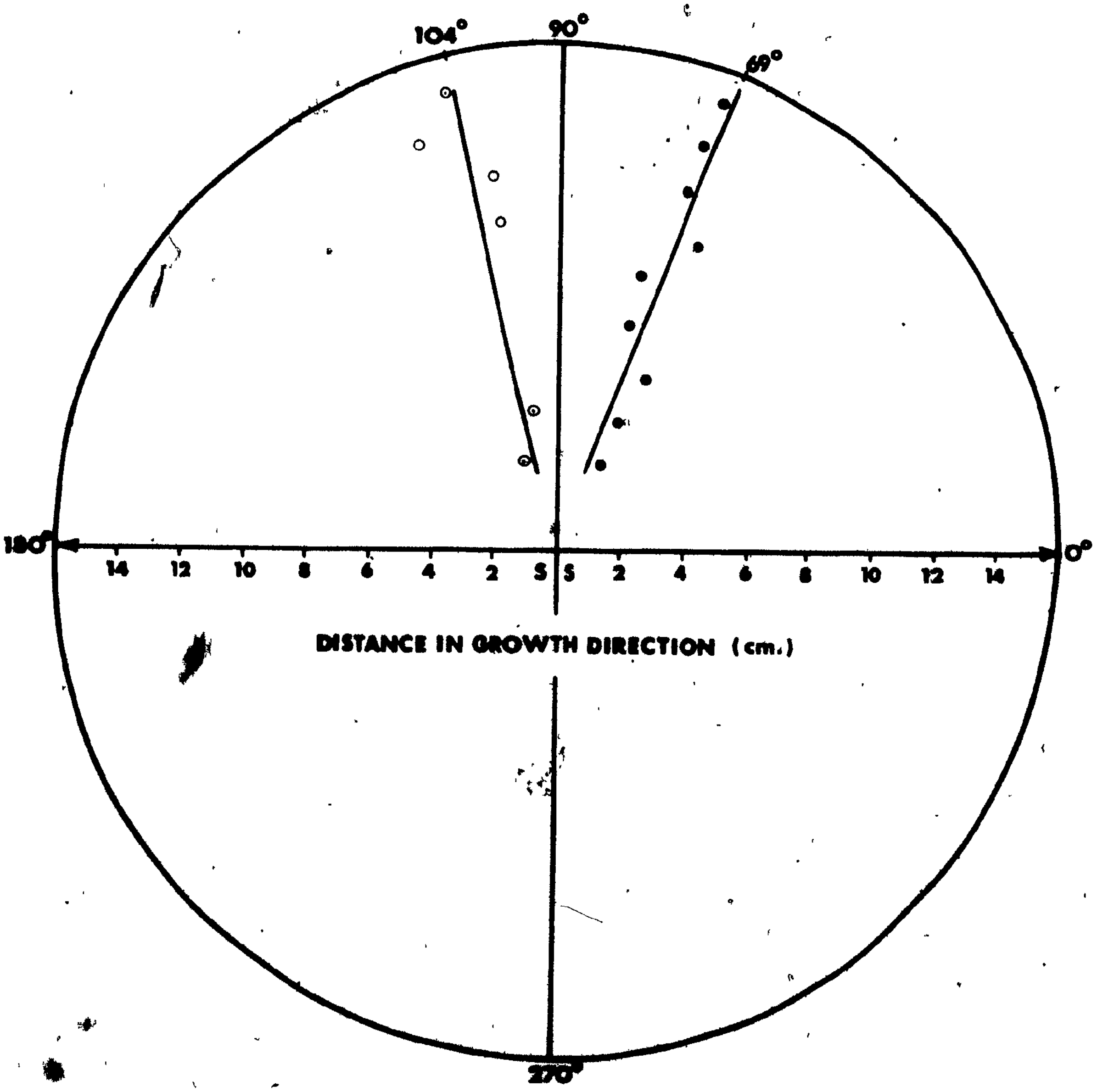

104°
90°
69°
180°
0°
270°
14
12
10
8
6
4
2
S
S
2
4
6
8
10
12
14
DISTANCE IN GROWTH DIRECTION (cm.)

FIGURE 3.10 Plot of lamellar orientations as a function of solidification distance for a directionally frozen Sn-Cd sample (23 cm. long) containing faulted grains (R = 1.3 cm/hr., G = 8.0°C/cm)

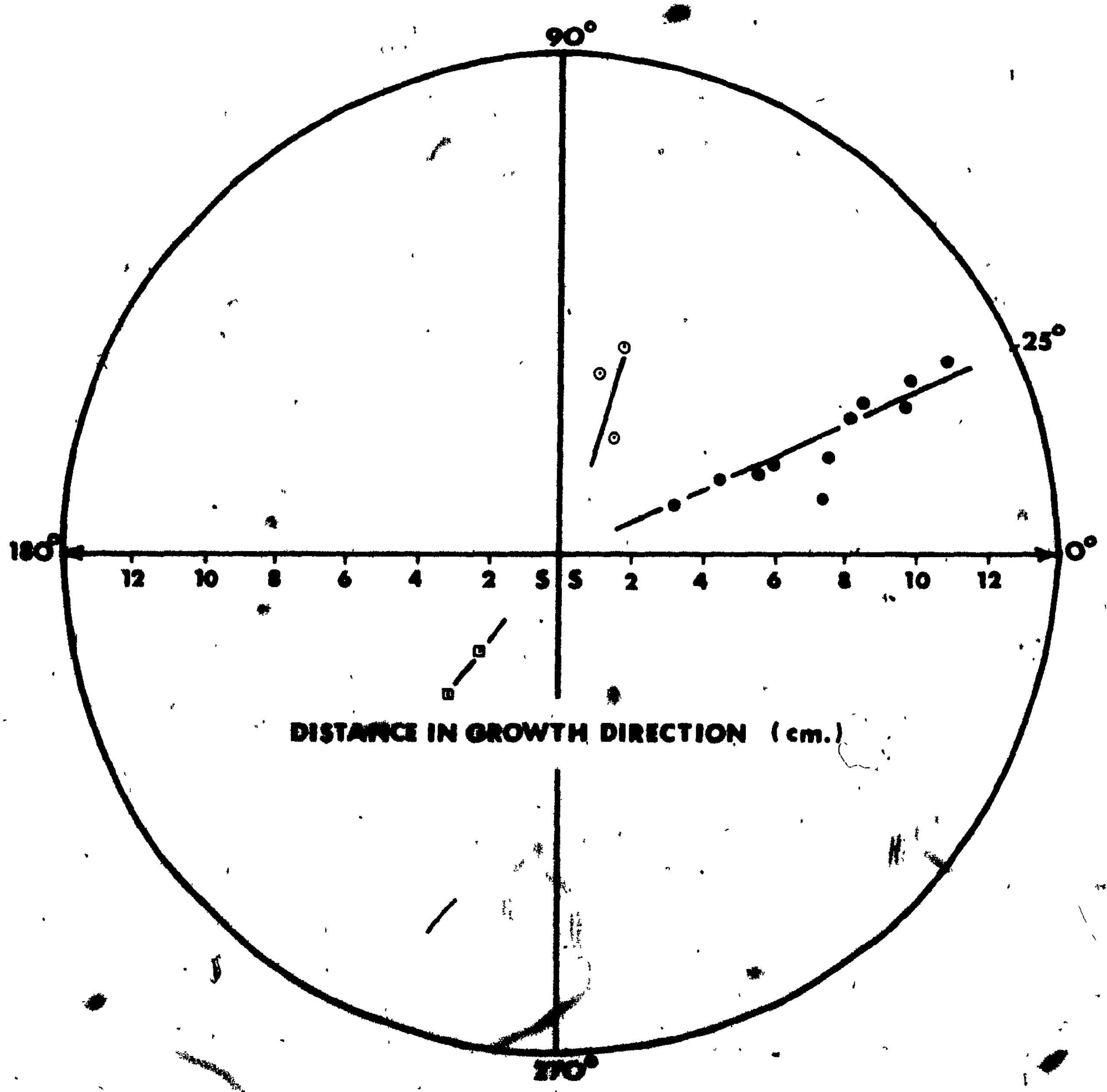
90°
25°
180°
0°
12
10
8
6
4
2
S
S
2
4
6
8
10
12
DISTANCE IN GROWTH DIRECTION (cm.)
270°

TABLE 3.2 Growth Conditions used for Pb-Sn Specimens

Sample #	R(cm/hr)	G(^{o}C/cm)	Remarks
B1	2.3	7.1	lamellar structure
B2	11.0	5.5	degenerate structure

that in comparison to the other systems studied, the number of grains is quite small. In fact, in sample B1 only two grains were nucleated and both persisted during growth indicating that both were quite stable.

The spiralling of grain (1) is shown in Figure 3.11(a) and that of grain (2) in Figure 3.11(b). Although the rate of lamellar rotation was found to be constant for both grains, the sense of rotation was not: the lamellae of the first grain rotated in a clockwise sense, while those of grain (2) rotated in a counterclockwise sense. The progressive variation of the lamellar traces in both grains is shown in Figure 3.12. The rate of spiralling was obtained from the slope of the straight lines and was found to be about 160^{o}/cm, the negative slope of the line corresponding to grain (2) implying a counterclockwise rotation in that grain. The results obtained by Hopkins and Stewart (1970) for a Pb-Sn sample directionally frozen by the Bridgeman technique at 2.6 cm/hr. are also included in Figure 3.12. The previously reported results were found to be roughly comparable with the present results with the exception that the two grains present in the sample of Hopkins and co-worker (1970) both rotated in the same sense. It has previously been shown for the

FIGURE 3.11 Variation of lamellar orientations with solidification distance for a directionally frozen Pb-Sn sample (R = 2.3 cm/hr, G = 7.1°C/cm):
(a) grain (1);
(b) grain (2)

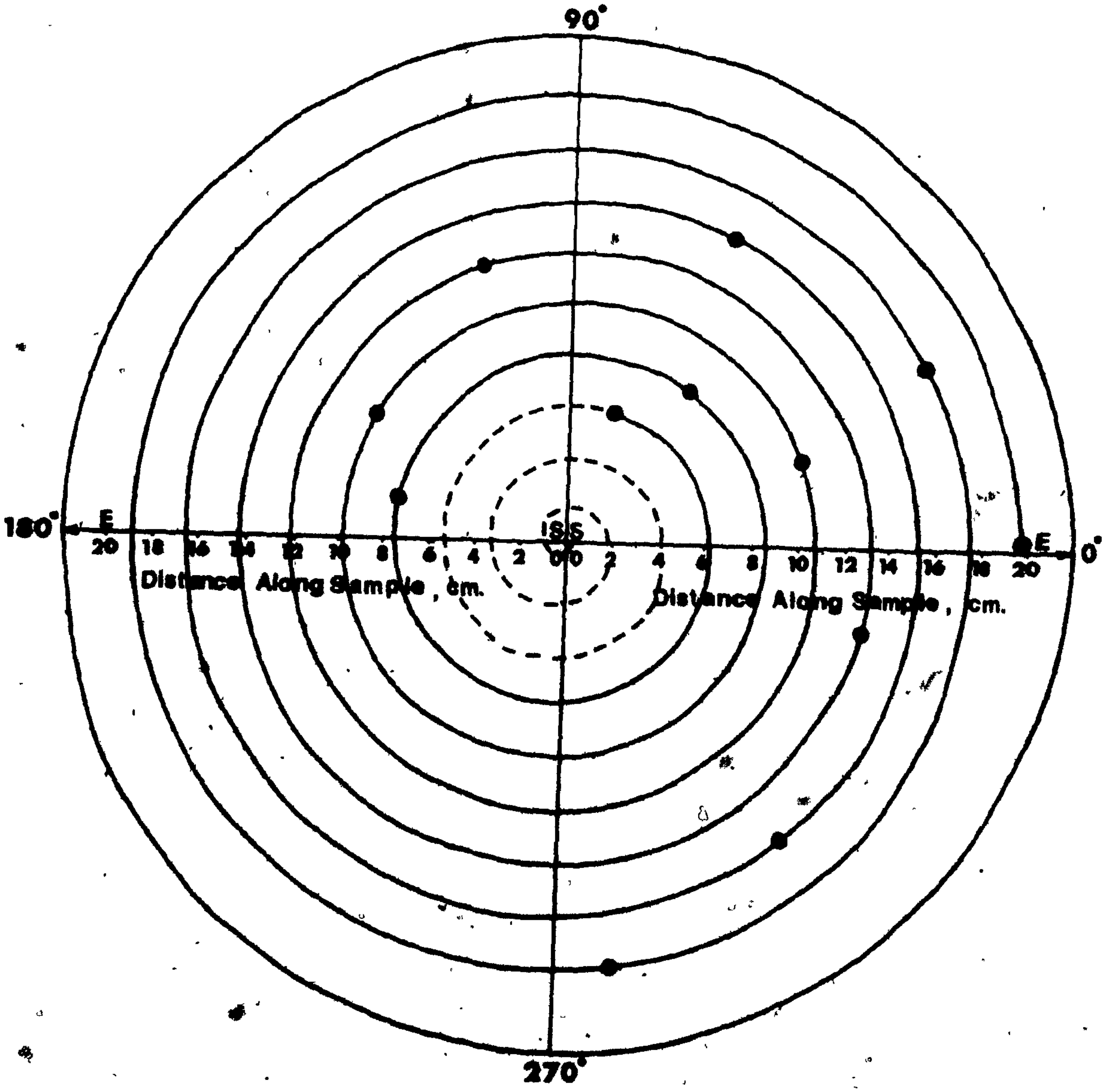

90°
180°
0°
270°
E
E
ISS
20 18 16 14 12 10 8 6 4 2 0
0 2 4 6 8 10 12 14 16 18 20
Distance Along Sample, cm.
Distance Along Sample, cm.

(a)

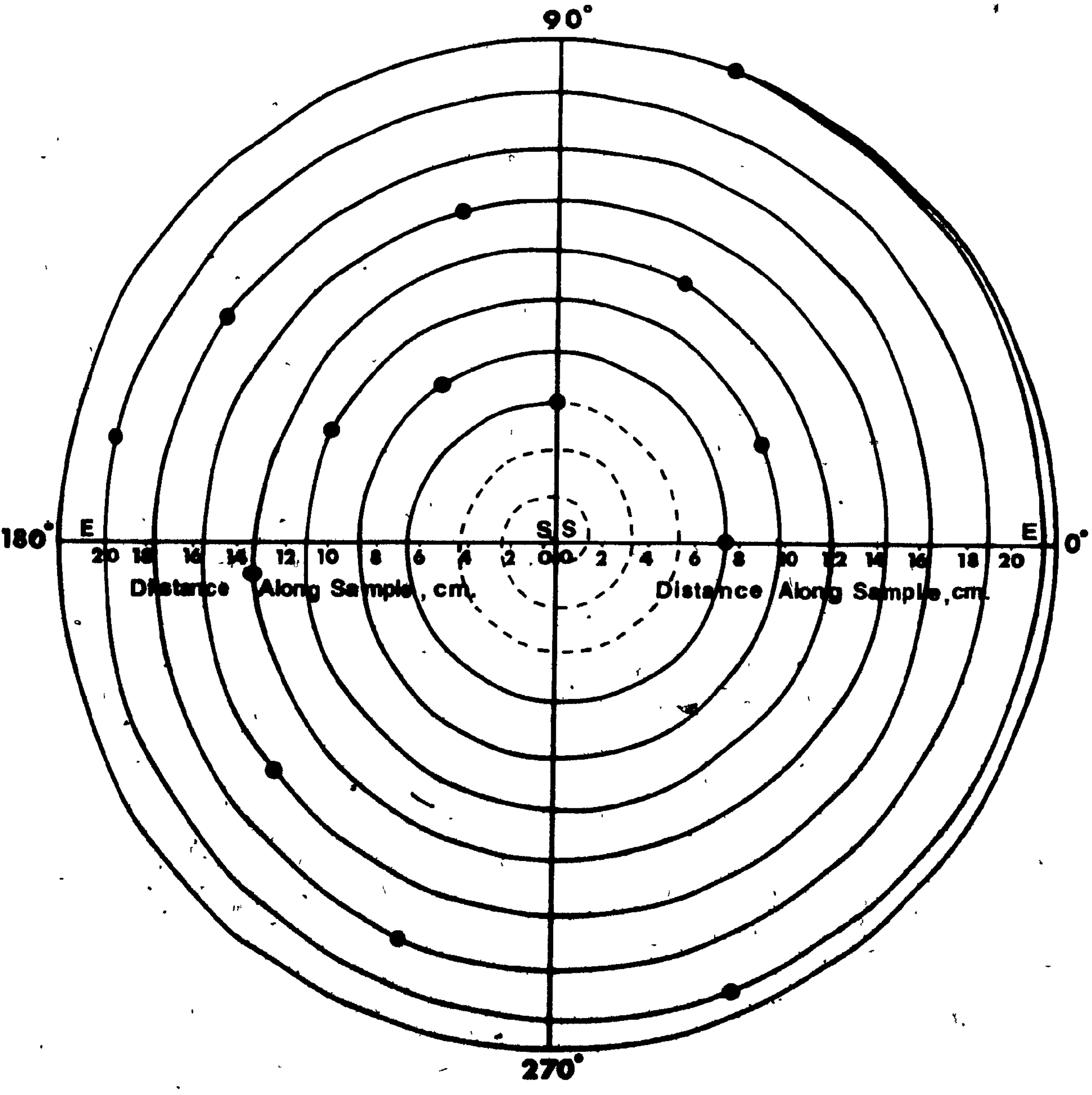

90°
180°
0°
270°
E
E
S S
20 18 16 14 12 10 8 6 4 2 0
0 2 4 6 8 10 12 14 16 18 20
Distance Along Sample, cm.
Distance Along Sample, cm.

(b)

FIGURE 3.12 Cumulative variation of lamellar orientations with solidification distance for a directionally frozen Pb-Sn sample ($R = 2.3$ cm/hr, $G = 7.1^{\circ}C/cm$)

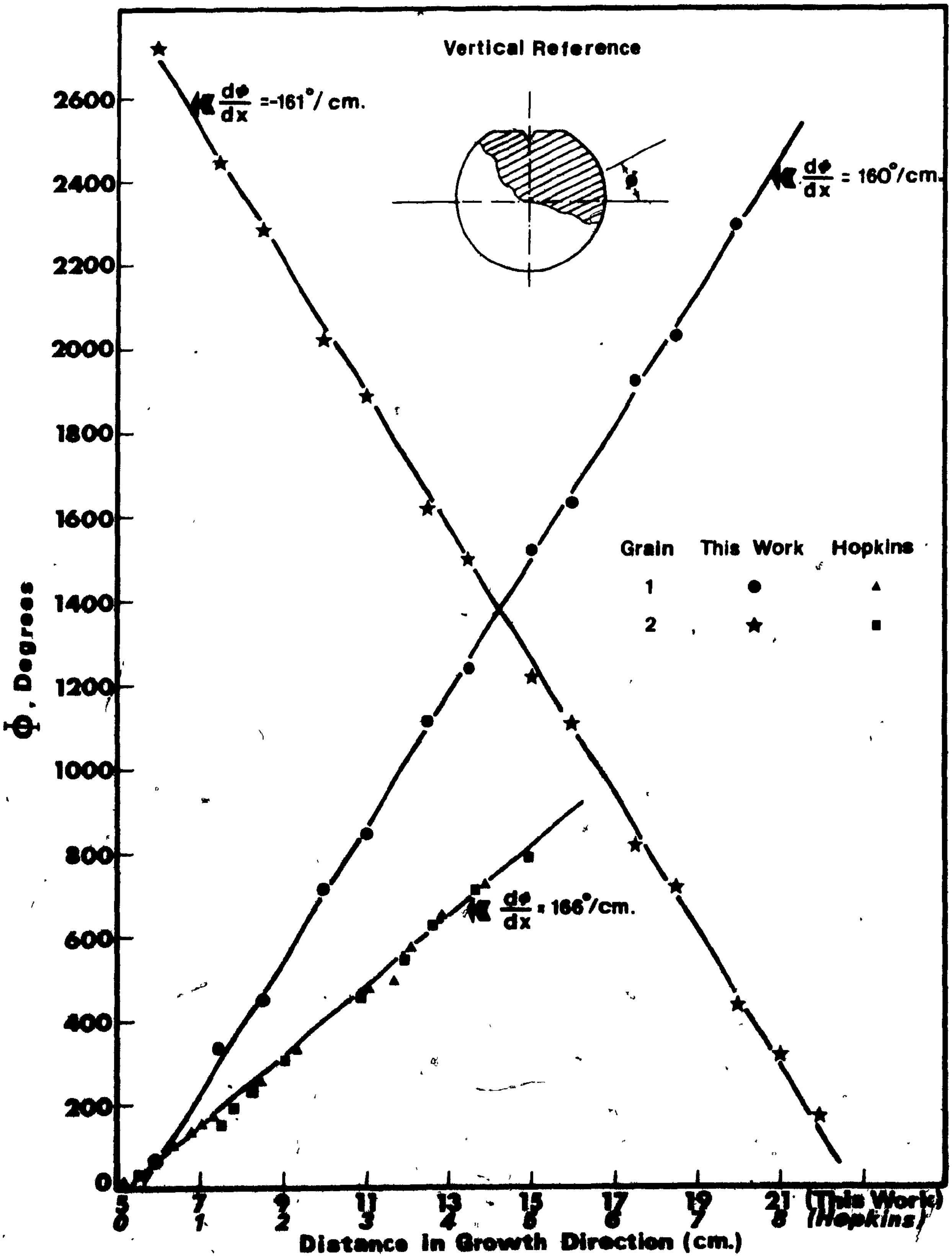
Vertical Reference
φ
dφ/dx = -161°/cm.
dφ/dx = 160°/cm.
dφ/dx = 166°/cm.
Grain
This Work
Hopkins
1
●
▲
2
★
■
φ, Degrees
0
200
400
600
800
1000
1200
1400
1600
1800
2000
2200
2400
2600
5
7
9
11
13
15
17
19
21
(This Work)
0
1
2
3
4
5
6
7
8
(Hopkins)
Distance in Growth Direction (cm.)

Al-Zn eutectic (Double et al. 1968) that grains have the freedom to rotate during growth in either clockwise or counterclockwise senses as long as their rates of rotation are the same. Hopkins and Stewart (1970) found that in another specimen grown using the Czockralski technique two grains spiralled in opposite directions.

A degenerate structure was produced in Pb-Sn by growth at 11 cm/hr. under a temperature gradient of 5.5°C/cm. Lamellar orientation measurements showed that the degenerate structure did not exhibit the spiralling effect. The results are shown in Figure 3.13. Although there is a relatively high degree of scatter in the average orientation of the two grains, it is evident that the mean orientation of the grains did not vary with distance in the growth direction.

3.2.3 Cadmium-Zinc

Two Cd-Zn samples were directionally solidified under the different growth conditions given in Table 3.3.

TABLE 3.3 Growth Conditions used for Cd-Zn Specimens

Sample #	R(cm/hr)	G(°C/cm)	Remarks
C1	2.5	8.0	faulted structure - constant R
C2	30.0 - 6.0	13.0	faulted structure - varying R

FIGURE 3.13 Plot of degenerate lamellar orientations as a function of solidification distance for a directionally frozen Pb-Sn sample (R = 11.0 cm/hr, G = 5.5°C/cm)

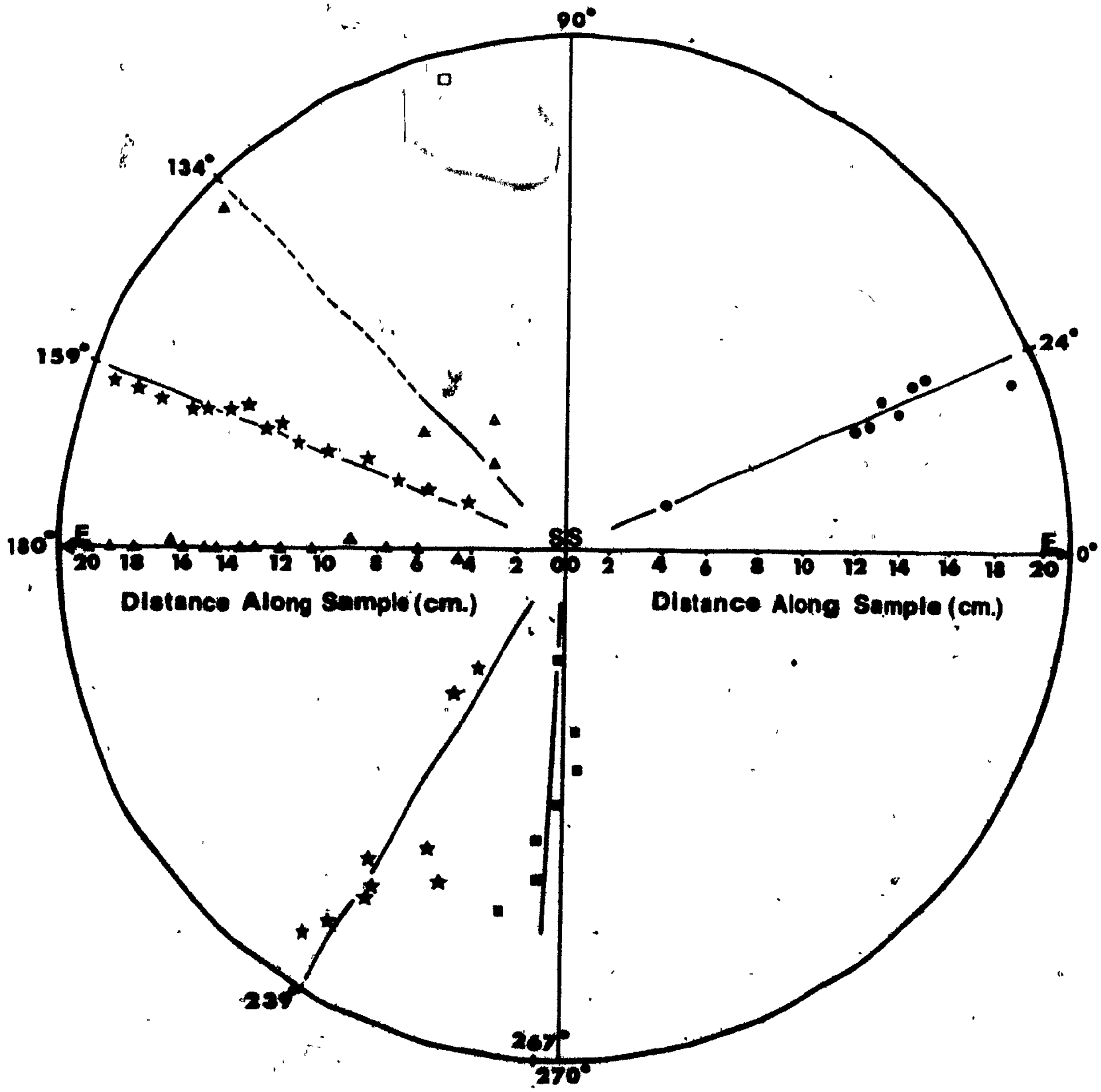
90°
134°
159°
24°
180°
E
SS
E
0°
20 18 16 14 12 10 8 6 4 2 0
0 2 4 6 8 10 12 14 16 18 20
Distance Along Sample (cm.)
Distance Along Sample (cm.)
239°
267°
270°

Lamellar spiralling was measured in sample C1; while sample C2 was grown by Berthou's method in an attempt to produce a perfect structure similar to that of Sn-Cd. Faults could not be eliminated in this system (Figure 3.5(a)) although from a crystallographic point of view this eutectic is very similar to the Sn-Cd. Results on lamellar spiralling are shown in Figure 3.14 in which the mean orientation of five grains are shown. Although the lamellae definitely did not rotate, a relatively higher scatter was observed in the mean grain orientations as compared to the Sn-Cd system. Lamellar spiralling measurements were also undertaken on a few sections of sample C2 and indicated that no spiralling occurred during growth.

3.2.4 Tin-Zinc

It was decided to search for spiralling in the Sn-Zn eutectic because it exhibits a typical broken lamellar structure and furthermore, both phases have different crystal structures. Measurements were made on a sample directionally frozen at 3.0 cm/hr. under a temperature gradient of 6.6°C/cm. Variation of the average grain orientation with distance in the growth direction is shown in Figure 3.15. The results indicated that the Sn and Zn lamellae, although crystallographically dissimilar, did not spiral during growth. Faults were found to be a characteristic of the structure just as is the case for most lamellar structures (see Figure 3.6(a)).

FIGURE 3.14 Plot of lamellar orientations as a function of solidification distance for a directionally frozen Cd-Zn sample (R = 2.5 cm/hr, G = 8.0°C/cm)

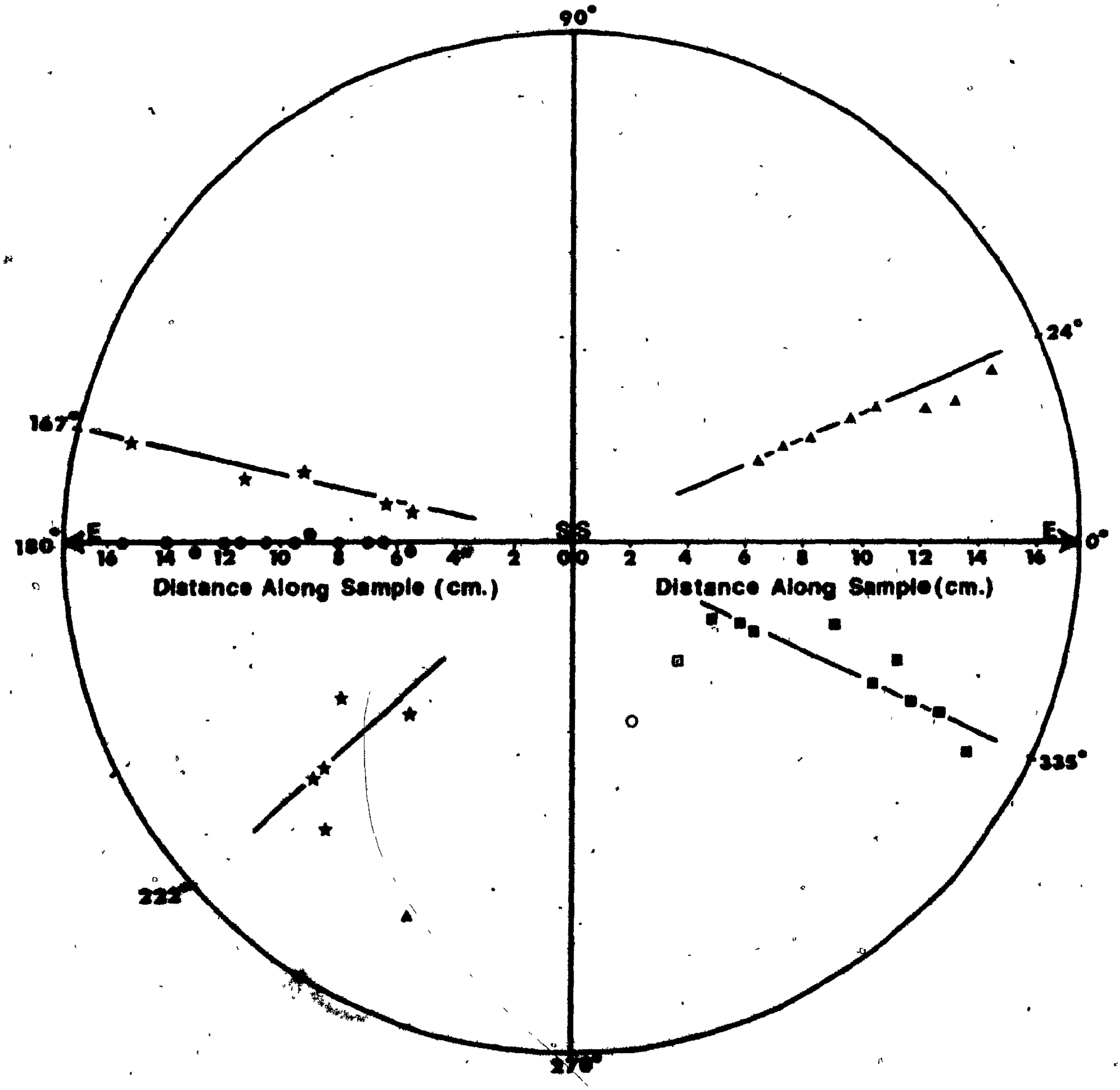
90°
24°
167°
180°
E
16
14
12
10
8
6
4
2
SS
0 0
2
4
6
8
10
12
14
16
E
0°
Distance Along Sample (cm.)
Distance Along Sample (cm.)
335°
222°
270°

FIGURE 3.15 Plot of lamellar orientations as a function of solidification distance for a directionally frozen Sn-Zn sample (R = 3.0 cm/hr, G = 6.6°C/cm)

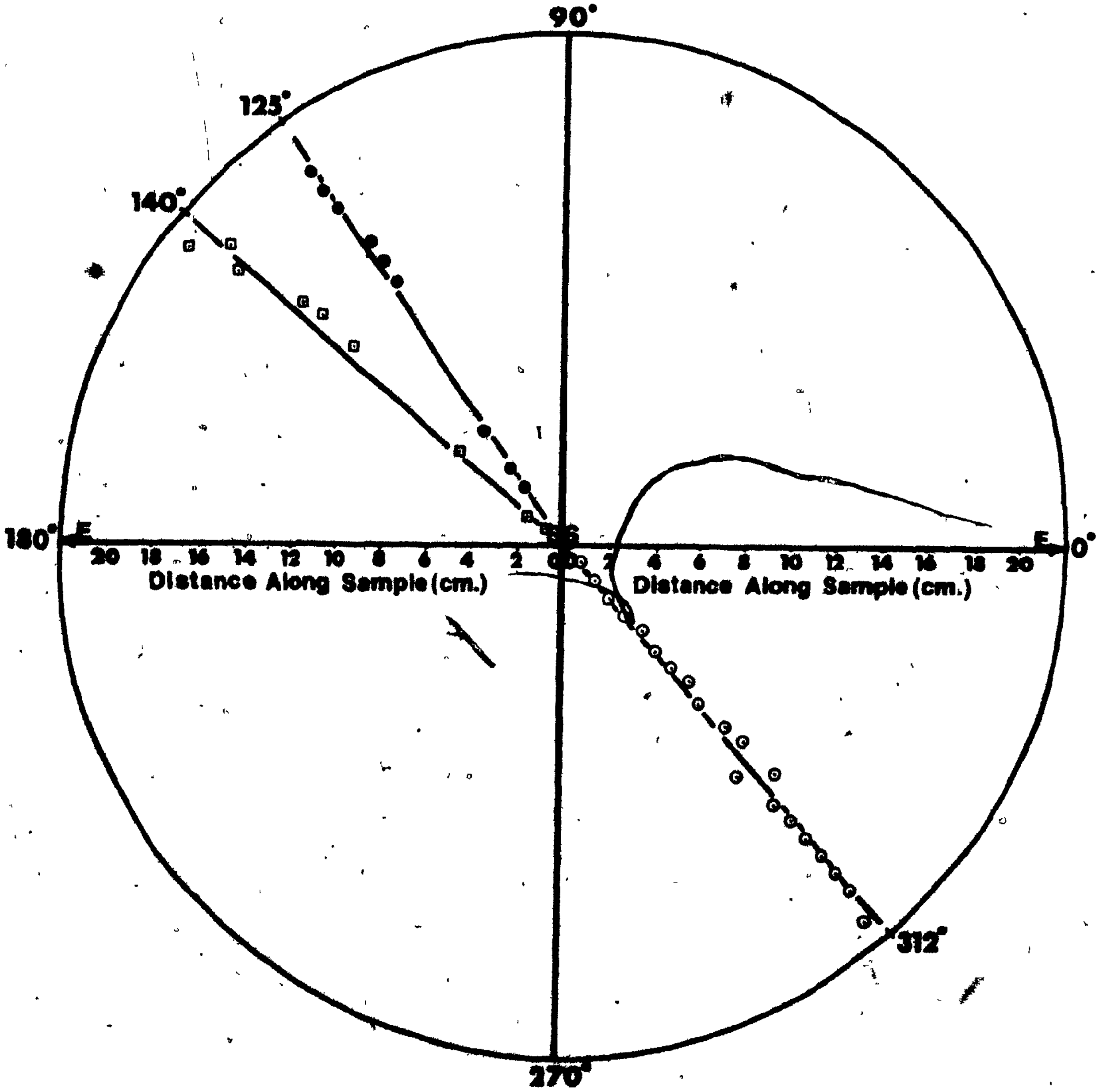
90°
125°
140°
180°
E
20
18
16
14
12
10
8
6
4
2
0
Distance Along Sample (cm.)
2
4
6
8
10
12
14
16
18
20
E
0°
Distance Along Sample (cm.)
312°
270°

The Sn-Zn eutectic was observed to grow relatively large grains. The results shown in Figure 3.15 indicate that three grains were encountered during lamellar orientation measurements. No grain boundaries were microscopically visible so that probably two of the grains shown in Figure 3.15 are subgrains since the difference between their average lamellar orientations is small. The subgrain represented by the open circles in Figure 3.15 had an average orientation of 312° (≡ 132°) which is very close to the 140° mean orientation of the subgrain represented by the open squares.

3.2.5 Aluminum-Copper and Lead-Cadmium

The Al-$CuAl_2$ system was also investigated in this work, but in a less detailed way than the other eutectics. This system has been previously reported (Double et al. 1968; Hellawell 1967; Double 1973; Dean 1973) to exhibit lamellar spiralling. Under certain conditions the Al-$CuAl_2$ eutectic is similar to the Pb-Sn in that it forms a degenerate structure. The major difference between the two systems is that the degenerate structure forms only at low growth rates in Al-$CuAl_2$ (Chadwick 1972) while in Pb-Sn it has been observed at both high and low growth rates (Hunt 1963). Furthermore, Al-$CuAl_2$ undergoes the lamellar-to-fibrous structural transition in the presence of impurities, and although both systems have almost equal volume fractions of the discontinuous phase (46% $CuAl_2$ versus 37% Pb), this transition does not occur in Pb-Sn (Hunt and Chilton 1962).

Lamellar orientation measurements were undertaken in Al-CuAl$_2$ on five consecutive sections each about 2 cm. apart. The results are given in Figure 3.16 and the cumulative variation of lamellar orientations is shown in Figure 3.17 from which the rate of spiralling has been determined to be about 2^0/cm. Bending of the lamellae in transverse sections has been previously reported for this eutectic (Dean 1973) and was also observed during this work (see Figure 3.18). As was the case for the Pb-Sn and Sn-Zn eutectics, large grains of Al-CuAl$_2$ were obtained, and in fact, the sample on which measurements were taken consisted of a single grain.

A Pb-Cd sample was also directionally solidified for lamellar spiralling studies, but unfortunately this system was found to nucleate very small grains which did not easily grow out so that it was not possible to trace individual grains from one section to the next. Plots of lamellar orientations versus distance across the transverse section gave angular values ranging at random from 0^0 to 180^0 due to the large number of small grains encountered. Lamellar grains could therefore not be followed from one section to the next and hence a spiralling rate determination was not possible. Lamellar bending was also observed in this system as shown in Figures 3.19(a) and 3.19(b) and the structure was always found to be faulted.

FIGURE 3.16 Variation of lamellar orientations with solidification distance in a directionally frozen Al-$CuAl_2$ sample

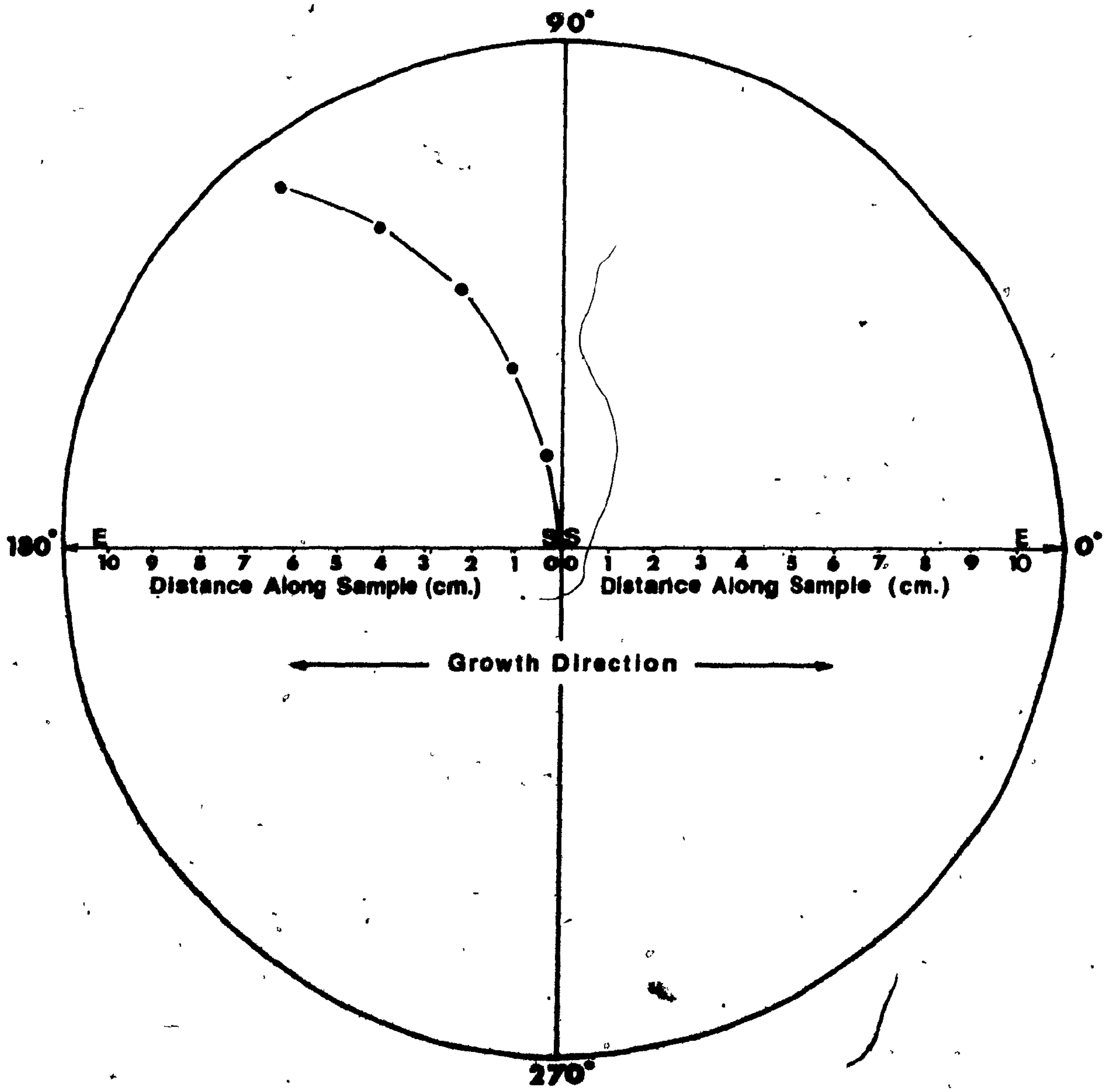
90°
180°
0°
270°
E
E
S
S
10 9 8 7 6 5 4 3 2 1 0
0 1 2 3 4 5 6 7 8 9 10
Distance Along Sample (cm.)
Distance Along Sample (cm.)
Growth Direction

FIGURE 3.17 Cumulative variation of lamellar orientations with solidification distance in a directionally frozen Al-CuAl$_2$ sample

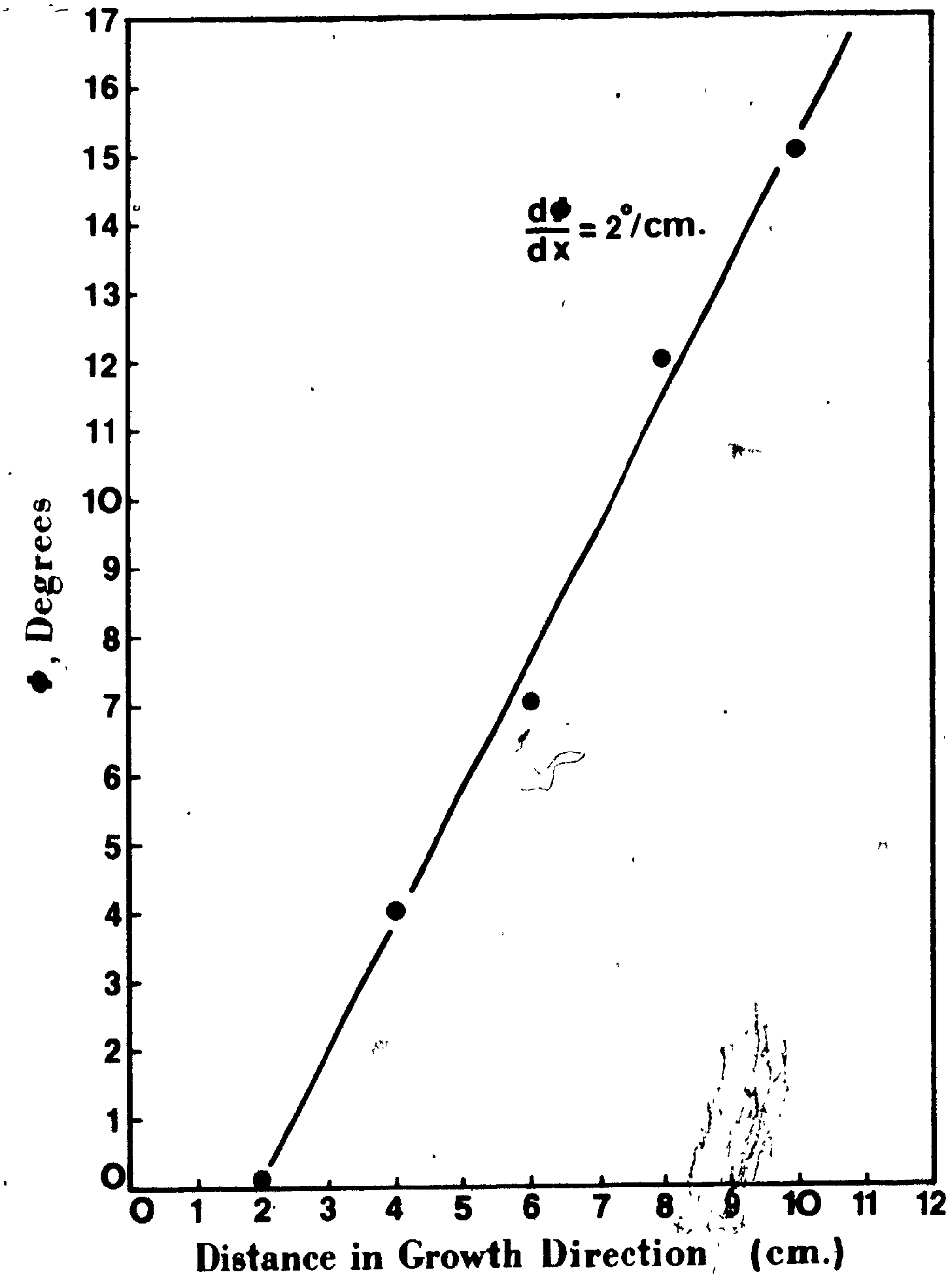

$\frac{d\phi}{dx} = 2°/cm.$
ϕ, Degrees
0
1
2
3
4
5
6
7
8
9
10
11
12
13
14
15
16
17
Distance in Growth Direction (cm.)

FIGURE 3.18 Al-$CuAl_2$ lamellar structure:
(a) transverse section (x350);
(b) Moiré pattern showing lamellar bending

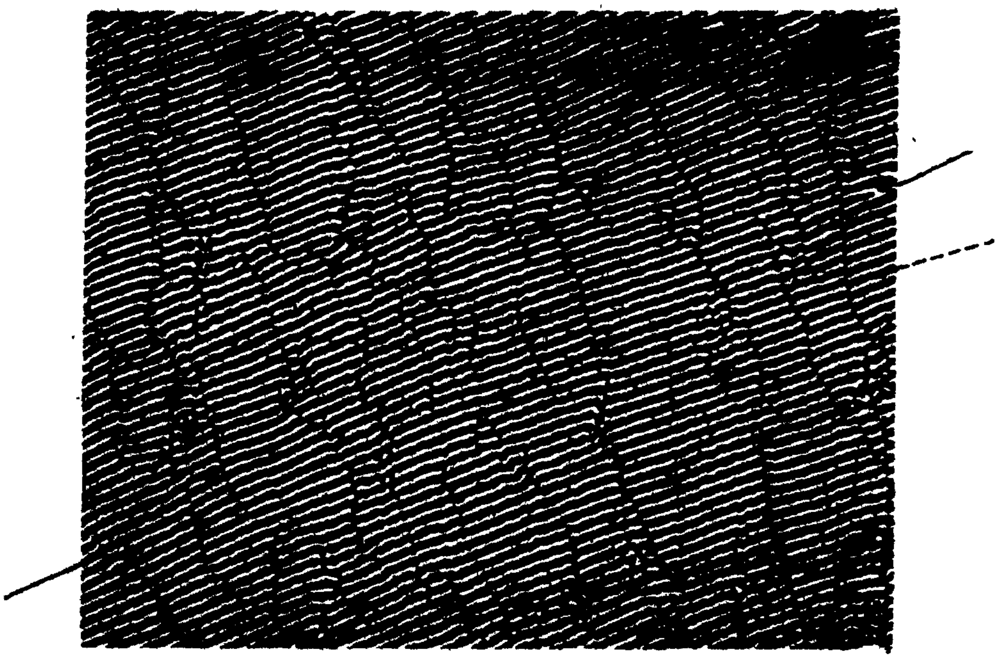

(a)

(b)

FIGURE 3.19 Pb-Cd lamellar structure:
(a) transverse section (x300);
(b) Moiré pattern showing lamellar bending

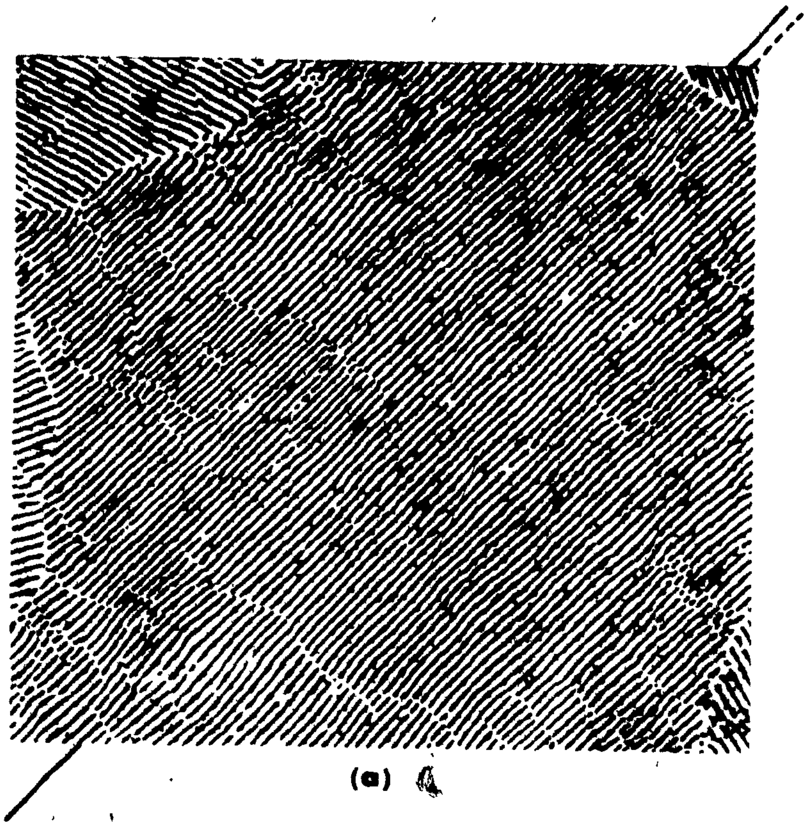

(a)

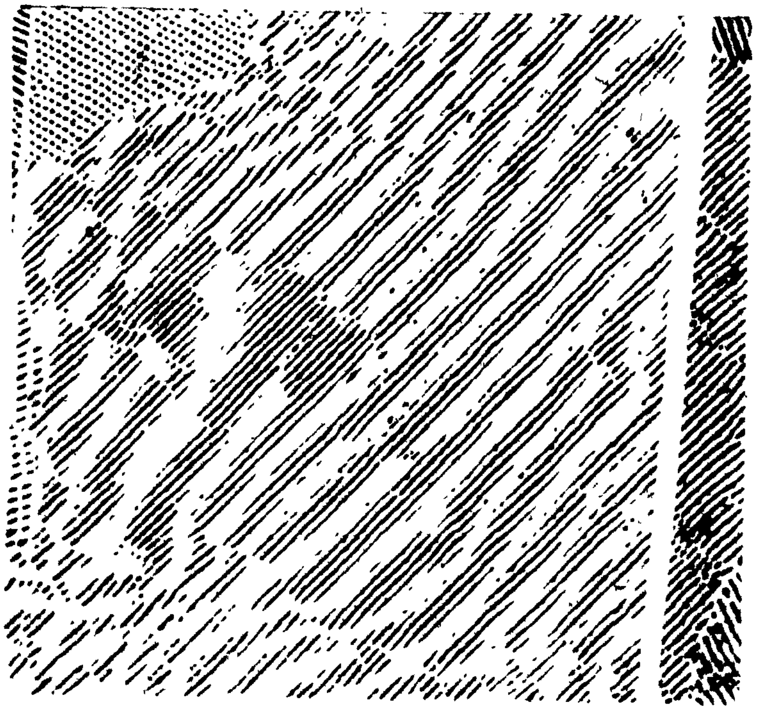

(b)

3.3 EFFECT OF GROWTH CONDITIONS ON SPIRALLING

3.3.1 Temperature Gradient

Of all the systems investigated during the present work Pb-Sn exhibited the highest spiralling rate. For this reason it was chosen for further study because any effect of growth conditions should be more easily detectable. The spiralling rate was previously reported to be fairly constant for a given set of freezing conditions and was directly related to the substructural perfection, to the sub-grain density and range of misorientations, the rate decreasing with an increase in the imposed temperature gradient (Double et al. 1968). During the present investigation a single sample was grown under varying conditions: the growth rate increased and the temperature gradient decreased from the bottom to the top of the specimen. Table 3.4 summarizes the growth conditions and the spiralling measurements. The growth rate values were determined by measuring λ and using the plot of R against λ obtained by Hunt (1963). From Figures 3.20 and 3.21 representing the variation of spiralling rate with solidified distance and temperature gradient, respectively, it is evident that the rate of spiralling is directly related to the temperature gradient, R being assumed to have no effect on lamellar spiralling as previously reported by Double et al. (1968). As a consequence of the increase in growth rate from the bottom to the top of the sample, the interlamellar spacing λ was observed to decrease along the length of the specimen (Table 3.4). Measurements on subgrain density and grain misorientation showed no appreciable change so that little can be said about the effect of structural imperfection on lamellar

TABLE 3.4 Pb-Sn Spiralling Measurements for Varying G and R

Section #	Section Length (mm)	λ (μ)	R (cm/min)	dT/dt (°C/min)	G (°C/cm)	Average Grain Orientation	CCW Rotation (°/cm)	Grain Misorientation $\delta\phi$(degrees)	Subgrain Density /3mm. length
1	9.80	2.38	0.04	2.0*	50	TOO MANY GRAINS FOR MEASUREMENT PURPOSES			
2	9.75	2.38	0.04	2.2	55				
3	9.90	1.85	0.06	2.4	40				
4	4.80	1.67	0.07	2.5	36				
5	9.95	1.52	0.09	2.7	30				
6	4.80	1.39	0.10	2.8	28				
7	9.75	1.28	0.12	3.0	25	22°	-	40	9
8	4.70	1.28	0.12	3.1	26	112°	204	30/35	8
9	9.80	1.19	0.14	3.3	24	114°	180	40	9/10
10	5.05	1.19	0.14	3.4	24	169°	109	25	11/12
11	9.80	1.11	0.16	3.6	23	152°	166	45	12/13
12	4.80	1.08	0.17	3.7	22	38°	138	40	11/12
13	9.65	1.04	0.18	3.9	22	168°	135	30/35	8/9
14	4.80	1.01	0.19	4.0	21	44°	117	40	11
15	10.10	1.04	0.18	4.2*	23	170°	125	30	10
15	4.80	0.98	0.21	3.9	19	60°	146	40	11
17	9.70	0.93	0.23	3.3	16	172°	115	25	9
18	4.70	0.90	0.24	3.0	13	58°	136	35	11
19	9.80	0.93	0.23	2.4	10	160°	104	35	10
20	4.80	0.90	0.24	2.1	9	30°	104	25/30	12
21	9.75	0.88	0.26	1.7	7	128°	101	30	12
22	4.75	0.90	0.24	1.4	6	170°	88	25	8
23	9.80	0.88	0.26	0.8	3	92°	104	30	8
24	4.80	0.83	0.29	0.5	2	150°	121	40	10
25	7.85	0.76	0.34	0.2*	1	110°	178	40	11/12

* Values measured experimentally, the others are estimated.

FIGURE 3.20 Variation of spiralling rate with solidification distance for a Pb-Sn sample directionally solidified under varying G and R

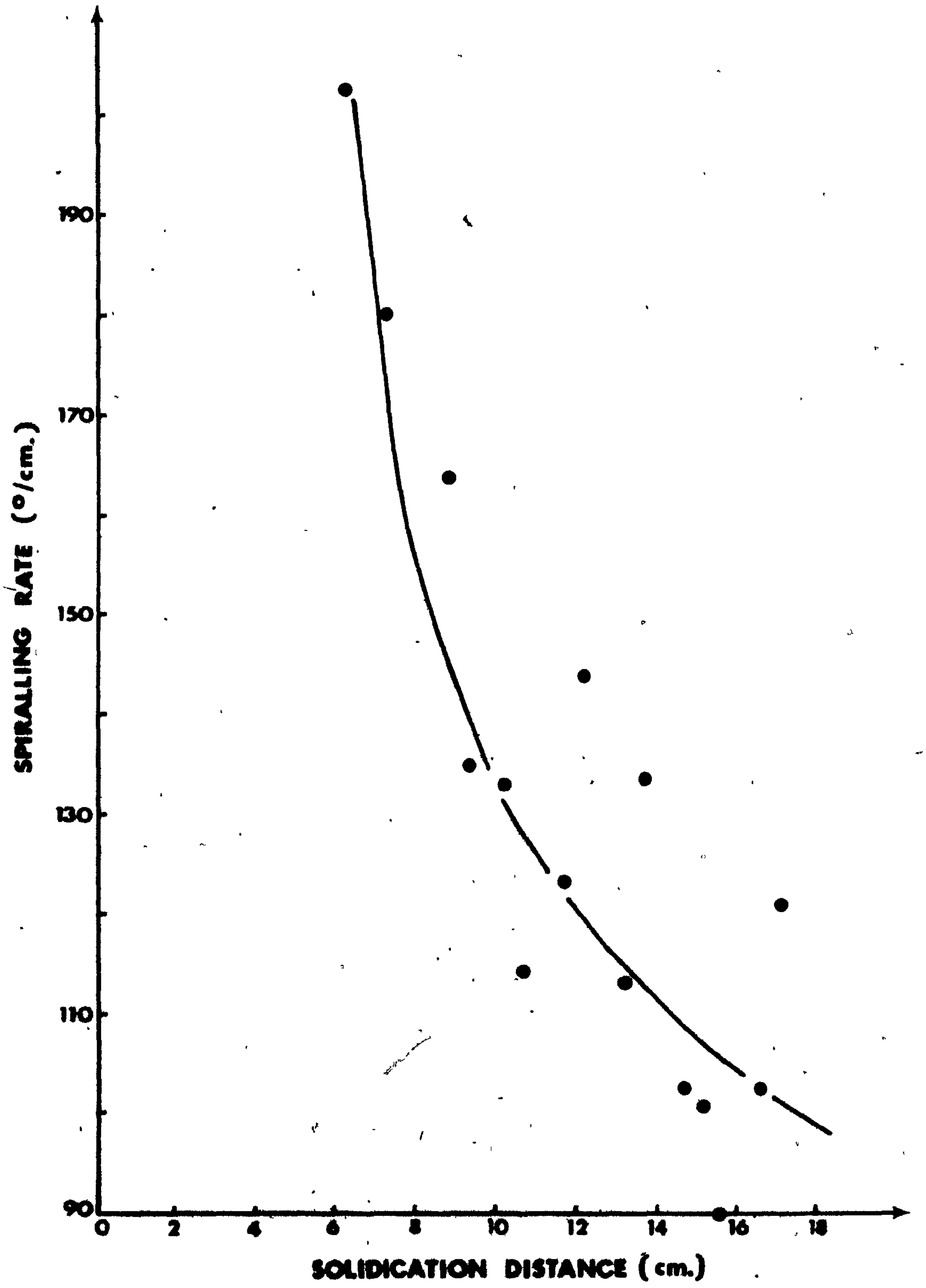
SPIRALLING RATE (°/cm.)
190
170
150
130
110
90
0
2
4
6
8
10
12
14
16
18
SOLIDICATION DISTANCE (cm.)

FIGURE 3.21 Variation of spiralling rate with temperature gradient for a Pb-Sn sample directionally frozen under varying R

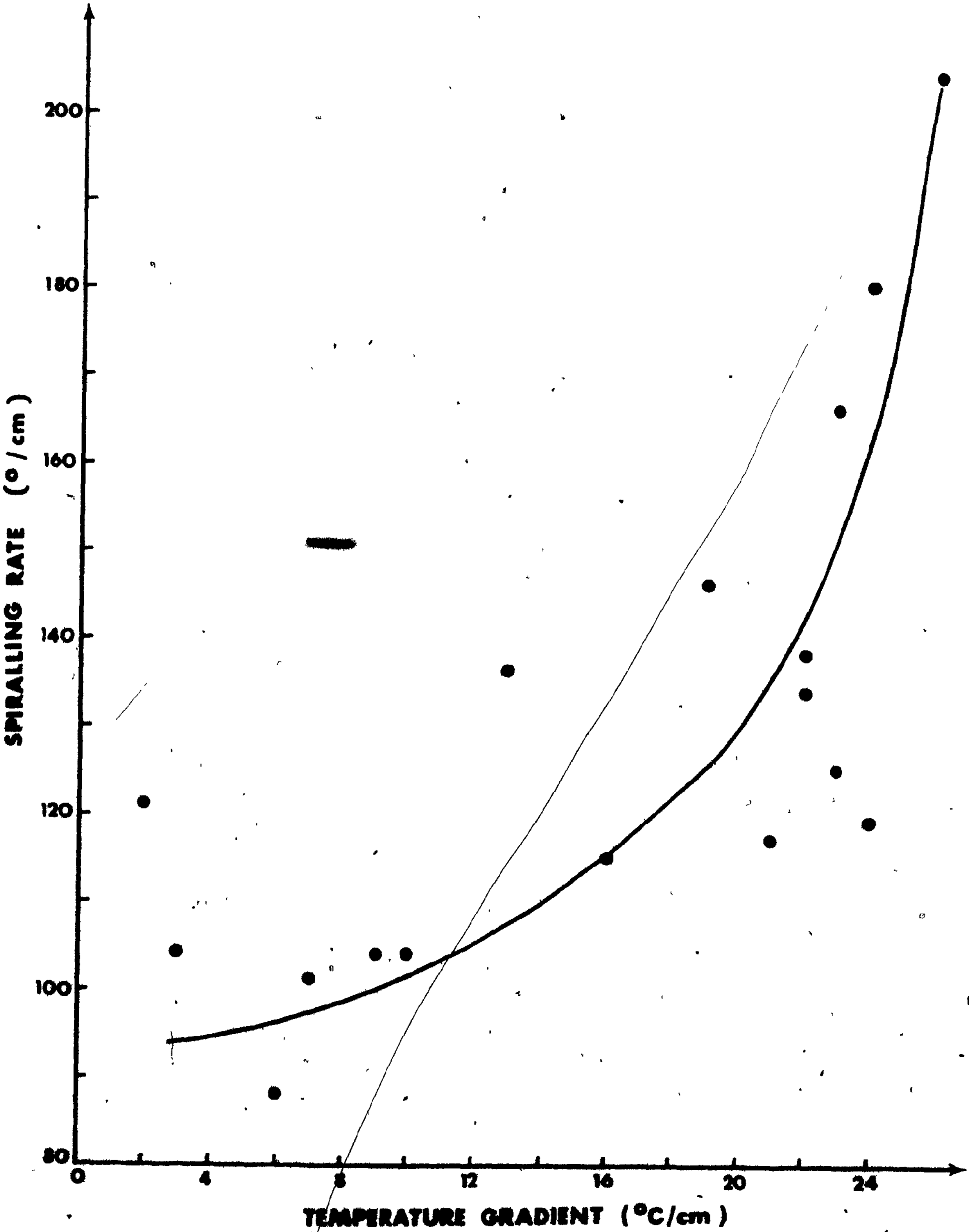
SPIRALLING RATE (°/cm)
TEMPERATURE GRADIENT (°C/cm)
200
180
160
140
120
100
80
0
4
8
12
16
20
24

spiralling from these results. It is to be noted that in order to decide whether the rotation of the grain was clockwise or counterclockwise, both being possible, extra lamellar orientation measurements were taken in a few 2 mm. thick sections.

3.3.2 Mold Shape

The effect of mold shape on lamellar spiralling was investigated in a 2 x 0.5 x 20 cm. Pb-Sn eutectic sample directionally solidified under steady growth conditions (R — 1.7 cm/m, G — 4^{o}C/cm. measured on the wide side). Two V-notches were carved along the length of the sample, one on the wide edge and the other on the thin edge (Figure 3.22 (b)). Rectangular sections 1 cm. and 0.5 cm. apart were cut by means of a spark cutter and then mounted and polished for lamellar orientation measurements. After etching, the grains were observed macroscopically to be aligned perpendicular to the wide side as shown in Figure 3.22(c), this probably being the shortest distance the grain boundaries could grow along. Spiralling measurements were carried out on both sides of the sample, the results being shown in Figures 3.23(a) and 3.23(b). The observed spiralling rate was about 50^{o}/cm. and was the same in directions both parallel and perpendicular to the fibre axis. In both cases measurements were taken on a single grain, grain A, shown in Figure 3.22.

FIGURE 3.22 Rectangular-shaped sample:
(a) as directionally frozen;
(b) reference marks (v-notches) made on both edges;
(c) schematic transverse section showing shape of grains and directions along which lamellar orientation measurements were taken in grain (A)

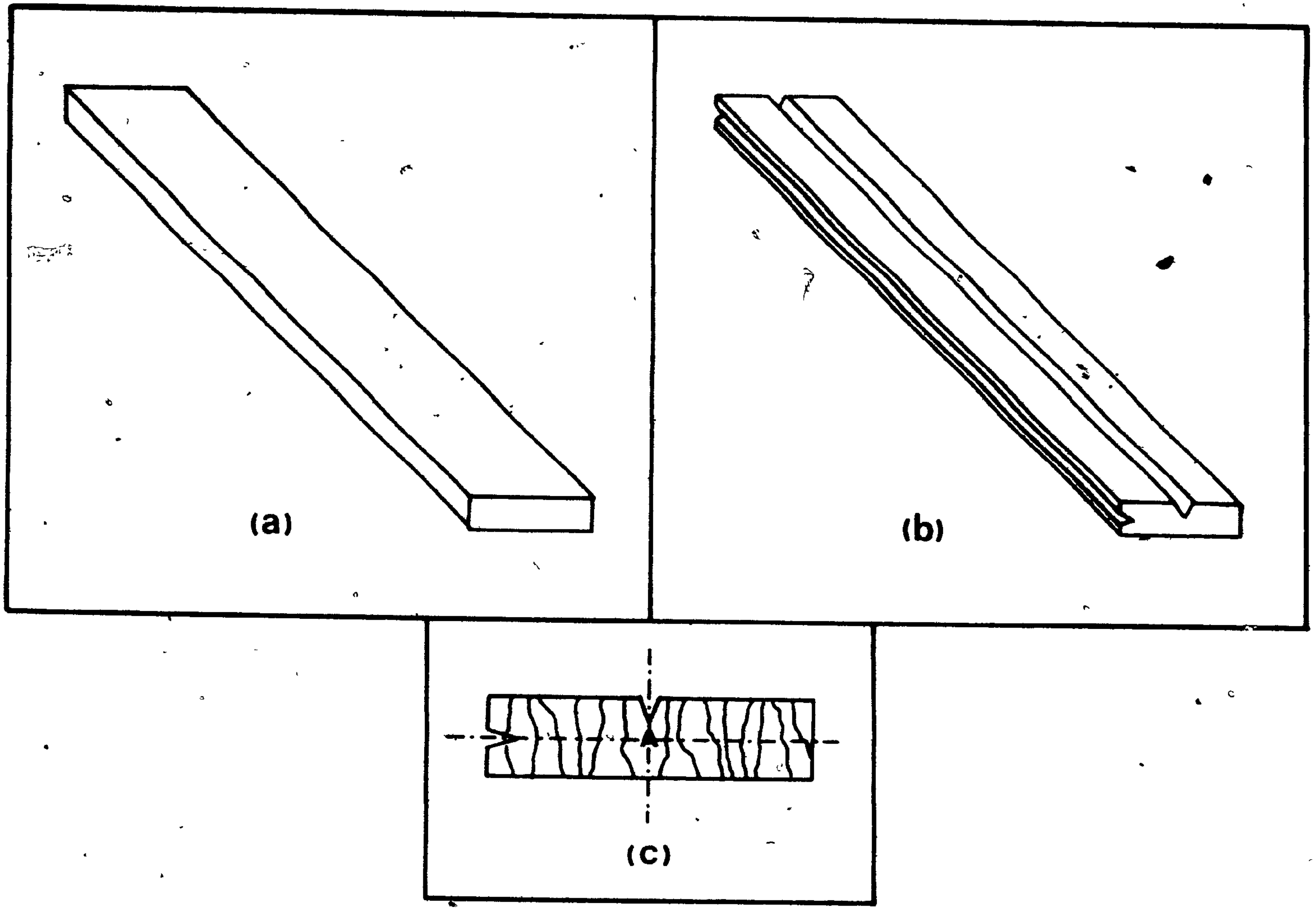
(a)
(b)
(c)

FIGURE 3.23 Variation of lamellar orientations with solidification distance for a directionally frozen Pb-Sn rectangular sample ($R = 1.7$ cm/hr, $G = 4.0^{\circ}C/cm$):

(a) measured in a direction parallel to the grain fiber axis;

(b) measured in a direction perpendicular to the grain fiber axis

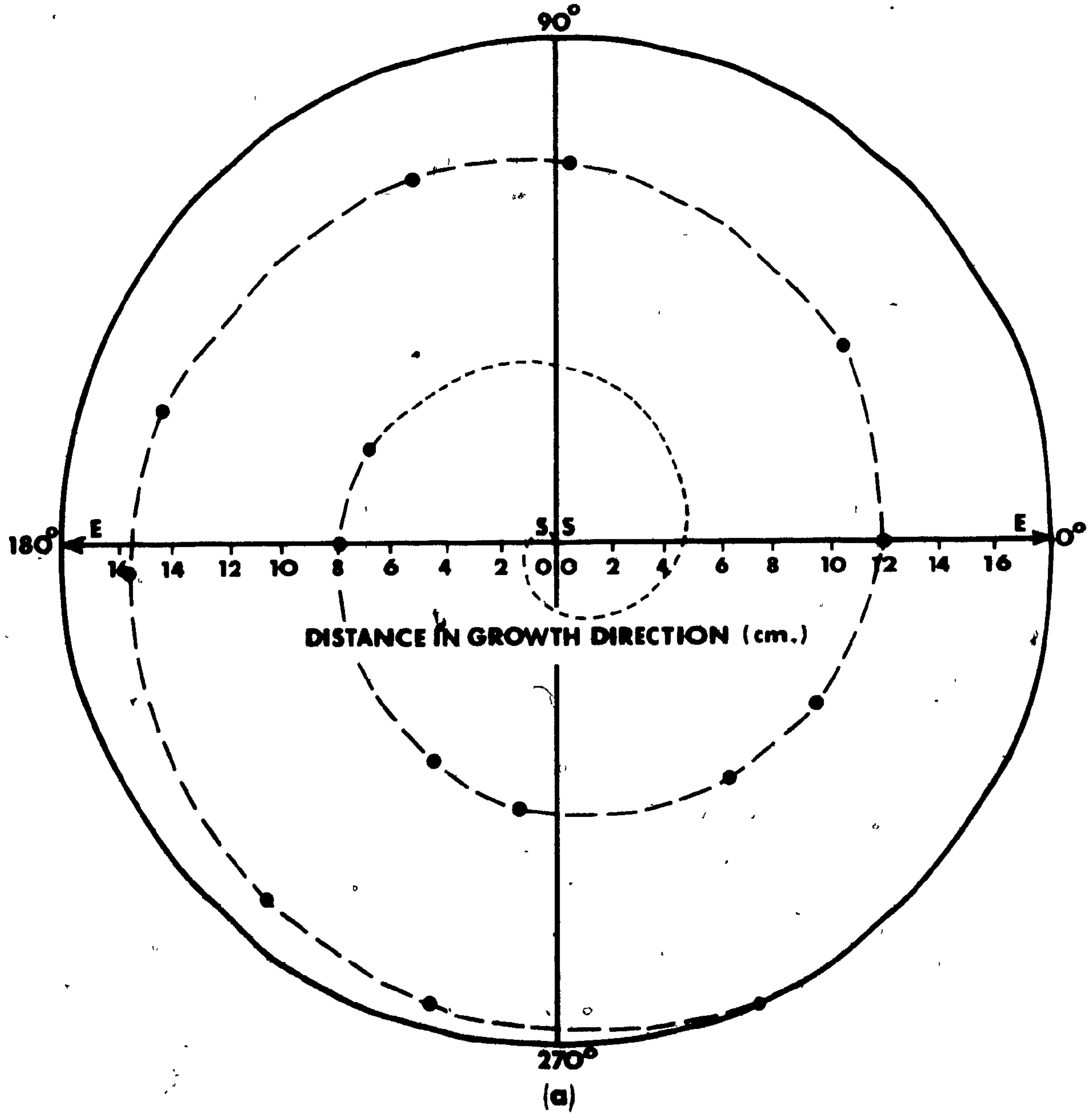

90°
180°
0°
270°
E
E
S
S
16
14
12
10
8
6
4
2
0
0
2
4
6
8
10
12
14
16
DISTANCE IN GROWTH DIRECTION (cm.)

(a)

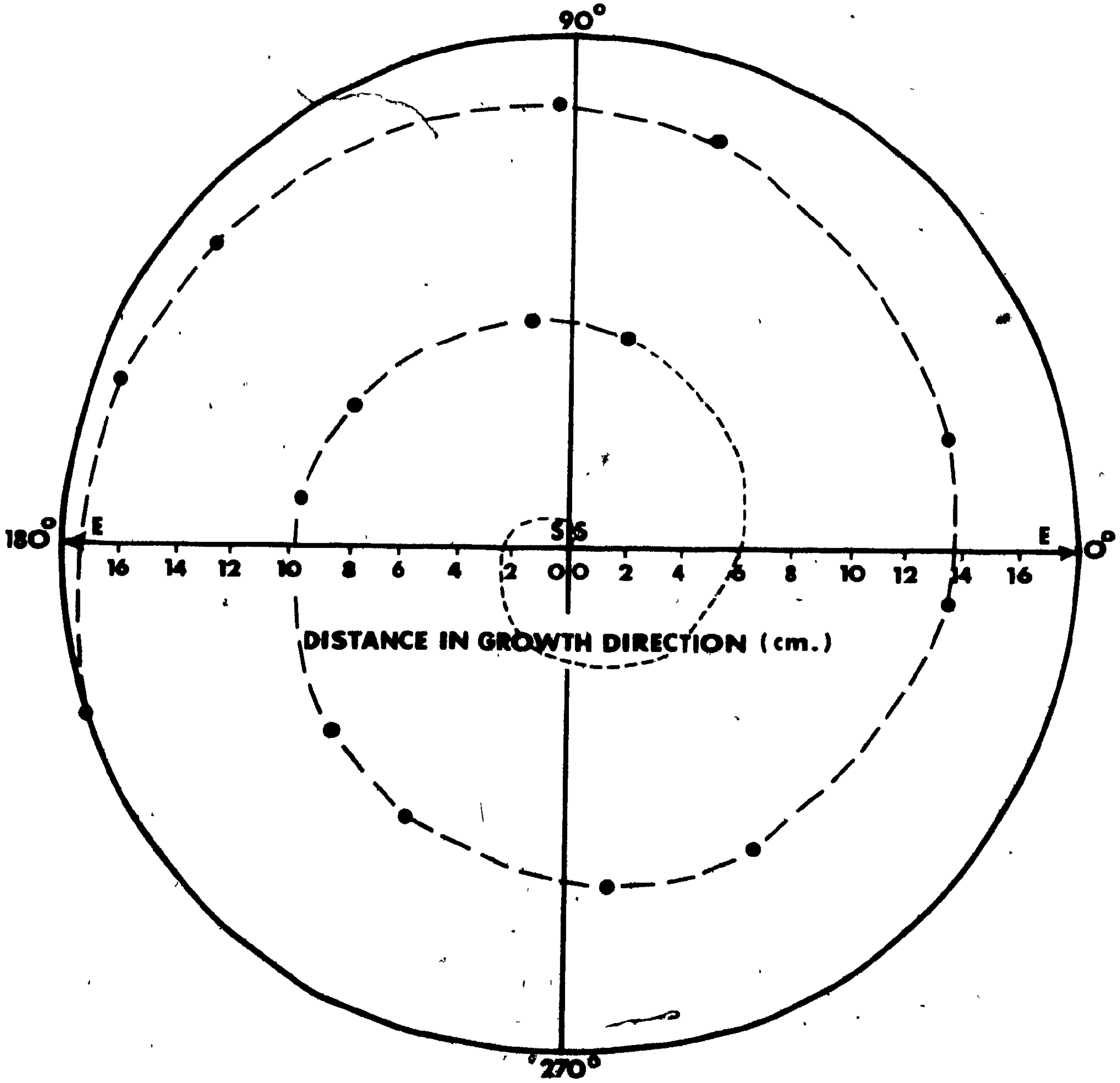
90°
180°
0°
270°
E
E
S S
16 14 12 10 8 6 4 2 0 0 2 4 6 8 10 12 14 16
DISTANCE IN GROWTH DIRECTION (cm.)

(b)

CHAPTER IV

DISCUSSION

4.1 SPIRAL GROWTH

Since lamellar spiralling was first observed, no consistent approach to the problem has ever been given in the literature. In this section an analysis of spiralling is presented based on the fact that the preferred growth direction of each phase as imposed by its crystal structure may be different from the overall growth direction of the system. The eutectic is under severe restraints to grow in the normal direction due to the coupled growth tendency and to heat flow considerations. The crystallographic orientation relationships of the systems studied are therefore important parameters in this analysis.

4.1.1 Crystallographic Relationships in Eutectic Systems

A brief discussion of the interface crystallography of the systems investigated during the present work is presented below and a list of the crystallographic orientation relationships of the studied systems (as well as Al-Zn and Al-Ag_2Al, both reported to exhibit lamellar spiralling (Double et al. 1968)) is given in Table 4.1.

4.1.1.1 Lead-Tin

According to Kraft (1962,1963), the free energy of eutectic interfaces attains a minimum when "puckered planes", i.e. planes of high atomic density and wide spacing are brought into contact at the

TABLE 4.1 Interface Crystallographic Relationships of Systems Reported and Observed to Spiral

System	Interface Crystallographic Relationships	References
Sn-Cd	(100)Sn // (0001)Cd [001]Sn // [01$\bar{1}$0]Cd	Straumanis and Brakss 1937
	Interfaces // (0001)Cd Growth Direction // [10$\bar{1}$0]Cd	Gruzleski and Kraft, reported by Hogan et al. 1970, p.126
Cd-Zn	Interface // (0001)Cd // (0001)Zn Growth Direction // [10$\bar{1}$0]Cd //[10$\bar{1}$0]Zn	Straumanis and Brakss 1935; Double and Hellawell 1969b
Pb-Sn	Interface // (1$\bar{1}\bar{1}$)Pb // (0$\bar{1}$1)Sn Growth Direction // [211]Pb // [211]Sn	Hopkins 1967; Hopkins and Kraft 1968
	Interface // (111)Pb // (101)Sn Growth Direction // [$\bar{1}\bar{1}$2]Pb // [010]Sn	Takahashi and Ashinuma 1958-59
	Interface // (01$\bar{1}$)Pb // ($\bar{1}$10)Sn Growth Direction // [100]Pb // [110]Sn	Labulle and Petipas 1975
Sn-Zn	Interface // (100)Sn // (0001)Zn Growth Direction // [001]Sn // [01$\bar{1}$0]Zn	Straumanis and Brakss 1937
Al-CuAl$_2$	Interface // {111}Al // {211}CuAl$_2$ Growth Direction // <101>Al // <120>CuAl$_2$	Kraft 1961,1962; Kraft and Albright 1962; Cantor and Chadwick 1974
	Interface // {001}Al // {001}CuAl$_2$ Growth Direction // <100>Al // <100>CuAl$_2$	Ellwood and Bagley (1950)
	Interface // (001)Al // (001)CuAl$_2$ Growth Direction // [110]Al // [100]CuAl$_2$	Takahashi 1960
	Interface // (001)Al // (001)CuAl$_2$ Growth Direction [310]Al // [100]CuAl$_2$ Equivalent to [1$\bar{1}$0]Al // [1$\bar{2}$0]CuAl$_2$	Mehl et al. 1932

TABLE 4.1 (cont'd)

System	Interface Crystallographic Relationships	References
Al-$CuAl_2$	$\{111\}$Al // $\{211\}CuAl_2$ $<111>$Al // $<012>CuAl_2$ Interface 13° away from $\{111\}$Al // $\{211\}CuAl_2$	Davies and Hellawell 1969a
	$\{111\}$Al // $\{211\}CuAl_2$ $<110>$Al // $<120>CuAl_2$ Interface 12° away from $\{111\}$Al // $\{211\}CuAl_2$	Davies and Hellawell 1969a, 1970
Al-Ag_2Al	Interface // (111)Al // (0001)Ag_2Al Growth Direction // $[1\bar{1}0]$Al // $[11\bar{2}0]Ag_2Al$	Cantor 1971
Al-Zn	Interface // $(10\bar{1}8)$Zn Growth Direction // $[11\bar{2}0]$Zn Lamellar Interface $\nparallel$ Growth Direction	Double et al. 1968 Double and Hellawell 1969b

lamellar interface. This hypothesis implies that the atomic spacings and densities of the mating planes are similar in order to lower the interfacial strain energy.

From X-ray diffraction results on Pb-Sn one finds the habit planes to be {111} and {011} for the Pb-and Sn-rich phases respectively. Using lattice parameters corrected for temperature and composition, Hopkins (1967) has worked out a detailed analysis of the interfacial planes of the Pb-Sn eutectic. The presence of the Pb {111} planes at the lamellar interface is justified by the fact that they are the most widely separated and densely populated planes. On the other hand, the most densely packed planes for body centred tetragonal Sn are the {100} which are not those established at the interface under equilibrium conditions. Hopkins attributed this selection to the fact that the difference in atomic density and spacing between {100} Sn and the Pb mating plane is larger than that of the {110} Sn with {111} Pb.

Although the mold shape and mode of growth seem to affect the common growth direction of each eutectic phase in the habit plane, the lamellar interface itself is unaffected by these variables, but prefers to be parallel to the most densely packed and widely spaced planes of each phase. In fact, Takahashi and Ashinuma (1958-59) grew Pb-Sn eutectic films by withdrawing a loop from the melt. From the crystallographic orientation relationships given in Table 4.1 one can see that the interfacial planes were not changed by this essentially two-dimensional growth mode. Little is known about the crystallography of the degenerate lamellar interface although an unsuccessful attempt at its determination was made by Hunt (1963) using the back-reflection Laue technique.

4.1.1.2 Aluminum-Copper

Different sets of crystallographic relationships have been reported for this system although in most cases a single growth technique was used. Edmund's analysis (1941) on the development of preferred orientations in castings based on Bravais' law of crystal growth, was extended by Kraft (1962) to explain preferred growth in the Al-$CuAl_2$ eutectic. It should be noted that although the habit planes forming the equilibrium interface are supposed to be unaffected by the shape of the sample and growth technique, more than one set of interfacial planes have been observed for the Al-$CuAl_2$ system (see Table 4.1).

4.1.1.3 Tin-Cadmium and Cadmium-Zinc

Because of the solid state transformation during which the β phase (Sn + Cd) changes its crystal structure from close packed hexagonal to body centred tetragonal, very little is known about the Sn-Cd lamellar interface crystallography during solidification. However, there seems to be some similarity between the Sn-Cd and Cd-Zn eutectics at their equilibrium temperatures, both being composed of two close packed hexagonal phases. As is usually the case, hexagonal phases tend to have the basal plane in contact at the solid/solid interface boundary, so that it is very likely that the β phase in the Sn-Cd eutectic would also be oriented in this way. This point will be considered later in the analysis of spiral growth.

4.1.1.4 Tin-Zinc

The most densely packed and widely spaced {100} Sn planes are those established under equilibrium conditions at the interface in contact with the densely populated {0001} Zn planes. The interface crystallography of this system is similar to the room temperature crystallography of the Sn-Cd eutectic (see Table 4.1) in which case the {100} Sn planes are those restricting growth, resulting in a {100} growth direction. This point will be reconsidered later in the analysis of spiral growth.

4.1.2 Growth Directions of Single Phases

All of the B-type statements (Table 4.1) have been postulated on the assumption that the lamellae grow perpendicular to the solid/liquid interface, implying that the specified directions lie within the habit planes described in statement A. It is unclear as to why the system should prefer any particular direction in a habit plane. Theories have been proposed to account for the development of preferred orientations in columnar grains of commercial purity castings (Edmunds 1941). A list of the preferred orientations in castings is given in Table 4.2. Barrett (1952) collected data from different sources showing that face

TABLE 4.2 Preferred Orientations in Castings
(ASM Metals Handbook 1973, p.232)

Crystal Structure		Texture
F.C.C.		$\langle 100 \rangle$
B.C.C.		$\langle 100 \rangle$
β-Sn	B.C.T.	$\langle 110 \rangle$
Cd	C.P.H.	$\langle 10\bar{1}0 \rangle //, (0001) \perp$
Zn		$\langle 10\bar{1}0 \rangle //, (0001) \perp$

centered cubic metals grow preferentially in ~~the~~ [100] direction, although zone refined lead was found to have a [111] direction parallel to the heat flow in the columnar zone (Bolling 1963). A small addition of Ag (0.0005 wt.%) changed this [111] texture to [100] (Rosenberg 1957).

The preferred growth direction of Cd and Zn has been found to be $\langle 10\bar{1}0 \rangle$ (Edmunds 1941,1945) and from studies on the binary eutectic it was observed that each phase tends to have the same texture that it would have had in uncoupled growth (Edmunds 1941; Nix and Schmid 1929).

Body centred cubic metals always grow in the $\langle 100 \rangle$ direction whereas body centred tetragonal β-Sn has been found to adopt the $\langle 110 \rangle$ direction as the fiber axis of columnar grains (ASM Metals Handbook 1973, p.232).

Edmunds (1941) postulated a theory to explain the selection of preferred growth directions by metals of different crystal structure.

His theory was based on Bravais' law stating that the higher the atomic density of a plane, the greater is the growth velocity perpendicular to this plane and less is its chance of survival during continued growth. Furthermore, Edmunds proposed that the growth direction observed in a casting will be the maximum dimension of a solid bounded by these dense planes. This rule was found to apply readily to cubic metals. In F.C.C. structures, the octahedral {111} planes are the most closely packed. The longest distance through an octahedron is between opposite vertices along the axes of the cube and from Bravais' rule the maximum growth rate should be along the [100] direction in agreement with the experimental results.

4.2 ANALYSIS OF SPIRAL GROWTH

4.2.1 Introduction

Since upon solidification metals tend to develop specific preferred growth directions depending on their crystal structure (Edmunds 1941), then if this phenomenon is combined with coupled lamellar growth, there is no evidence to suggest that the eutectic phases do not continue to grow in the direction imposed by their own crystal structure. Indeed the experimental results on Cd-Zn (Edmunds 1941; Nix and Schmid 1929) support this hypothesis. This combined growth effect is thought to promote lamellar spiralling in certain eutectic systems.

An attempt is made here to illustrate qualitatively the development of lamellar spiralling. The analysis is based on the anisotropic growth tendency of both phases although this might not be the only factor causing the complex spiralling phenomenon (another factor could be anisotropy of either solid/solid or solid/liquid or both interfacial energies).

Three assumptions are made for the purpose of handling the problem numerically:

(1) The anisotropic growth tendency of each phase is assumed to act as a force so that the two forces can be added vectorially to obtain a resultant "force of coupled growth" at the solid/liquid interface. The real force causing the growth directions of the individual phases to deviate from the overall growth direction of the system is of course quite complex, involving growth kinetics, surface tensions and free energy changes due to diffusion. No attempt has been made here to evaluate this force.

(2) The magnitudes of both vectors $\vec{A}$ and $\vec{B}$ (Figure 4.1) representing the anisotropic growth of both phases are related to their volume fractions, the most abundant phase being the one exerting the strongest effect during coupled growth.

(3) The behaviour of the eutectic phases (solid solutions) is considered to be the same as that of the pure metals.

FIGURE 4.1 Schematic representation of a lamellar interface. The preferred growth directions of the two phases are represented by vectors $\vec{A}$ and $\vec{B}$, while the coupled growth resultant is represented by vector $\vec{R}$. Each vector forms angles α, β and γ with the x, y and z axes, respectively; both x and y axes lying on the solid/liquid interface plane the former being at right angles and the latter parallel to the solid/solid interface boundary. The z-axis representing the growth direction of the system specified in statement B is drawn parallel to the lamellar interface and hence perpendicular to the solid/liquid interface.

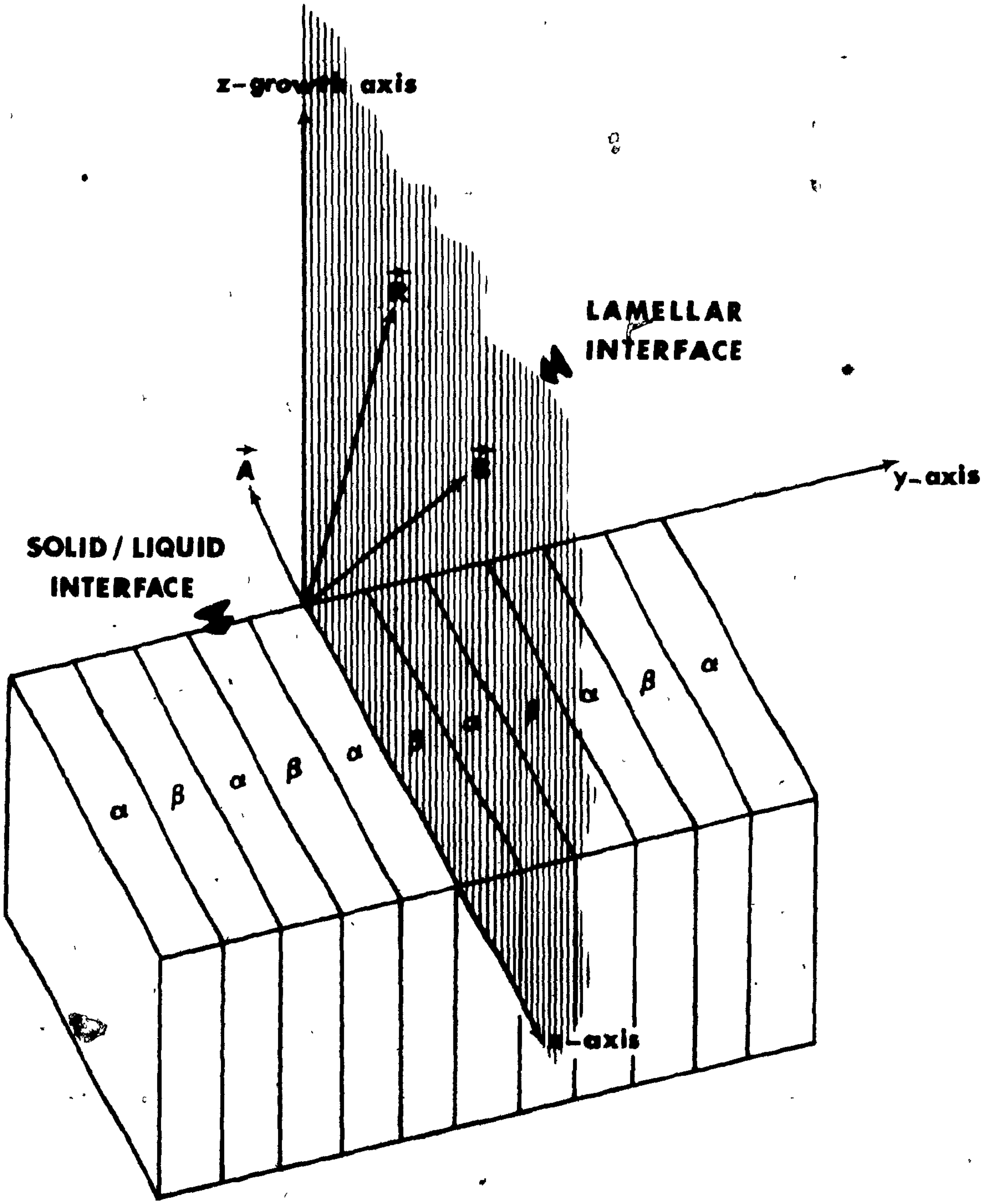
z-growth axis
LAMELLAR INTERFACE
$\vec{R}$
$\vec{B}$
$\vec{A}$
y-axis
SOLID / LIQUID INTERFACE
α
β
α
β
α
β
α
β
α
β
α
x-axis

This has been shown to be valid for the Cd-Zn eutectic (Edmunds 1941; Nix and Schmid 1929).

Figure 4.1 depicts in a general way the crystallography of the equilibrium interface of a lamellar eutectic formed when the directions specified in the B statement are brought into coincidence by overlapping the two habit planes given in statement A. The preferred growth directions of the two phases are represented by vectors $\vec{A}$ and $\vec{B}$, while the coupled growth resultant is represented by vector $\vec{R}$. Each vector forms angles α, β and γ with the x, y and z axes respectively; both x and y axes lying on the solid/liquid interface plane, the former being at right angles and the latter parallel to the solid/solid interface boundary. The z-axis representing the growth direction of the system is drawn parallel to the solid/solid interface boundary and hence perpendicular to the solid/liquid interface plane. Vectors $\vec{A}$ and $\vec{B}$ are chosen to be the closest directions within the appropriate crystallographic family to the z-growth axis of the system which is made to coincide with the directions described in statement B.

Lamellar spiralling in the five systems investigated during the present work along with the others listed in Table 4.1 will be treated below in the light of these assumptions.

4.2.2 Lead-Tin

The eutectic orientation relationships have been stated to be (Hopkins and Kraft 1968; Hopkins 1967)

LAMELLAR INTERFACE // $(0\bar{1}1)_{Sn}$ // $(1\bar{1}\bar{1})_{Pb}$ STATEMENT A

GROWTH DIRECTION // $[211]_{Sn}$ // $[211]_{Pb}$ STATEMENT B

The magnitudes and orientations of vectors $\vec{A}$, $\vec{B}$ and the coupled growth vector, $\vec{R}$, are given in Table 4.3 wherein two possible ways in which the two phases can be brought into contact at the interface are considered. A sample calculation is given in the Appendix.

From Table 4.3 and Figure 4.1 it is evident that if the two phases have the same texture that they would have in independent growth, then the interface will try to tilt by 26.67° to the z-axis and twist either to the right or to the left (Case 1 and Case 2 in Table 4.3, respectively) depending on the direction (positive or negative) in which the two eutectic constituents choose to approach one another. The solid/solid interface on the other hand will change its spatial position only if it has the degree of freedom to do so. The solid/liquid interface is isothermal, and in normal unidirectional growth the isotherms are flat and the interface is unable to tilt away from the z-axis. To explain the spiralling phenomenon we consider the three components of $\vec{R}$ and attempt to understand the relationship of each to unidirectional coupled growth of the eutectic.

(1) The vector $\vec{R}$ should be parallel to the z-axis, in other words the preferred growth directions imposed by the system should coincide with those which are operative in the absence of the coupled growth constraint. In this case the system should not exhibit lamellar spiralling as indeed will be shown later to be true for

TABLE 4.3 Coupled Growth of Phases at the Pb-Sn Eutectic Interface (Hopkins 1967; Hopkins and Kraft 1968)

Growth Direction // z-axis // $[2\underline{1}\underline{1}]_{Pb}$ // $[2\underline{1}1]_{Sn}$
Lamellar Interface // x-z plane // $(1\bar{1}1)_{Pb}$ // $(0\bar{1}1)_{Sn}$

Case 1	y-axis ⊥ lamellar interface // // $[\bar{1}11]_{Pb}$ // $[0\bar{1}1]_{Sn}$				Case 2	y-axis ⊥ lamellar interface // // $[1\bar{1}\bar{1}]_{Pb}$ // $[01\bar{1}]_{Sn}$			
	Phase Volume Fraction	Magnitude (Units of Force)	α	β	γ	$\vec{x}$	$\vec{y}$	$\vec{z}$	Preferred Growth Direction
$\vec{A}$(β-Sn*)	63%	1.7†	79.08°	1) 109.80° 2) 70.20°	22.83°	$+0.322\bar{i}$	1) $-0.576\bar{j}$ 2) $+0.576\bar{j}$	$+1.569\bar{k}$	[110]
$\vec{B}$(Pb)	37%	1.0†	90.00°	1) 125.26° 2) 54.74°	35.26°	0	1) $-0.578\bar{j}$ 2) $+0.578\bar{j}$	$+0.816\bar{k}$	[100]
$\vec{R}$(Pb+Sn)	-	2.7 (calculated)	83.06°	1) 115.61° 2) 64.39°	26.67°	$+0.322\bar{i}$	1) $-1.154\bar{j}$ 2) $+1.154\bar{j}$	$+2.385\bar{k}$	-

* β-Sn is body centred tetragonal: $a = 5.8311$ A°; $c = 3.1817$ A° at 20°C (Barrett 1952). No correction has been made for either temperature or composition.

† Values estimated from the respective phase volume fractions.

Cd-Zn. However, when $\vec{R}$ is not parallel to the z-axis, the system will try to keep the z-component of $\vec{R}$ as large as possible in order to minimize the interfacial boundary area. In extreme cases when the z-component becomes relatively small, the departure from equilibrium conditions increases, the lamellar structure would no longer be stable and as a result a degenerate structure may be produced.

(2) The x-component represents the coupled growth force resolved along the lamellae in the direction in which they elongate and would seem to be the least important of the three, although it contributes to the reduction of the z-component.

(3) The y-component would seem to be the key to the spiralling problem. If this component is large, the lamellae will tend to grow sideways and thus coupled growth becomes difficult. In the ideal case this component is zero so that the system will grow in a direction perpendicular to the solid/liquid interface. However, cases in which the lamellar interface was not parallel to the growth axis and yet lamellar coupled growth was retained have been reported: Al-Zn (Double et al. 1968), $Al-Ag_2Al$ (Ellwood and Bagley 1950) and $Al-CuAl_2$ (Davies and Hellawell 1969,1970).

Hunt (1963) suggested that when the eutectic phases are growing in a direction which is slightly off the preferred orientation imposed by the system (the deviation in our case is large), the eutectic should grow with the minimum energy interface for a short distance, then form a small step of atomic dimensions. The presence of these steps along the boundary will produce an increase in the average interphase interfacial energy so that the lamellar spacing will become wider (see Figure 4.2). Lamellae at this stage should still be stable. However, if the size of the step increases, in other words, the deviation from the preferred growth direction increases, the steps become more frequent and the average interfacial energy becomes so high that the lamellae will no longer be stable and a degenerate structure may be produced. Hunt suggested that the lamellae should break down when the rate of production of steps is greater than the rate at which they grow out.

There does not seem to be any doubt about the fact that lamellar breakdown will occur when the coupled eutectic growth direction deviates substantially from the heat flow direction. This is supported by the results of experiments carried out by Hunt and Chilton (1962-63). The system will therefore try to eliminate or at least to reduce the y-component which disturbs interfacial

FIGURE 4.2 Schematic plot of lamellar spacing, λ, against ΔT_C and ΔT_D, where ΔT_C is the average undercooling due to interfacial curvature and ΔT_D is the average undercooling due to solute building in the liquid ahead of the lamellae (Hunt 1963)

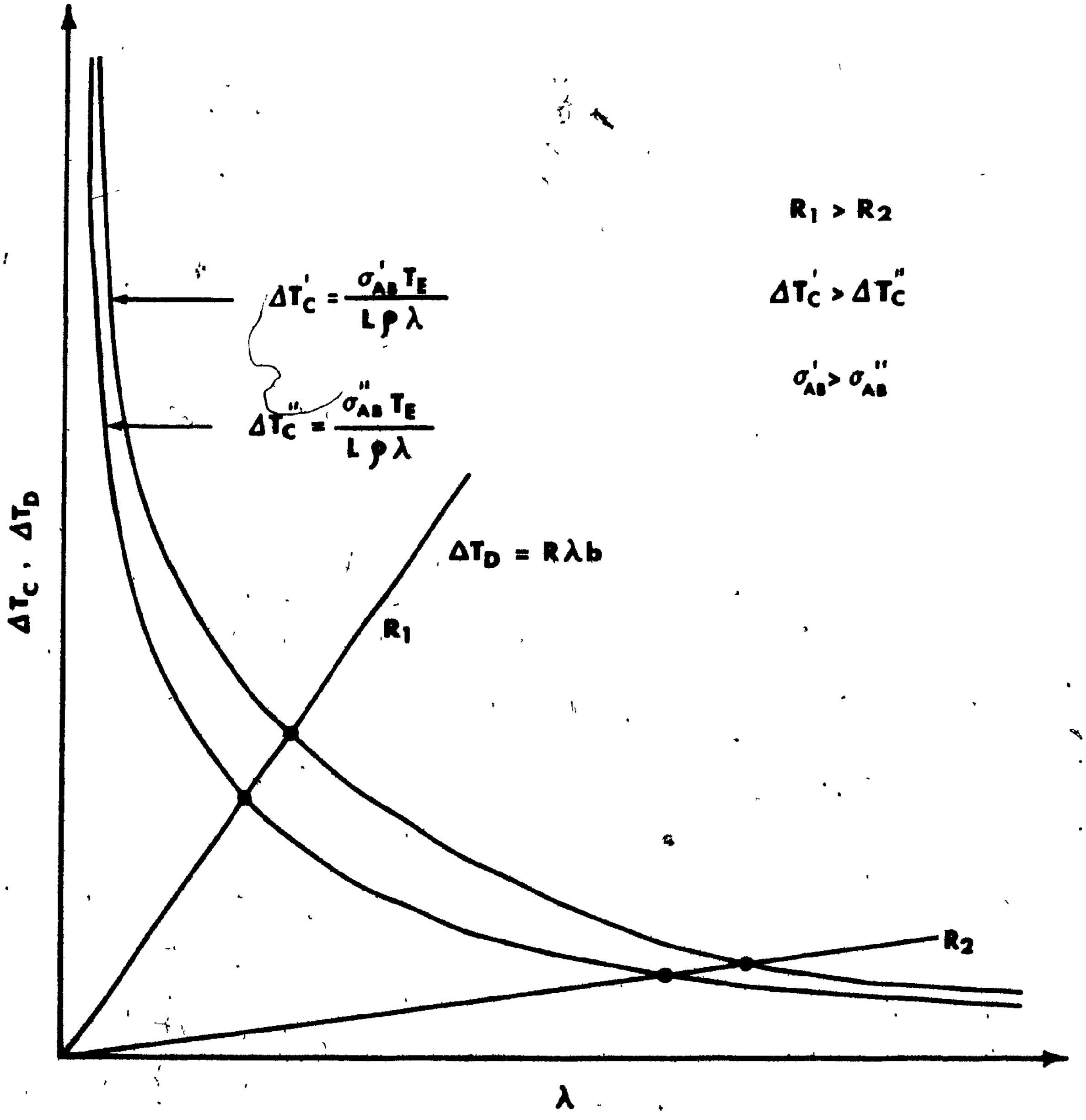
$\Delta T'_C = \frac{\sigma'_{AB} T_E}{L \rho \lambda}$
$\Delta T''_C = \frac{\sigma''_{AB} T_E}{L \rho \lambda}$
$R_1 > R_2$
$\Delta T'_C > \Delta T''_C$
$\sigma'_{AB} > \sigma''_{AB}$
$\Delta T_D = R \lambda b$
R_1
R_2
$\Delta T_C \cdot \Delta T_D$
λ

stability, and it is suggested that to do so the interface will utilize its rotational degree of freedom about the z-axis. However, as the interface rotates in an attempt to minimize $\vec{y}$, the resultant growth force, $\vec{R}$, also changes position since the crystallographic orientations are fixed. Thus the system never achieves a smaller value of $\vec{y}$ although it keeps on trying to do so, resulting in the spiralling phenomenon.

When the Pb-Sn eutectic interface in the thin films produced by the loop method (Takahashi and Ashinuma 1958-59) is analysed in the preceding manner, the system is again predicted to spiral (Table 4.4). The y-component in this case is larger than it is in the case of bulk specimens probably indicating that the spiralling rate should be higher. However, since the growth conditions are so much different from those of unidirectional freezing, it may be unwise to apply this analysis to the thin film work.

Very recently perfect grains of Pb-Sn eutectic were produced in 10 to 20 μm thick eutectic samples grown by unidirectional solidification, and the crystallographic relationship was found to be (Labulle and Petipas 1975):

LAMELLAR INTERFACE // $(\bar{1}10)_{Sn}$ // $(01\bar{1})_{Pb}$ STATEMENT A
GROWTH DIRECTION // $[110]_{Sn}$ // $[100]_{Pb}$ STATEMENT B

TABLE 4.4 Coupled Growth of Phases at the Pb-Sn Eutectic Interface
(Takakashi and Ashinuma 1958-59)

<table>
<tr><td colspan="10">Growth Direction // z-axis // $[\bar{1}\bar{1}2]_{Pb}$ // $[010]_{Sn}$
Lamellar Interface // x-z plane // $(111)_{Pb}$ // $(101)_{Sn}$</td></tr>
<tr><td colspan="5">Case 1 y-axis ⊥ lamellar interface // // $[111]_{Pb}$ // $[101/(c/a)^2]_{Sn}$</td><td colspan="5">Case 2 y-axis ⊥ lamellar interface // // $[\bar{1}\bar{1}\bar{1}]_{Pb}$ // $[\bar{1}0\bar{1}/(c/a)^2]_{Sn}$</td></tr>
<tr><td></td><td>Phase Volume Fraction</td><td>Magnitude (Units of Force)</td><td>α</td><td>β</td><td>γ</td><td>$\vec{x}$</td><td>$\vec{y}$</td><td>$\vec{z}$</td><td>Preferred Growth Direction</td></tr>
<tr><td>$\vec{A}$(β-Sn)</td><td>63%</td><td>1.7†</td><td>76.74°</td><td>1) 65.14°
2) 111.86°</td><td>28.62°</td><td>$+0.391\bar{i}$</td><td>1)$+0.716\underline{j}$
2)$-0.716\bar{j}$</td><td>$+1.495\bar{k}$</td><td>[011]</td></tr>
<tr><td>$\vec{B}$(Pb)</td><td>37%</td><td>1.0†</td><td>90.00°</td><td>1) 54.74°
2) 125.26°</td><td>35.26°</td><td>0</td><td>1)$+0.577\underline{j}$
2)$-0.577\bar{j}$</td><td>$+0.816\bar{k}$</td><td>[001]</td></tr>
<tr><td>$\vec{R}$(Pb + Sn)</td><td>-</td><td>2.7
(calculated)</td><td>81.61°</td><td>1) 61.11°
2) 118.99°</td><td>30.31°</td><td>$+0.391\bar{i}$</td><td>1)$+1.293\underline{j}$
2)$-1.293\bar{j}$</td><td>$+2.311\bar{k}$</td><td>-</td></tr>
</table>

† Values calculated from the respective phase volume fractions

Analyzing the interface of these Pb-Sn fault-free grains, the system is predicted not to spiral since the directions described in statement B for both the Pb- and Sn-rich phases coincide with those operative in the absence of coupled growth constraint (see Table 4.2). It should be noted that for the Pb-and Sn-rich phases the growth directions of the lamellae of the fault free grains, of precipitates (Tu and Turnbull 1969), of impure crystals (Hellawell and Herbert 1962) and of dendrites (Weinberg and Chalmers 1952; Walton and Chalmers 1959; Barrett 1952) are the same.

4.2.3 Aluminum-Copper

The Al-$CuAl_2$ eutectic has also been found to exhibit lamellar spiralling in a large number of investigations (Dean 1973; Hellawell 1967; Double et al. 1968) including the present one. Many sets of crystallographic relationships (statements A and B) have been reported for this system and they are all listed in Table 4.1. It should be noted that two relationships were obtained using two different techniques on specimens grown in different ways (Elwood and Bagley 1950; Takahashi 1960). The most common Al-$CuAl_2$ interface would seem to be (Kraft 1961, 1962; Kraft and Albright 1962)

LAMELLAR INTERFACE	//	$\{111\}_{Al}$	//	$\{211\}_{CuAl_2}$	STATEMENT A
GROWTH DIRECTION	//	$<101>_{Al}$	//	$<120>_{CuAl_2}$	STATEMENT B

The analysis described above for Pb-Sn was repeated for this interface with the result, listed in Table 4.5, that spiralling should occur.

The present analysis does not provide a means of evaluating the spiralling rate, and even if it did the results would not be very reliable due to the nature of the assumptions made. However, from a comparison of the y components in both the Pb-Sn and Al-CuAl$_2$ systems it should be possible to estimate the relative magnitudes of the two spiralling rates. The ratio of the y-component in the Pb-Sn to that in Al-CuAl$_2$ (from Tables 4.3 and 4.5) is ~3. Since Pb-Sn spirals at a rate of 160°/cm., then the spiralling rate of the Al-CuAl$_2$ system should be lower than that of Pb-Sn, and considering the rates to be in the ratio 3:1, Al-CuAl$_2$ is predicted to spiral at 50°/cm. for similar growth conditions. The observed rates for the Al-CuAl$_2$ system have been previously reported to range between 3 and 30°/cm. (Hellawell 1967). In the present investigation the spiralling rate was observed to be as low as 2°/cm., the differences probably being due to differing growth conditions, mainly temperature gradient.

It is interesting to note that the present analysis predicts that the interfaces described by Elwood and Bagley (1950) and Takahashi (1960) should not twist about the z-axis. These results are presented in Tables 4.6 and 4.7. It is surprising that not only does the relative orientation of the two phases in the heat flow direction change with growth technique (as was observed for the Pb-Sn system), but the habit planes also change.

TABLE 4.5 Coupled Growth of Phases at the Al-$CuAl_2$ Eutectic Interface
(Kraft 1961,1962; Kraft and Albright 1962)

Growth Direction // z-axis // $[110]$Al // $[210]CuAl_2$
Lamellar interface // x-z plane // $(\bar{1}11)$Al // $(2\bar{1}1)CuAl_2$

Case 1: y-axis ⊥ lamellar interface // $[\bar{1}11]$Al // $[2\bar{1}\ /(c/a)^2]CuAl_2$

Case 2: y-axis ⊥ lamellar interface // $[1\bar{1}\bar{1}]$Al // $[\bar{2}1\bar{1}\ /(c/a)^2]CuAl_2$

	Phase Volume Fraction	Magnitude (Units of Force)	α	β	γ	$\vec{x}$	$\vec{y}$	$\vec{z}$	Preferred Growth Direction
$\vec{A}$(Al)	55%	$1.1^\dagger$	65.91^o	1) 125.26^o 2) 54.74^o	45.00^o	$+0.454\bar{i}$	1) $-0.642\bar{j}$ 2) $+0.642\bar{j}$	$+0.786\bar{k}$	[100]
$\vec{B}(CuAl_2)$*	45%	$1.0^\dagger$	81.14^o	1) 73.87^o 2) 106.03^o	18.43^o	$+0.154\bar{i}$	1) $+0.276\bar{j}$ 2) $-0.276\bar{j}$	$+0.949\bar{k}$	[110]
$\vec{R}(Al+CuAl_2)$	-	1.3 (calculated)	71.08^o	1) 101.24^o 2) 78.76^o	22.23^o	$+0.608\bar{i}$	1) $-0.365\bar{j}$ 2) $+0.365\bar{j}$	$+1.745\bar{k}$	-

† Values calculated from the respective phase volume fractions

* $CuAl_2$ is body centred tetragonal: $a = 6.07$ A° $c = 4.87$ A° $c/a = 0.80$ (ASM Metals Handbook 1973)

TABLE 4.6 Coupled Growth of Phases at the Al-$CuAl_2$ Eutectic Interface
(Ellwood and Bagley 1950)

Growth Direction // z-axis // [100]Al // [100]$CuAl_2$
Lamellar Interface // x-z plane // (001)Al // (001)$CuAl_2$
y-axis ⊥ Lamellar Interface // [001] Al // [001] $CuAl_2$
x-axis // Lamellar Interface // [010]Al // [010]$CuAl_2$

	Phase Volume Fraction	Magnitude (Units of Force)	α	β	γ	$\vec{x}$	$\vec{y}$	$\vec{z}$	Preferred Growth Direction
$\vec{A}$(Al)	55%	$1.1^{\dagger}$	90.00°	90°	0°	0	0	$+1.111\overline{k}$	[100]
$\vec{B}$($CuAl_2$)	45%	$1.0^{\dagger}$	45.00°	90°	45°	$+0.707\overline{i}$	0	$+0.707\overline{k}$	[110]
$\vec{R}$(Al+$CuAl_2$)	-	2.0 (calculated)	68.75°	0°	21.25°	$+0.707\overline{i}$	0	$+1.818\overline{k}$	

† Values calculated from the respective phase volume fractions

TABLE 4.7 Coupled Growth of Phases at the Al-$CuAl_2$ Eutectic
(Takahashi 1960)

Growth Direction // z-axis , // [011]Al // [100]$CuAl_2$
Lamellar Interface // x-z plane // (001)Al // (001)$CuAl_2$
y-axis // [001]Al // $[001/(c/a)^2]CuAl_2$
z-axis // $[1\bar{1}0]$Al // [010]$CuAl_2$

	Phase Volume Fraction	Magnitude (Units of Force)	α	β	γ	$\vec{x}$	$\vec{y}$	$\vec{z}$	Preferred Growth Direction
$\vec{A}$(Al)	55%	1.1†	45.00^o	90.00^o	45.00^o	$+0.786\bar{i}$	0	$+0.786\bar{k}$	[100]
$\vec{B}$($CuAl_2$)	45%	1.0†	45.00^o	90.00^o	45.00^o	$+0.707\bar{i}$	0	$+0.707\bar{k}$	[110]
$\vec{R}$(Al+$CuAl_2$)	-	2.1 (calculated)	45.00^o	90.00^o	45.00^o	$+1.493\bar{i}$	0	$+1.493\bar{k}$	-

† Values calculated from the respective phase volume fractions

4.2.4 Cadmium-Zinc

The equilibrium interface in Cd-Zn has been described as (Double and Hellawell 1969b; Straumanis and Brakss 1935):

LAMELLAR INTERFACE // $(0001)_{Cd}$ // $(0001)_{Zn}$ STATEMENT A.
GROWTH DIRECTION // $[10\bar{1}0]_{Cd}$ // $[10\bar{1}0]_{Zn}$ STATEMENT B

Since the preferred growth direction of Cd and Zn individually has been found to be $<10\bar{1}0>$ which coincides with the coupled growth direction, then the fact that this eutectic does not exhibit lamellar spiralling requires little further rationalization or explanation.

4.2.5 Tin-Cadmium

It is rather unfortunate that the Sn-Cd eutectic undergoes a solid state transformation at 133^{o}C during which the hexagonal Sn-rich phase becomes body-centred tetragonal. Since only the crystallographic relationship pertaining to the equilibrium interface at room temperature has been reported for Sn-Cd (Straumanis and Brakss 1937), it is difficult to ascertain whether the system should spiral or not. However, two assumptions have been made in order to consider this problem further:

(1) The Sn-Cd system formed by the two close packed hexagonal constituents is treated as if it was similar to Cd-Zn. In other words the β-phase is assumed to have similar growth characteristics to either pure Zn or pure Cd.

(2) The room temperature interface as described by Straumanis and Brakss (1937) is considered as a eutectic growth interface:

LAMELLAR INTERFACE // $(100)_{Sn}$ // $(0001)_{Cd}$ STATEMENT A
GROWTH DIRECTION // $[001]_{Sn}$ // $[01\bar{1}0]_{Cd}$ STATEMENT B

With the first assumption no lamellar spiralling should be exhibited for the same reasons as given for Cd-Zn. No spiralling should again result from the second assumption since no y component exists because the [011] preferred growth direction in Sn lies within the lamellar interface plane (the X-Z plane) and hence only x and z components exist (see Table 4.8). These predictions agree with the experimental observations.

4.2.6 <u>Tin-Zinc</u>

This eutectic was found not to exhibit spiralling even though it is formed from two crystallographically different phases. The equilibrium eutectic interface has been described as (Straumanis and Brakss 1937):

LAMELLAR INTERFACE // $(001)_{Sn}$ // $(01\bar{1}0)_{Zn}$ STATEMENT A
GROWTH DIRECTION // $[001]_{Sn}$ // $[01\bar{1}0]_{Zn}$ STATEMENT B

For the reasons given in the section on Sn-Cd, the analysis again predicts that no spiralling should occur (see Table 4.8).

TABLE 4.8 Coupled Growth of Phases in the Sn-Cd and Sn-Zn Eutectics
(Straumanis and Brakss 1937)

Growth Direction // z-axis // [001]Sn // $[01\bar{1}0]$Zn,Cd
Lamellar Interface // x-z plane // (100)Sn // (0001)Zn,Cd
y-axis ⊥ Lamellar Interface // $[\bar{1}00]$Sn // [0001]Zn,Cd

	Phase Volume Fraction	Magnitude (Units of Force)	α	β	γ	$\vec{x}$	$\vec{y}$	$\vec{z}$	Preferred Growth Direction
$\vec{A}$(Sn)	91% 75%	10.1† 3.0†	28.62°	90.00°	61.38°	$+8.875\bar{i}$ $+2.633\bar{i}$	0 0	$+4.843\bar{k}$ $+1.436\bar{k}$	[011]
$\vec{B}$(Zn,Cd)	9% 25%	1.0† 1.0†	90.00°	90.00°	0	0 0	0 0	$+1.000\bar{k}$ $+1.000\bar{k}$	$[\bar{0}1\bar{1}0]$
$\vec{Z}$(Sn+Zn, Sn+Cd)	- -	10.6 3.6 (calculated)	33.36° 42.78°	90.00° 90.00°	56.64° 47.22°	$+8.875\bar{i}$ $+2.633\bar{i}$	0 0	$+5.843\bar{k}$ $+2.436\bar{k}$	-

† Values calculated from the respective phase volume fractions

4.2.7 Aluminum-Silver

This system was not investigated in the present study, but it has previously been found to exhibit lamellar spiralling (Double et al. 1968). The equilibrium interface was described as (Cantor 1971):

LAMELLAR INTERFACE // $(111)_{Al}$ // $(0001)_{Ag_2Al}$ STATEMENT A
GROWTH DIRECTION // $[1\bar{1}0]_{Al}$ // $[11\bar{2}0]_{Ag_2Al}$ STATEMENT B

The analysis has been applied to this system and it predicts that lamellar spiralling should occur (see Table 4.9). The close-packed hexagonal Ag_2Al phase was assumed to grow preferentially in the $[10\bar{1}0]$ direction as has been reported for Cd and Zn. It was reported (Double et al. 1968) that this system spirals more rapidly than $Al\text{-}CuAl_2$ but no figures were given. Comparing the y-components determined for both systems (Table 4.10), the analysis predicts that $Al\text{-}Ag_2Al$ should spiral more rapidly than $Al\text{-}CuAl_2$, the spiralling rate amounting to $\sim 110^\circ/cm$.

4.2.8 Aluminum-Zinc

This is the only remaining system which is known to exhibit lamellar spiralling. The equilibrium interface was studied by both X-ray analysis (Double et al. 1968) and transmission electron microscopy (Double and Hellawell 1969b). Both techniques showed that in the Zn-rich phase the lamellar interface was inclined by about 18° to the (0001) basal plane but contains the $[11\bar{2}0]$ growth direction imposed by the

TABLE 4.9 Coupled Growth of Phases at the Al-Ag_2Al Eutectic Interface (Cantor 1971)

Growth Direction // z-axis // $[\bar{1}\bar{1}0]$Al // $[11\bar{2}0]$$Ag_2$Al
Lamellar Interface // x-z plane // (111)Al // (0001)Ag_2Al

Case 1: y-axis ⊥ lamellar interface // [111]Al // [0001]Ag_2Al

Case 2: y-axis ⊥ lamellar interface // $[\bar{1}\bar{1}\bar{1}]$Al // $[000\bar{1}]$$Ag_2$Al

	Phase Volume Fraction	Magnitude (Units of Force)	α	β	γ	$\vec{x}$	$\vec{y}$	$\vec{z}$	Preferred Growth Direction
$\vec{A}$(Al)	60%	$1.5^{\dagger}$	65.91°	1) 54.74° 2) 125.26°	45.00°	+0.564$\overline{i}$	1)+0.866$\overline{j}$ 2)-0.866$\overline{j}$	+1.061$\overline{k}$	[100]
$\vec{B}$(Ag_2Al)	40%	$1.0^{\dagger}$	60.00°	1) 90.00° 2) 90.00°	30.00°	+0.500$\overline{i}$	0	+0.866$\overline{k}$	$[10\bar{1}0]$
$\vec{R}$ (Al+Ag_2Al)	-	2.4 (calculated)	62.23°	1) 68.73° 2) 111.27°	36.19°	+1.112$\overline{i}$	1)+0.866$\overline{j}$ 2)-0.866$\overline{j}$	+1.927$\overline{k}$	-

† Values calculated from the respective phase volume fractions

TABLE 4.10 List of Measured and Predicted Spiralling Rates

System	$\lvert y \rvert$ (Units of Force)	Predicted Rate of Spiralling	Observed Rate of Spiralling	References
Pb-Sn	1.154	-	160°/cm	Hopkins and Stewart 1970; Present Work
Al-Ag$_2$Al	0.866	†110°/cm	-	Double et al. 1968
Al-CuAl$_2$	0.365	† 50°/cm	2°/cm* - 3 to 30°/cm	*Present Work; Hellawell 1967; Double et al. 1968
Cd-Zn	0	0	0	Present Work
Sn-Cd	0	0	0	Present Work
Sn-Zn	0	0	0	Present Work
Al-Zn	-	-	4.3°/cm	Double et al, 1968

† Roughly estimated values based on the fact that the Pb-Sn rate of spiralling in round samples is 160°/cm at $R = 2.3$ cm/hr. and $G = 7.1^{\circ}$C/cm

system, so that the habit planes correspond approximately to $(10\bar{1}8)$. The reported rates of spiralling were $\sim 4.3^{\circ}$/cm. (Double et al. 1968). No orientation relationship for the Al-rich phase could be obtained because of the eutectoid reaction which takes place at 265°C. For this reason the equilibrium interface could not be treated by the present method. A list of all the y-components evaluated by the above analysis is given in Table 4.10.

4.3 EFFECT OF GROWTH CONDITIONS ON SPIRALLING

4.3.1 Temperature Gradient

During this study the spiralling rate in Pb-Sn specimens grown by the Bridgeman technique was found to be directly related to the temperature gradient. These results do not agree either with the observations of Double et al. (1968) on specimens of Bridgeman-grown Al-Zn eutectic, or with those of Hopkins and Stewart (1970). Although no appreciable variations in subgrain density and grain misorientation were found to result from varying temperature gradients in a single Pb-Sn specimen, a marked increase in subgrain density and grain misorientation was noticed in going from a Pb-Sn sample grown under a constant relatively low temperature gradient (7.1°C/cm.) to another grown under varying G, the temperature gradient decreasing from the beginning of the sample where it was (50°C/cm.). The grain misorientations varied from 10-20° in the first case to 30-40° in the second case, while the subgrain density increased from an average of 5 to an average of 11. These results also do not confirm the observations of Double et al. (1968) and Hopkins and Stewart (1970). The reason for which no appreciable changes in grain misorientation and subgrain density could be detected as G varied is probably due to the fact that the system, in order to spiral at a higher rate, nucleated quite a large number of faults which could not be eliminated as fast as G was decreased. In longer samples grown under a temperature gradient decreasing at a slower rate, the variation in subgrain density and grain misorientation may be noticeable.

The mechanism of lamellar spiralling seems to be related to eutectic structural defects. In fact an increase in spiralling rate was observed to be accompanied by an increase in grain misorientation and subgrain density. From Figure 1.7 showing a near longitudinal ($<5^o$) taper section through an Al-$CuAl_2$ eutectic specimen, it is evident that lamellar twisting takes place through the nucleation and elimination of faults. However, the presence of faults in a lamellar structure does not necessarily imply the existence of lamellar spiralling. This point is supported by the fact that both faulted and fault-free Sn-Cd grains as well as faulted Cd-Zn and Sn-Zn grains did not spiral.

4.3.2 Mold Shape

It is not yet understood why temperature gradient and mold shape should affect lamellar spiralling. It seems, however, that this growth phenomenon is highly surface tension dependent and that the shape of the solid/liquid interface may control the spiralling rate. This might explain why Hopkins and Stewart (1970) observed a higher spiralling rate for Bridgeman-grown samples than for Czochralski-grown samples since interfacial curvature is more convex during the second growth technique. As suggested by Hunt (1963) surface energy anisotropy might be the reason for which the eutectic phases prefer to grow in certain directions, growth being facilitated by lower undercoolings. If these preferred directions do not lie on the lamellar interface plane, the system will spiral trying to bring them onto the interface boundary but this condition will never be achieved because the habit planes have been presumably selected to form an interface of minimum energy and cannot for this reason be changed, so the system will spiral indefinitely. If the preferred growth directions lie on the interface plane, the lamellae will tend to grow in the heat flow direction as observed for the Cd-Zn, Sn-Cd and Sn-Zn systems.

The shape of the solid/liquid interface (concavity or convexity) might increase or decrease the deviation of the resultant coupled growth direction from the z-growth axis and a higher or lower spiralling rate might result. When the deviation increases to the point that coupled growth is destroyed, there is no longer any need for the system to spiral as was observed for the case of the degenerate Pb-Sn structure.

4.4 THE LAMELLAR BENDING EFFECT

Double and Hellawell (1969a) using an interference technique observed that lamellae have a tendency to fan out at subgrain boundaries (Figure 1.8). As a result of these studies they attributed the spiral growth phenomenon to the fact that lamellae could be tilted and at the same time grow in a fan-like arrangement as shown in Figure 1.9. Thus, when viewed on consecutive transverse sections the lamellae will seem to change their position from section to section, in other words they will give the impression of moving in a spiral fashion due to the combination of fanning and tilting effects. Although this explanation of spiralling is quite plausible, it is not substantiated by observation on lamellar systems which spiral. The fanning proposed by Double and Hellawell (1969a) will occur only in the presence of high angle subgrain boundaries which are relatively uncommon and moreover do not appear to occur with a variable frequency in systems which spiral on the one hand and do not on the other. Thus, although the explanation is plausible in principle, metallographic observations would seem to indicate that situations such as those described by Double and Hellawell (1969a) occur infrequently.

Using the same interference technique, the lamellae in all systems investigated in this work (except Sn-Zn) were observed to curve across transverse sections whether the eutectic exhibited spiralling or not (see Figures 3.1(b), 3.2(c), 3.3(b), 3.5(b), 3.19(b) and 3.20(b)). The bending effect would therefore seem to be a feature associated with lamellar eutectic growth in general and is probably not related to spiralling. It should be noticed in the transverse microsections of the systems investigated, that bending takes place through faults and other structural imperfections, such as lamellar distortions. The only case in which the lamellae were observed to be smoothly curved was in the perfect Sn-Cd grains within which structural imperfections were completely absent (Figure 3.2(c)).

The bending effect is believed to be caused by a stress which is generated either at the solid/liquid interface or at the solid/solid interface during growth. At this stage, it is not possible to state the nature of this stress, but it may be due to thermal effects or to a consequence of atomic mismatch across the solid/solid boundary. For example, it is known that partial complete coherency of even two similar crystals having different lattice parameters results in a state of stress at the interface. This concept is substantiated by the observation that Sn-Zn lamellae do not bend. They have been shown to be of a broken or "swiss-cheese" nature and it would be expected that a large measure of stress relief would occur in such a structure.

4.5 DEGENERACY IN LEAD-TIN

Lamellar structures generally result from unidirectional solidification when the alloys are prepared from high purity materials. In the presence of impurities lamellar eutectics generally undergo the lamellar-to-rod transition. This was first thought to be due solely to impurities until Hunt and Chilton (1962-63) proved that impurities are only indirectly responsible for this morphological transition as their function is to stabilize a curved cellular solid/liquid interface. They reached this conclusion as a result of growing very pure eutectic alloys in a graphite boat containing a graphite inset around which the solid/liquid interface was forced to curve. The lamellae broke down into rods near the inset, indicating that the direction of growth, being subject to changes due to interfacial curvature, is the main determining factor in causing the lamellar-to-rod transition, and that neither the growth rate (Tiller 1958) nor the presence of impurities (Chilton and Winegard 1960-61) have a direct effect on structural stability. Systems showing this type of morphological transition are Sn-Cd, Cd-Zn, Pb-Cd, Al-Zn and Sn-Zn. On the other hand, the Pb-Sn structure was observed to become degenerate under conditions for which the other systems formed rods (Hunt and Chilton 1962-63; Hunt 1963). According to Hunt's and Chilton's analysis such a behaviour is to be expected since the volume fraction of the minor Pb-rich phase exceeds their 32% limit, actually approaching 50%. It should be noted, however, that the Al-$CuAl_2$ eutectic with about 45% by volume of $CuAl_2$ has been found to solidify in lamellar (Kraft and Albright 1962; Takahashi 1960; Chadwick 1962-63a; Cooksey et al. 1964; Dean and Gruzleski 1973), degenerate (Davies and Hellawell 1970; Dean and Gruzleski 1973) and rod-like morphologies (Hogan 1965; Chadwick 1962-63b).

The Pb-Sn degeneracy has been investigated by Hunt (1963) who concluded that the stable lamellar structure tends to break down at growth rates lower than 3 cm/hr. and greater than 36 cm/hr. The breakdown was at first attributed to the repeated nucleation of Pb on the tips of the Sn lamellae. However, Hunt observed a small degree of undercooling associated with the solid/liquid interface at the low growth rates at which degenerate grains are produced and he consequently felt that degeneracy results when the two eutectic phases grow under conditions of unfavourable relative orientation. High growth-rate degeneracy was attributed to the concave shape of the solid/liquid interface which prevents the unsuitably oriented grains from growing out (Figure 4.3). This was substantiated by growing a Pb-Sn sample with a concave solid/liquid interface at a growth rate (12 cm/hr.) at which lamellar grains had normally been produced. As a result, degenerate grains were obtained which were absent when the same sample was regrown with a planar solid/liquid interface. The concept that degeneracy is orientation dependent is also supported by the fact that degenerate eutectic grains have been found to grow adjacent to stable lamellar grains (Figure 3.4(b)), relative orientation presumably being the only parameter that differs between adjacent grains within the same sample.

Degenerate structures similar to those found in the Pb-Sn system have also been observed in the $Al-CuAl_2$ eutectic (Davies and Hellawell 1970; Chadwick 1972; Dean and Gruzleski 1973); however, the degenerate structure is observed only at very low growth rates (Chadwick 1972). For this reason, Hunt (1963) suggested that degeneracy in general tends to be a low growth rate effect, and that higher rate degeneracy is particular to the Pb-Sn eutectic and other eutectics in which one phase readily nucleates on the other. Even if grain selection is much faster at high growth rates because of the larger difference in undercooling between grains of different interphase boundary energy (Figure 4.2), degenerate grains will always be present if they are

FIGURE 4.3 Diagram showing that grains tend to grow out at a convex interface whereas new grains tend to be nucleated at concave interfaces (Hunt 1963)

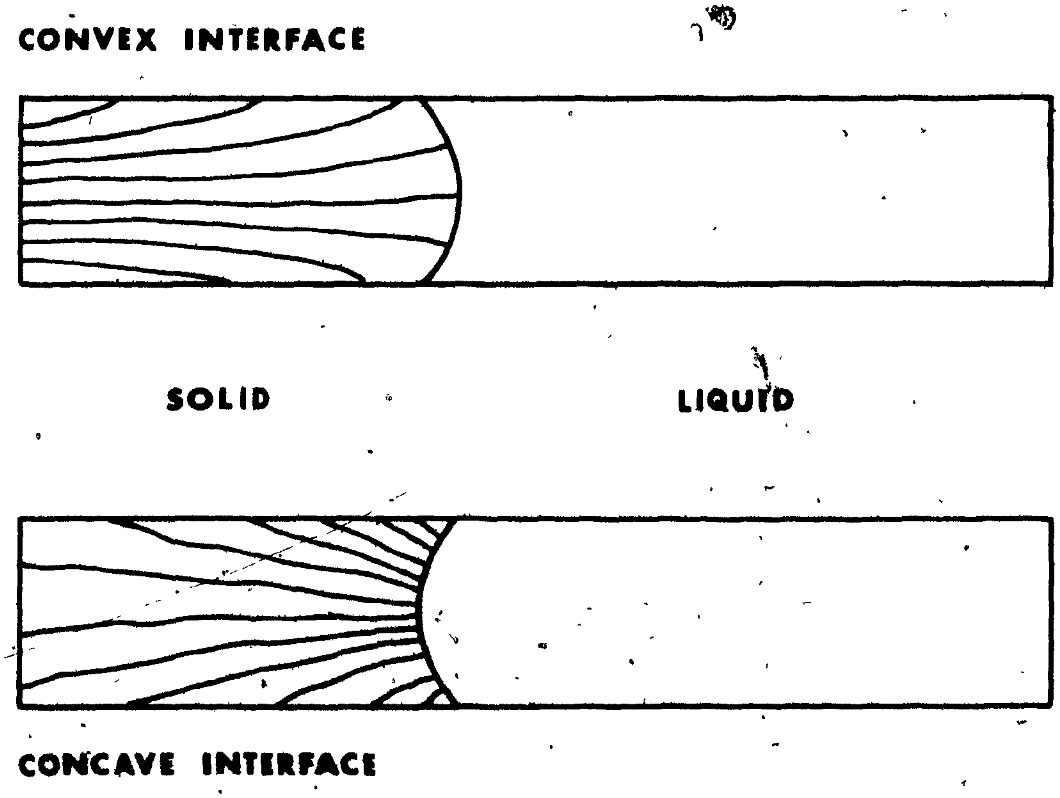
CONVEX INTERFACE
SOLID
LIQUID
CONCAVE INTERFACE

nucleated faster than they grow out. As Sundquist and Mondolfo (1961b) and Hunt (1963) have shown, the Pb-rich phase nucleates very easily on the Sn-rich phase with a supercooling as small as 1.25°C. Undercoolings of this size may exist at the solid/liquid interface when the eutectic is grown rapidly thereby leading to the nucleation of new eutectic grains or irregularities in the structure (Hunt 1963). Hunt observed that the grain size tended to be very small at high growth rates and that new grains which were continually nucleated at the edge of the boat did not grow out easily due to the concave shape of the solid/liquid interface.

Hogan et al. (1970) suggested that steep temperature gradients would be expected to flatten the solid/liquid interface, thereby diminishing the variation in local growth direction along the interface itself. The high-growth-rate degeneracy can therefore be delayed until much higher growth rates are attained if the imposed temperature gradient is high enough to sufficiently flatten the interface, thus increasing the rate at which unfavourably oriented grains grow out. On the other hand, degenerate structures can be obtained at intermediate growth rates if the imposed temperature gradient is so low that the solid/liquid interface cannot be prevented from becoming concave.

During the present investigation Pb-Sn samples were grown at rates varying from 2.3 to 15.0 cm/hr. under temperature gradients ranging between 5.5 and 28.6°C/cm. The various growth conditions are listed in Table 4.11.

TABLE 4.11 Growth Conditions for Pb-Sn Samples

Sample #	R(cm/hr)	G(^{o}C/cm)	G/R	Morphology
1	15.0 - 4.0	7.0 - 12.0	0.5 - 3.0	degenerate
2	2.3	7.1	3.4	lamellar
3	11.0	5.5	0.5	degenerate
4	11.0	8.5	0.8	lamellar
5	12.0	28.6	2.4	lamellar
6	10.2	22.0	2.2	lamellar

Samples containing only degenerate grains were obtained under two conditions:

(1) when the G/R ratio was less than 0.8°C hr/cm^2

(2) when the eutectic specimen was grown rapidly for the first centimeter and then the growth rate was lowered in an attempt to produce fault-free grains.

A plot of G vs. R (Figure 4.4) yields a line passing through the origin and separating the graph into two regions, one in which only lamellar morphologies are produced and the other in which degenerate lamellae are stable. Due to the lack of experimental points it is not possible to determine exactly the slope of the line which defines the limiting value of G/R. At this stage it is possible to state only that the G/R limit lies somewhere between 0.5 and 0.8°C hr/cm^2. Of course this limit can vary with impurity content with which it would be expected to increase.

In order to investigate the effect of growth rate and temperature gradient individually on the morphological stability, G and 1/R were plotted vs. G/R (Figure 4.5). From a comparison of the slopes of the two straight lines it may be concluded that the stability of the lamellae is most strongly affected by temperature gradient, the growth rate having a less marked effect. This observation partly supports Hunt's and Chilton's experimental results (1962-63) which indicated that the direction of growth, being subject to localized variations at a curved solid/liquid interface, is the major factor in determining structural stability. It should be noted that in sample 1 (Table 4.11)

FIGURE 4.4 Plot of G vs. R for zone refined Pb-Sn alloys

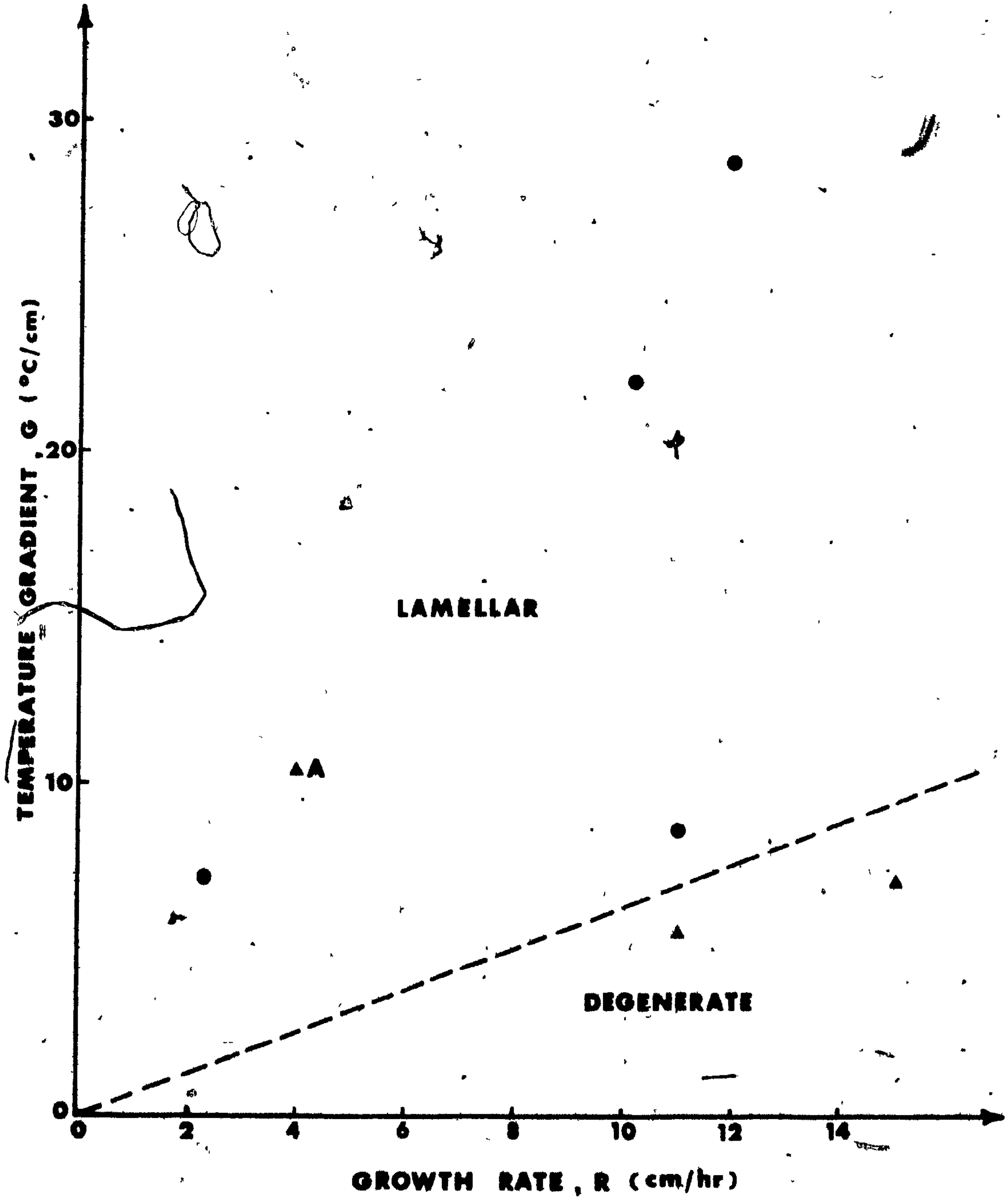

TEMPERATURE GRADIENT, G (°C/cm)
30
20
10
0
LAMELLAR
▲A
DEGENERATE
0
2
4
6
8
10
12
14
GROWTH RATE, R (cm/hr)

FIGURE 4.5 Effect of G and R on the Pb-Sn morphological stability

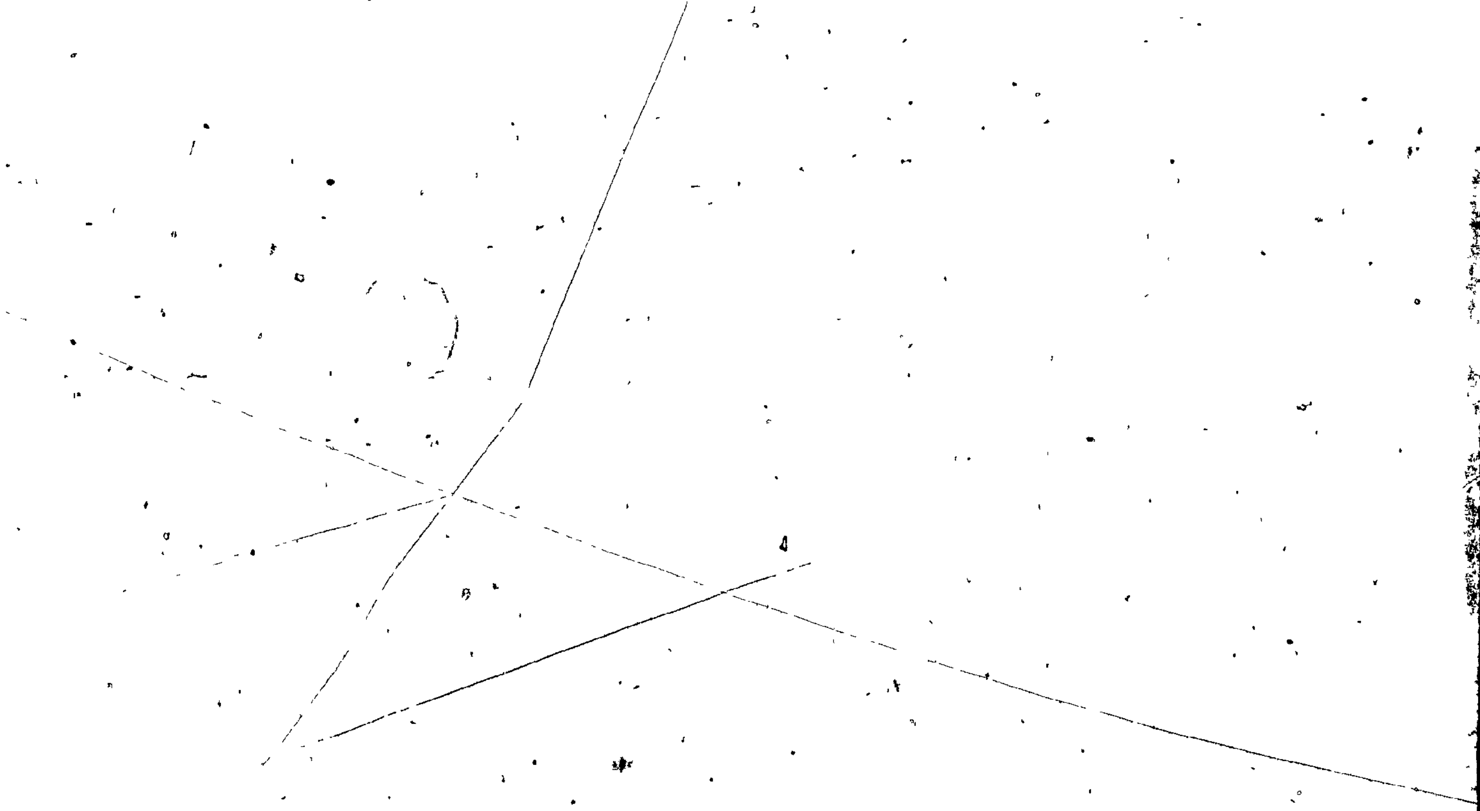

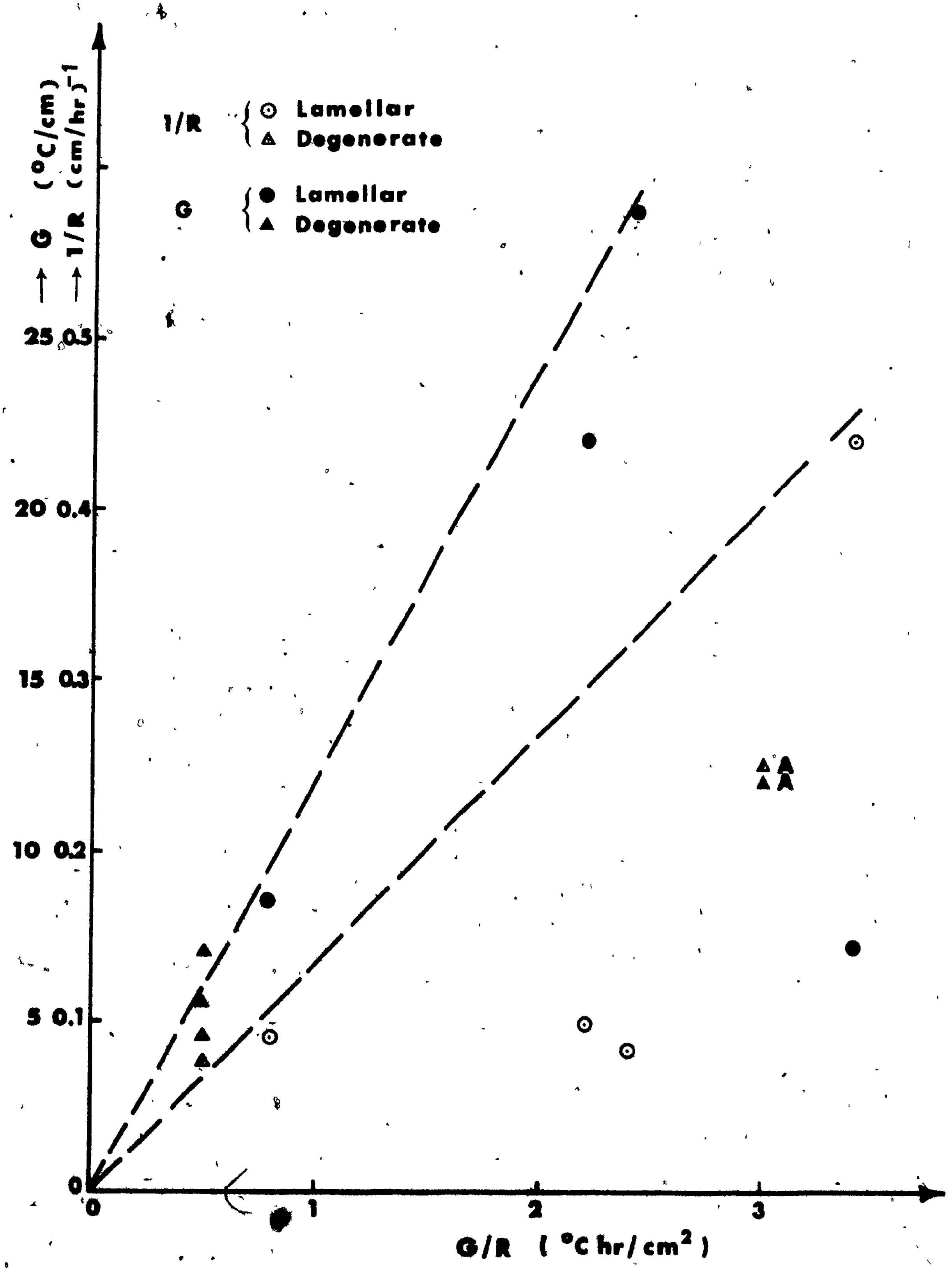

1/R { ⊙ Lamellar
△ Degenerate
G { ● Lamellar
▲ Degenerate
→ G (°C/cm)
→ 1/R (cm/hr)$^{-1}$
25 0.5
20 0.4
15 0.3
10 0.2
5 0.1
0
0
1
2
3
G/R (°C hr/cm^2)

grown first rapidly with a low G/R ratio and then slowly with a G/R ratio higher than the limit value, only degenerate grains were obtained. This might be due to the fact that when the growth rate is high (low G/R), the elimination of unfavourably oriented grains is slow due to the concave shape of the interface. However, even when the growth conditions were changed to favour stable grains on a flat interface (high G/R), the less stable grains did not grow out easily within the solidification distance used. This explains the presence of point A representing degenerate structure in the stable lamellar region in Figures 4.4 and 4.5.

4.6 SUGGESTIONS FOR FURTHER WORK

On the basis of the above discussion it is thought that the following experiments are necessary to eluciditate further certain aspects of lamellar spiralling and to test the validity of the spiral growth analysis:

(1) Investigation of the effect of growth rate on lamellar spiralling.

(2) Determination of the Pb-Cd interface crystallography to predict through the spiral growth analysis if the system should spiral or not.

(3) Production of Pb-Cd grains of sizes suitable for grain detection from section to section through lamellar orientation measurements indicating if the system does or does not spiral during growth.

(4) Other systems which can possibly be investigated for lamellar spiralling and whose interface crystallographies have been determined (Hogan et al. 1973, p.120) are: Ag-Cu, Bi-Cd, Co-CoAl, Ni-NiBe, Ni-Ni_3Cb, Ni-Cr, Ni-NiMo and Ni-Ni_3Ti.

(5) Investigation of the effect of structural imperfection on lamellar spiralling. This is suggested to be done on a sample grown at constant growth rate under varying temperature gradient which should increase from the bottom to the top of the specimen to see if the fault density increases with solidification distance.

CONCLUSIONS

The present thesis involved an investigation of the spiralling behaviour observed in certain lamellar eutectics. The systems studied were systems of low eutectic melting point whose interface crystallographic orientation relationships were previously determined.

As a result of the study, the following general conclusions can be made:

(1) The Sn-Cd system does not exhibit lamellar spiralling whether in the faulted or fault-free state.

(2) Spiralling is a feature of Pb-Sn stable lamellae. The spiralling rate was observed to be 160°/cm in cylindrical ingots (6 mm. in diameter) directionally solidified at a growth rate of 2.3 cm/hr. under a temperature gradient of 7.1°C/cm; however, when the structure broke down into degenerate lamellae, the system failed to exhibit lamellar spiralling.

(3) Cd-Zn and Sn-Zn eutectics do not spiral.

(4) The Al-$CuAl_2$ system spirals during growth although the rate of spiralling is lower than that observed in Pb-Sn for similar growth conditions.

(5) The spiral growth analysis leads to the following conclusions which are in agreement with the experimental results obtained:

(i) The Sn-Cd, Cd-Zn and Sn-Zn systems should not exhibit lamellar spiralling since the preferred growth direction of the individual phases lies within the habit plane forming the solid/solid interface boundary.

(ii) The Pb-Sn systems should exhibit lamellar spiralling when forming stable lamellae. The crystallographic orientation relationships for the degenerate structure have not yet been investigated so that no predictions can be made in this case.

(iii) The Al-CuAl$_2$ eutectic is expected to spiral due to the existing y-component of growth the magnitude of which, being smaller than that predicted for Pb-Sn, probably indicates a lower spiralling rate.

(iv) The Al-Ag$_2$Al system is also predicted to spiral at a faster rate than Al-CuAl$_2$.

(6) Growth conditions affect lamellar spiralling in the following ways:

(i) An increase in temperature gradient leads to an increase in spiralling rate accompanied by an increase in grain misorientation and subgrain density. This indicates that spiralling takes place through faults without implying that the presence of faults necessitates lamellar spiralling since Sn-Cd, Cd-Zn and Sn-Zn faulted grains failed to exhibit lamellar spiralling.

(ii) Varying the mold shape changes the spiralling rato. In rectangular Pb-Sn ingots (2 cm x 0.5 cm x 20 cm) directionally solidified at a growth rate of 1.7 cm/hr. under a temperature gradient of 4.0^{o}C/cm, the spiralling rate was observed to be lower than in the case of cylindrical ingots (50^{o}/cm vs. 160^{o}/cm). It seems that by making the samples flatter, the crystallographic orientation relationships are varied due to the different heat flow conditions resulting in a smaller y-component which leads to a lower spiralling rate. In fact, perfect grains were obtained in very thin Pb-Sn films in which the interface crystallography indicated that both the Pb- and Sn-rich phases grow in the directions operative under uncoupled growth conditions. (Labulle and Petipas 1975)

(7) Lamellar bending across transverse sections was observed in all the systems investigated (except Sn-Zn) whether they spiralled or not. This seems to be associated with eutectic growth and is probably not related to spiralling. The bending effect is believed to be caused by a stress generated either at the solid/liquid or solid/solid interface by thermal effects or as a consequence of atomic mismatch across the lamellar interface.

REFERENCES

ASM Metals Handbook, Vol.8, 8th Edition (1973).

Barrett, C.S., "Structure of Metals", McGraw Hill (1952).

Berthou, P. and Gruzleski, J.E., J. Cryst. Growth, 10 (1971) 285.

Bibring, H., "Mechanical Behaviour of Unidirectionally Solidified Composites", Proceedings of The Conference on "Insitu Composites", Connecticut, U.S.A. (1973).

Bolling, G.F., Kramer, J.J. and Tiller, W.A., Trans. Met. Soc. AIME, 227 (1963) 47.

Cantor, B., Thesis, Cambridge University (1971) reported by Chadwick (1972) p.124.

Cantor, B. and Chadwick, G.A., J. Cryst. Growth, 23 (1974) 12.

Chadwick, G.A., Acta Met., 10 (1962) 1.

Chadwick, G.A., J. Inst. Metals, 91 (1962-63a) 169.

Chadwick, G.A., J. Inst. Metals, 91 (1962-63b) 298.

Chadwick, G.A., J. Inst. Metals, 10 (1965) 178.

Chadwick, G.A., Met. Sci. J., 1 (1967) 132.

Chadwick, G.A., "Metallography of Phase Transformations", Butterworth and Co. Ltd. (1972).

Chalmers, B., "Principles of Solidification", John Wiley and Sons (1964) 143.

Chilton, J.P. and Winegard, W.C., J. Inst. Metals, 89 (1960-61) 162.

Cooksey, D.J.S., Munson, D., Wilkinson, M.P., and Hellawell, A., Phil. Mag., 10 (1964) 745.

Davies, I.G. and Hellawell, A., Phil. Mag., 19 (1969) 1285.

Davies, I.G. and Hellawell, A., Phil. Mag., 22 (1970) 1255.

Davies, V. de L., J. Inst. Metals, 93 (1964) 10.

Day, M.G. and Hellawell, A., Proc. Roy. Soc. Ser. A., 305 (1968) 473.

Dean, H., M. Sc. Thesis, McGill University (1973).

Dean, H. and Gruzleski, J.E., J. Cryst. Growth, 19 (1973) 253.

Double, D.D., Truelove, P. and Hellawell, A., J. Cryst. Growth, 2 (1968) 191.

Double, D.D. and Hellawell, A., Phil. Mag., 19 (1969a) 1299.

Double, D.D. and Hellawell, A., J. Cryst. Growth, 6 (1969b) 107.

Double, D.D., Ph.D. Thesis, Oxford University (1971).

Double, D.D., Mat. Sci. and Eng., 11 (1973) 325.

Edmunds, G.E., Trans. Met. Soc. AIME, 143 (1941) 183.

Edmunds, G.E., Trans. Met. Soc. AIME, 161 (1945) 114.

Elbaum, C. and Chalmers, B., Canad. J. Physics, 33 (1955) 196.

Ellwood, E.C. and Bagley, K.Q., J. Inst. Metals, 76 (1950) 631.

Gruzleski, J.E. and Winegard, W.C., J. Inst. Metals, 96 (1968) 301.

Gruzleski, J.E. and Kraft, R.W., to be published, reported by Hogan et al. (1970) p.126.

Hellawell, A. and Herbert, P.M., Proc. Roy. Soc. (London)A, 269 (1962) 560.

Hellawell, A., Proceedings of the Conference on "The Solidification of Metals", Brighton (1967) 264.

Hertzberg, R.W., Lemkey, F.D. and Ford, J.A., Trans. Met. Soc. AIME, 233 (1965) 342.

Hirsch, P.B., Howie, A., Nicholson, R.B., Pashley, D.W. and Whelan, M.J., "Electron Microscopy of Thin Crystals", Butterworth (London), (1965) 375.

Hogan, L.M., J. Aust. Inst. Metals, 6 (1961) 279.

Hogan, L.M., J. Inst. Metals, 93 (1964-65) 505.

Hogan, L.M., J. Aust. Inst. Metals, 10 (1965) 78.

Hogan, L.M., Kraft, R.W. and Lemkey, F.D., "Advances in Materials Research, 5, John Wiley & Sons (1970).

Hopkins, R.H., Ph. D. Thesis, Lehigh University (1967).

Hopkins, R.H. and Kraft, R.W., Trans. Met. Soc. AIME, 242 (1968) 1627.

Hopkins, R.H. and Stewart, A.M., Phil. Mag., 22 (1970) 199.

Hunt, J.D. and Chilton, J.P., J. Inst. Metals, 91 (1962) 338.

Hunt, J.D., Ph. D. Thesis, Cambridge University (1963).

Hunt, J.D. and Jackson, K.A., Trans. Met. Soc. AIME, 236 (1966) 843.

Hurles, D.T.J. and Hunt, J.D., "Structure of Directionally Solidified Semiconductor Eutectics", Proceedings of the Conference on "The Solidification of Metals", Brighton (1967).

Jackson, K.A., "Liquid Metals and Solidification", ASM, Cleveland, Ohio (1958a) 174.

Jackson, K.A., "Growth and Perfection of Crystals", ed. by Doremus, R.H., Roberts, B.W. and Turnbull, D., John Wiley & Sons, N.Y., (1958b) 319.

Jackson, K.A. Progress in Solid State Chemistry, 4 (1967) 53.

Jaffrey, D. and Chadwick, G.A., J. Inst. Metals, 97 (1969) 118.

Kraft, R.W. and Albright, D.L., Trans. Met. Soc. AIME, 221 (1961) 95.

Kraft, R.W., Trans. Met. Soc. AIME, 221 (1961) 704.

Kraft, R.W., Trans. Met. Soc. AIME, 224 (1962) 65.

Kraft, R.W. and Albright, D.L., Trans. Met. Soc. AIME, 224 (1962) 1176.

Kraft, R.W., Trans. Met. Soc. AIME, 227 (1963) 393.

Labulle, B. and Petipas, C., J. Cryst. Growth, 28 (1975) 279.

Lee, J.A. and Raynor, G.V., Proc. Phys. Soc. (London), 367 (1954) 737.

Mehl, R.F., Barrett, C.S. and Rhines, F.N., Trans. Met. Soc. AIME, 99 (1932) 203.

Mondolfo, L.F., J. Aust. Inst. Metals, 10 No.2 (1965) 169.

Moore, A., Ph. D. Thesis, Manchester University (1967).

Moore, A. and Elliott, R., J. Inst. Metals, 96 (1968) 62.

Nix, F.C. and Schmid, E., Z. Metallk., 21 (1929) 286.

Oster, G., "The Science of Moiré Patterns", 2nd Edition, publ. Edmund Scientific, N.Y. (1969) 16.

Racek, R., Lesoult, G. and Turpin, M., J. Cryst. Growth, 22 (1974) 210.

Rosenberg, A. and Tiller, W.A., Acta Met., 5 (1957) 565.

Scheil, E., Z. Metallk., 37 (1946) 1.

Scheil, E., Giesserei, 24 (1959) 1313.

Southin, R.T. and Jones, B.L., J. Aust. Inst. Metals, to be published, reported by Jaffrey and Chadwick (1969) p.118.

Straumanis, W. and Brakss, N., Z. Phys. Chem., 30 B (1935) 117.

Straumanis, W. and Brakss, N., Z. Phys. Chem., 38 B (1937) 140.

Sundquist, B.E. and Mondolfo, L.F., Trans. Met. Soc. AIME, 221 (1961a) 157.

Sundquist, B.E. and Mondolfo, L.F., Trans. Met. Soc. AIME, 221 (1961b) 607.

Takahashi, N. and Ashinuma, K., J. Inst. Metals, 87 (1958-59) 19.

Takahashi, N., J. Appl. Phys., 31, No.7 (1960) 1287.

Taylor, P.J., Kerr, H.W. and Winegard, W.C., Canad. Met. Quart., 3 (1964) 235.

Tiller, W.A., "Liquid Metals and Solidification", ASM, Cleveland, Ohio (1958) 276.

Tu, K.N. and Turnbull, D., Acta Met., 17 (1969) 1263.

Tyzak, C. and Raynor, G.V., Acta Cryst. 7 (1954) 505.

Walton, D. and Chalmers, B., Trans. Met. Soc. AIME, 215 (1959) 447.

Weinberg, F. and Chalmers, B., Can. J. Phys., 30 (1952) 488.

Yue, A.S., Chang, Y.W. and Mathur, M.P., Proceedings of the Conference on "Insitu Composites", Lakeville (1972) 79.

Zener, C., Trans. Met. Soc. AIME, 167 (1946) 550.

APPENDIX

SAMPLE CALCULATION OF SPIRAL GROWTH ANALYSIS
FOR
THE Pb-Sn INTERFACE
(HOPKINS AND KRAFT 1968; HOPKINS 1967)

LAMELLAR INTERFACE // $(1\bar{1}\bar{1})_{Pb}$ // $(0\bar{1}1)_{Sn}$ STATEMENT A

GROWTH DIRECTION // $[211]_{Pb}$ // $[211]_{Sn}$ STATEMENT B

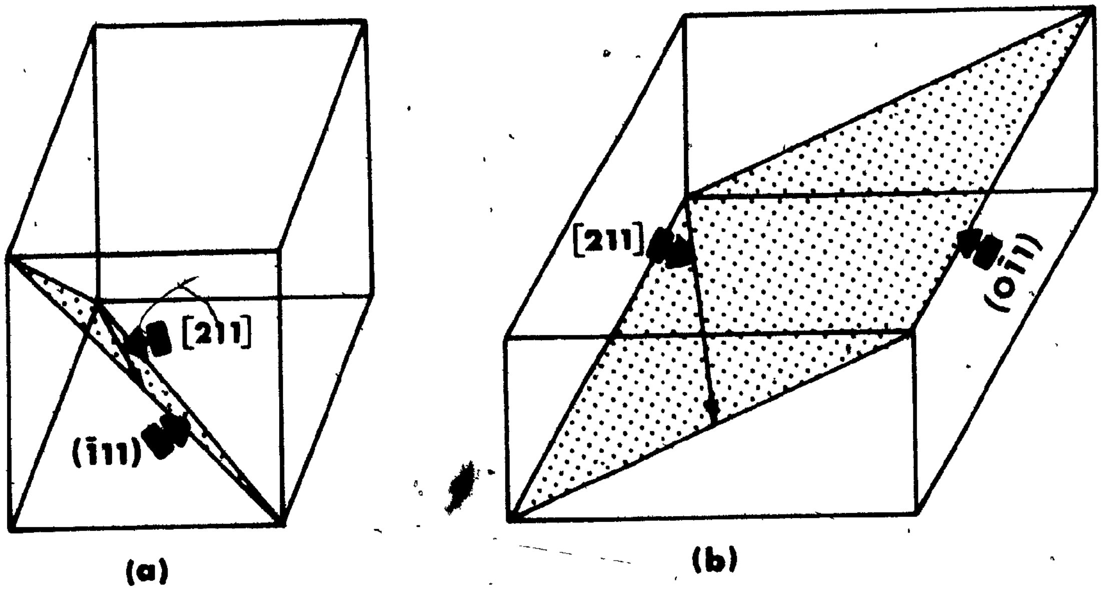

Figure showing planes and directions in contact at the solid/solid interface boundary: (a) Pb; (b) Sn.

According to Figure 4.1 and the above figure, the nominal growth directions $[211]_{Pb}$ and $[211]_{Sn}$ described in the B Statement coincide with the z-axis; while the lamellar interface (x-z plane) is parallel to the $(\bar{1}11)_{Pb}$ and $(0\bar{1}1)_{Sn}$ planes. Knowing that under uncoupled growth conditions face centered cubic (Pb) and body-centred-tetragonal

(Sn) metals tend to grow in the <100> and <110> directions respectively, then the angles α, β and γ formed by vectors $\vec{A}$ and $\vec{B}$ representing each phase preferred growth direction and by vector $\vec{R}$, the resultant coupled growth driving force can be determined.

Let's consider each phase separately:

(a) Pb - within the <100> preferred crystallographic family, the [100] direction is the closest to the [211] nominal growth direction coinciding with the z-axis.

γ ≡ angle between [100] and [211] (z-axis)

β ≡ angle between [100] and [$\bar{1}$11] (y-axis) case (1)

angle between [100] and [1$\bar{1}\bar{1}$] (y-axis) case (2)

α ≡ angle between [100] and x-axis. Can be determined knowing γ and β.

In general the angle between two directions is given by:

$$\cos\theta = \frac{u_1v_1a^2 + u_2v_2b^2 + u_3v_3c^2}{\sqrt{u_1^2a^2 + u_2^2b^2 + u_3^2c^2}\,\sqrt{v_1^2a^2 + v_2^2b^2 + v_3^2c^2}} \qquad (1)$$

For cubic structures where $a = b = c$, Equation (1) becomes:

$$\cos\theta = \frac{u_1v_1 + u_2v_2 + u_3v_3}{\sqrt{u_1^2 + u_2^2 + u_3^2}\,\sqrt{v_1^2 + v_2^2 + v_3^2}} \qquad (3)$$

So:

$$\cos\gamma = +2/\sqrt{6} \text{ and } \gamma = 35.26^\circ$$

$$\cos\beta = +1/\sqrt{3} \text{ and } \beta = 125.26^\circ \quad \text{case (1)}$$

$$\cos\beta = -1/\sqrt{3} \text{ and } \beta = 54.74^\circ \quad \text{case (2)}$$

From the direction cosines relation:

$$\cos^2\alpha + \cos^2\beta + \cos^2\gamma = 1 \tag{3}$$

$$\cos^2\alpha = 1 - \cos^2\gamma - \cos^2\beta$$

$$\therefore \cos^2\alpha = 1 - \frac{4}{6} - \frac{1}{3} = 0 \text{ and } \alpha = 90^\circ$$

(b) Sn - within the <110> preferred crystallographic family, the [110] direction is the closest to the [211] nominal growth direction coinciding with the z-axis.

$a = 5.8311$ A° $\qquad c = 3.1817$ A° $\qquad (c/a)^2 = 0.298$

(no correction made for either temperature or composition)

For tetragonal structures where $a = b \neq c$, directions are perpendicular to planes having the same Miller indices only when the c index is zero. When index $c \neq 0$, the direction normal to (hkl) plane will have Miller indices $[hk\frac{1}{(c/a)^2}]$ (i.e. [100] is perpendicular to (100) but $[21\frac{1}{(c/a)^2}]$ is perpendicular to (211)).

$\gamma \equiv$ angle between [110] and [211] (z-axis)

$\beta \equiv$ angle between [110] and $[0\bar{1}\frac{1}{(c/a)^2}]$ (y-axis) case (1)

angle between [110] and $[01\frac{\bar{1}}{(c/a)^2}]$ (y-axis) case (2)

$\alpha \equiv$ angle between [110] and x-axis. Can be determined knowing γ and β.

In the case of tetragonal structures, Equation (1) becomes

$$\cos \theta = \frac{u_1 v_1 a^2 + u_2 v_2 a^2 + u_2 v_3 c^2}{\sqrt{u_1^2 a^2 + u_2^2 a^2 + u_3 c^2}\sqrt{v_1^2 a^2 + v_2^2 a^2 + v_3^2 c^2}} \tag{4}$$

So:

$\cos \gamma = + 0.9216$ and $\gamma = 22.83$

$\cos \beta = - 0.3387$ and $\beta = 109.80$ case (1)

$\cos \beta = + 0.3387$ and $\beta = 70.20$ case (2)

$\cos \alpha = + 0.1894$ and $\alpha = 79.08^\circ$

The resultant growth force, $|R|$, is determined by adding vectorially vectors $\vec{A}$ and $\vec{B}$ taking into account the phases volume fractions (Pb — 37%, Sn — 73%):

$$\text{(Sn)} \quad \vec{A} = A_1 i + A_2 j + A_3 k \qquad |A| = 1.7 \text{ units of force} \tag{5}$$

$$\text{(Pb)} \quad \vec{B} = B_1 i + B_2 j + B_3 k \qquad |B| = 1.0 \text{ units of force} \tag{6}$$

$$B_1 = |B| \cos \alpha \qquad B_2 = |B| \cos \beta \qquad B_3 = |B| \cos \gamma$$

$$A_1 = |A| \cos \alpha \qquad A_2 = |A| \cos \beta \qquad A_3 = |A| \cos \gamma$$

$$|R| = \sqrt{(A_1 + B_1)^2 + (A_2 + B_2)^2 + (A_3 + B_3)^2} \tag{7}$$

The angles α, β and γ that $\vec{R}$ forms with the x, y and z axes are given by:

$$\cos\alpha = \frac{(A_1 + B_1)}{|R|} \qquad \cos\beta = \frac{(A_2 + B_2)}{|R|} \qquad \cos\gamma = \frac{(A_3 + B_3)}{|R|} \quad (8)$$

$|A_1 + B_1|$ being the x-component of R

$|A_2 + B_2|$ being the y-component of R

$|A_3 + B_3|$ being the z-component of R

Substituting the values of α, β and γ determined for vectors $\vec{A}$ and $\vec{B}$ in Equations (7) and (8), we obtain:

case (1)	case (2)
$\lvert R\rvert = 2.67$ units of force	$\lvert R\rvert = 2.67$ units of force
$\alpha = 83.06^\circ$	$\alpha = 83.06^\circ$
$\beta = 115.61^\circ$	$\beta = 64.39^\circ$
$\gamma = 26.67^\circ$	[illegible] $= 26.67^\circ$
$\vec{x} = +0.322\bar{i}$	$\vec{x} = +0.322\bar{i}$
$\vec{y} = -1.154\bar{j}$	$\vec{y} = +1.154\bar{j}$
$\vec{z} = +2.385\bar{k}$	$\vec{z} = +2.385\bar{k}$